LONG NONLINEAR INTERNAL WAVES

AND

QUASI-STEADY LEE WAVES

by

CHI-YUAN LEE

B.S., Cheng Kung University
(1964)

M.S., National Central University
(1966)

SUBMITTED IN PARTIAL FULFILLMENT OF THE
REQUIREMENTS FOR THE DEGREE OF
DOCTOR OF PHILOSOPHY

at the

MASSACHUSETTS INSTITUTE OF TECHNOLOGY

and the

WOODS HOLE OCEANOGRAPHIC INSTITUTION

June 1972

Signature of Author......................................
            Joint Program in Oceanography, Massachusetts
            Institute of Technology – Woods Hole Oceanographic
            Institution, and Department of Earth and Planetary
            Sciences, and Department of Meteorology,
            Massachusetts Institute of Technology, June 1972

Certified by..
                                            Thesis Supervisor

Accepted by...
            Chairman, Joint Oceanography Committee in the
            Earth Sciences, Massachusetts Institute of
            Technology – Woods Hole Oceanographic Institution

ABSTRACT

LONG NONLINEAR INTERNAL WAVES

AND QUASI-STEADY LEE WAVES

by

Chi-yuan Lee

Submitted to the Department of Meteorology, Massachusetts Institute of Technology and Woods Hole Oceanographic Institution on May 5, 1972 in partial fulfillment of the requirements for the degree of Doctor of Philosophy

Previous observation of large amplitude internal gravity waves generated by tidal flow over a submarine ridge in Massachusetts Bay have motivated us to consider the general problem of internal gravity wave generation by time-dependent flow of a stratified, inviscid fluid over topography. An internal Korteweg & deVries type equation for the stream function is derived using a three parameter expansion method, where the three small parameters correspond to nonlinear, dispersive, and non-Boussinesq effects. The nonlinear effect is found to depend crucially on the curvature of the basic density profile and vanishes for linear stratification, i.e., constant Brunt-Vaisala frequency. Numerical solutions to this KdV type equation for. variety of different conditions are then used to demonstrate the importance of nonlinearity on the generation of large amplitude internal waves in the breakdown of internal fronts. The numerical results are also in reasonable agreement with laboratory experiments in which a two-dimensional submarine ridge is moved to create transient internal disturbances. Additional numerical calculations show that a nonlinear model accurately describes the principal features observed in Massachusetts Bay.

Simple analytic models and laboratory experiments are also used to examine mixing and the generation of quasi-steady lee waves. A tall, rapidly oscillating ridge acts to mix the stratified fluid near the ridge; the circulation set up by the collapse of the mixed fluid is determined. In the second study, ray theory is used to analyse lee waves generated behind a low ridge being slowly towed periodically through a stratified fluid.

Thesis Supervisor: Robert C. Beardsley
                    Associate Professor of Oceanography

Table of Contents

1. <u>Introduction</u>

A. <u>General Motivation</u>:

Temperature measurements made by Halpern (1970) at station T
located 9 km west of Stellwagen Bank in Massachusetts Bay show that
large amplitude internal wave trains with wave periods of 6 to 8
minutes and lasting for about 3 hours are generated by the semi-
diurnal tidal flow. A warm front, i.e., a sudden rise in the general
temperature level, accompanies the onset of these internal wave trains.
Both the amplitude of the front and the amplitude of the internal wave
itself are so large (almost 10 m) in comparison to the characteristic
depth that nonlinearity which is neglected in linear wave theory can
not be overlooked in a general analysis of the generating wave mecha-
nics for this case. We shall assume that large internal disturbance
(say, a blocking front) with a horizontal characteristic length ℓ is
formed near Stellwagen Bank, and then use the smallness of the parame-
ter $(D/\ell)^2$, where D is the vertical characteristic length, to derive
a Korteweg & deVries-type governing equation (1895) for the internal
motion. This nonlinear KdV-type equation may then be used to analyse
the generation of internal waves from a long but otherwise arbitrary
initial internal disturbance. This is the general aim of this research;
we are not solely trying to explain the generation of these finite
amplitude waves in Massachusetts Bay.

In order to demonstrate the importance of the nonlinear effect,
two experimental records are shown in figure 1 and figure 2 . These
internal disturbances are measured using conductivity probes as shown
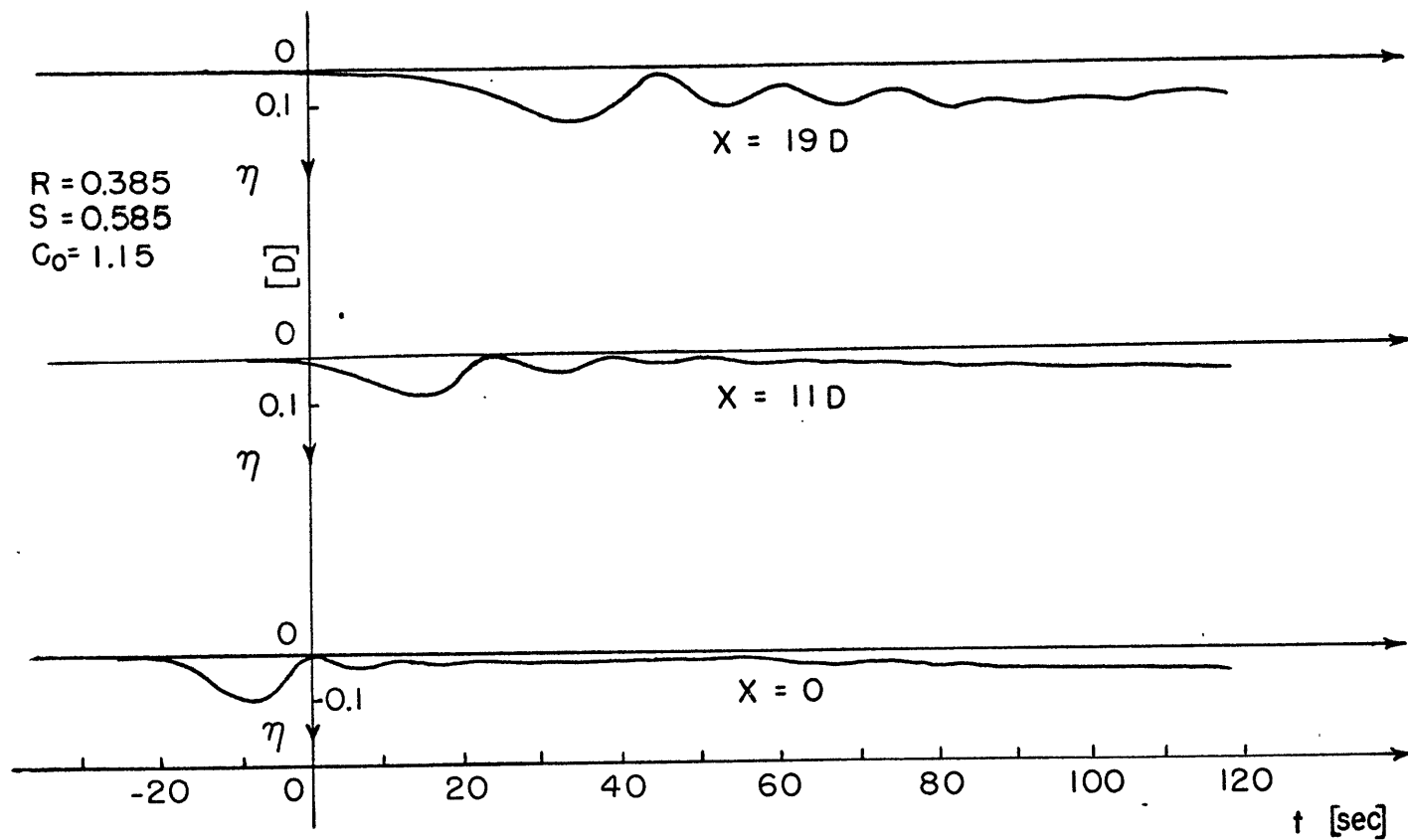
Figure / . Results of experiment / showing the generation of waves by
moving the ridge toward the probes for one half period of
a sinusoidal path (x = 0 corresponds to the position of
Probe A in figure 3 . Probe A is located approximately
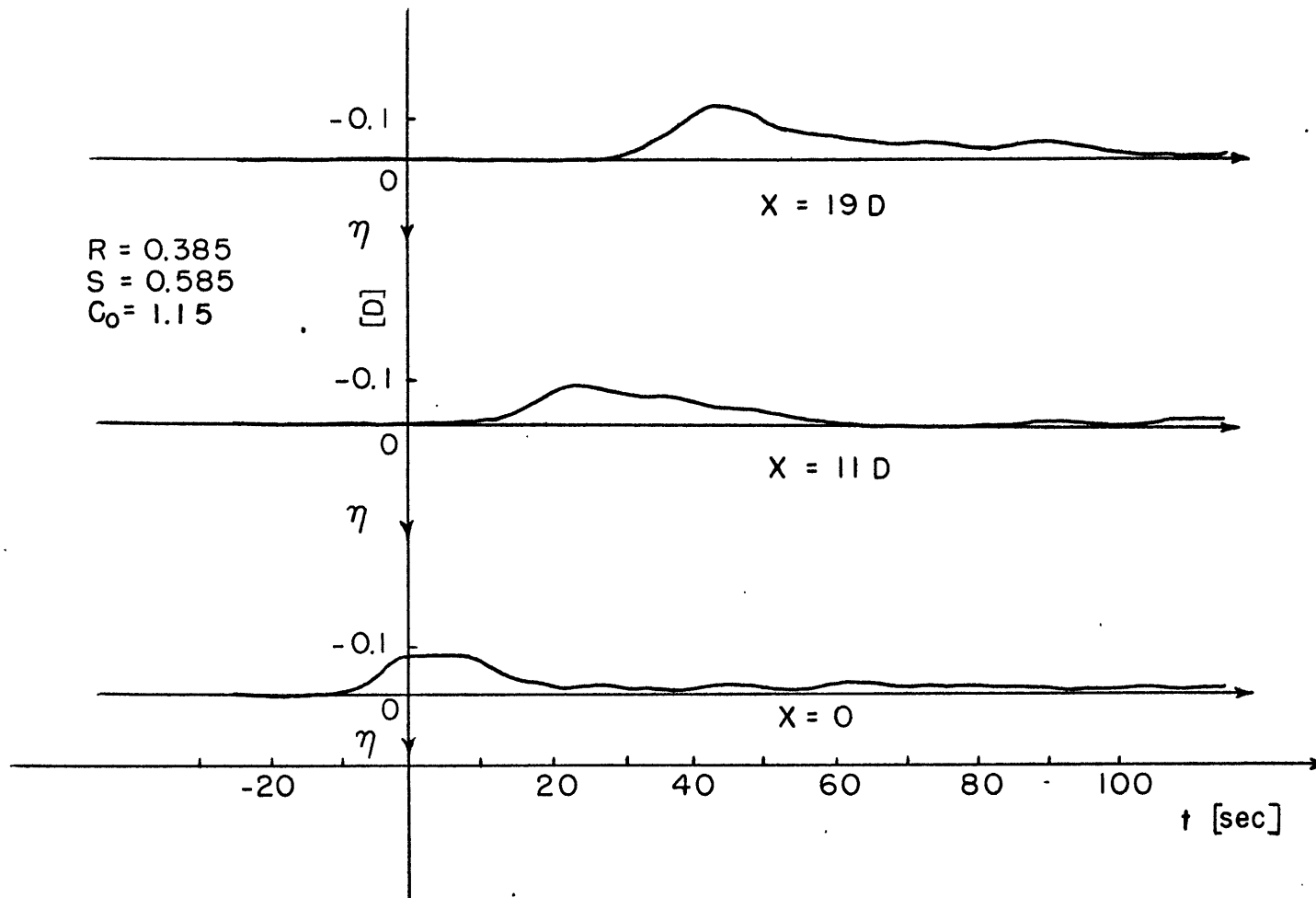55 cm from the final position of the ridge).

Figure 2 . Results of experiment 2 showing the generation of a solitary-type wave by moving the ridge away from the probes for one half period of a sinusoidal path (x = 0 corresponds to the position of Probe A in figure 3 . Probe A is located approximately 65 cm from the final position of the ridge).

in figure 3. The initial disturbances are produced by towing a ridge
horizontally over one half period a sinusoidal path. When the ridge
is moved toward the probes, the initial disturbance is a mound of
heavier fluid, with the local isopycnal surfaces being elevated.
The initial disturbance corresponds to a depression of the isopycnal
surfaces, when the ridge is moved away from the probes. For the
basic stratification used in our laboratory experiments, we will find
(in chapter 3) that an initial elevation will have a negative non-
linear effect, while an depression will have a positive nonlinear
effect. Thus, for a depression, the mass, momentum, and energy of
the initial disturbance are held together like a "solitary wave",
since the nonlinear effect tends to balance the dispersive effects.
An initial elevation will disperse into several waves behind the
initial front, however, since the negative nonlinear effect will
reinforce the dispersive effect. Detailed numerical calculations
for these two measurements will be given in chapter 3.

We will give in the remainder of this chapter a general discu-
ssion of the known nonlinear effects on surface and internal long
waves. In chapter 2 we try to model the wave phenomena observed in
Massachusetts Bay, develop a general classification of the internal
motion driven by a moving submarine ridge, and then describe the
experimental system and procedure used to illustrate our classifi-
cation scheme. In chapter 3, a three parameter expansion method
is used to derive a time dependent KdV equation for internal motion.
Both experimental data and numerical calculations are used to demon-
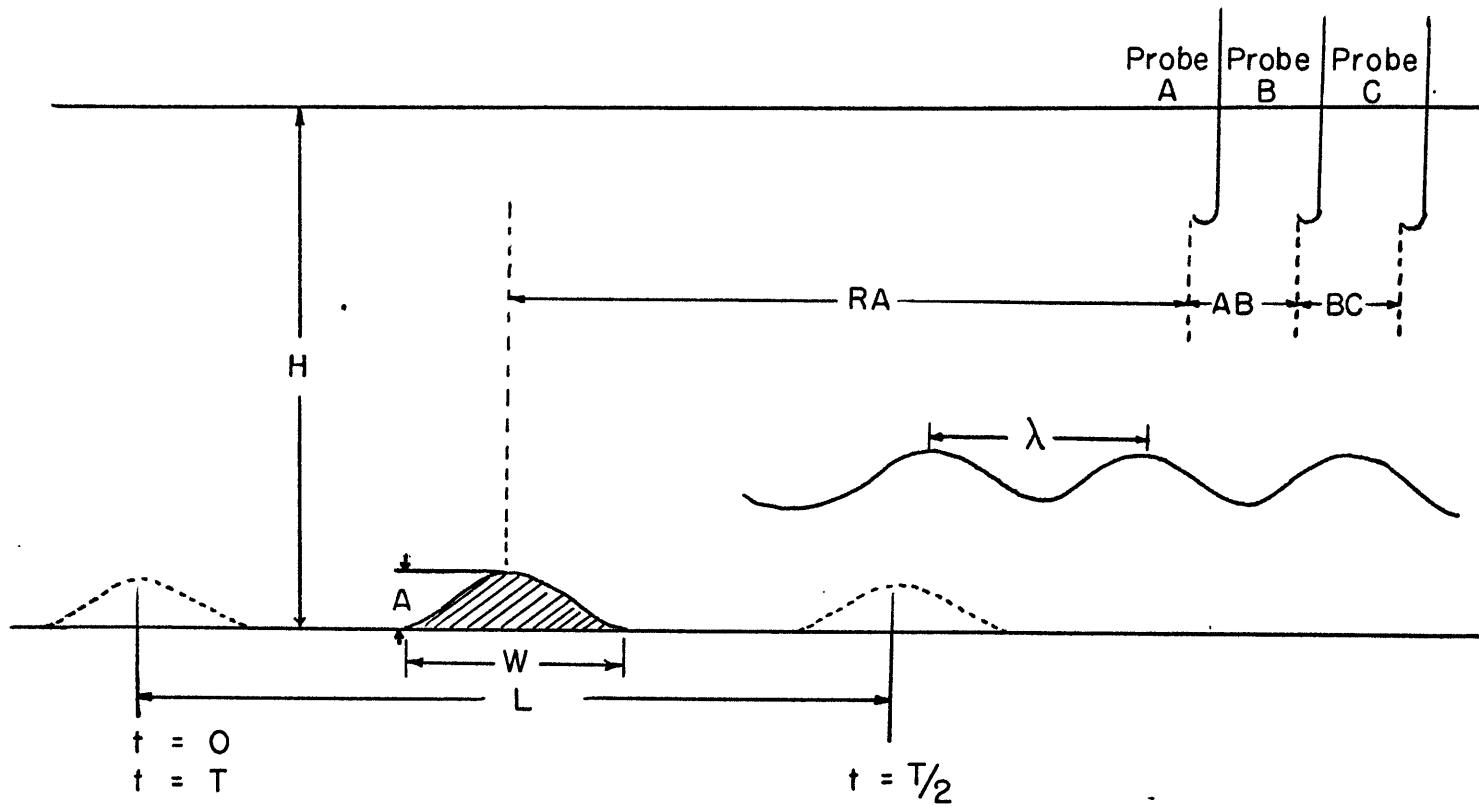strate the importance of nonlinearity in the generation of long

Figure 3 . Schematic of some of the physical dimensions in the experiment .

nonlinear internal waves, and the application to the large amplitude internal waves in Massachusetts Bay is explained. The influence of basic shear is analysed. The second order terms, i.e., the deviation from the classical KdV equation, are also obtained. In chapter 4, a ray theory and some experimental results are used to discuss quasi-steady lee trains. In chapter 5, we analyse mixing in a stratified fluid caused by rapid motion of the ridge.

B. Classical Long Surface Wave Theory:

We shall begin our analysis of long nonlinear internal waves by recalling some aspects of the classical long wave theory. Airy (1845) showed that when the pressure field is hydrostatic everywhere, the phase velocity of a progressive finite amplitude surface wave is equal to $(gH)^{1/2}$ everywhere where H is the local depth. It followed that the wave would tend to steepen ahead of their peaks, and the breaking of waves and consequent formation of "bores" could not be avoided. However, the lack of experimental support for Airy's theory led to the final discovery of solitary and cnoid waves by Scott Russell (1837, 1844), Rayleigh (1876), Stokes (1847, 1880), and Korteweg and deVries (1895). They showed that the tendency of a long surface wave to steepen ahead of its peak, which is proportional to the amplitude $a/H = \mathcal{E}$, may be balanced by an opposite tendency, due to the nonhydrostatic pressure field, which is proportional to the square of the wave number $H^2/\ell^2 = \delta$, where ℓ is the wave length. Thus, an infinite sequence of permanent wave profiles exist, each with a particular ratio of $\mathcal{E}/\delta$, the

Ursell parameter, such that the two tendencies to change the wave profile exactly cancel out. These waves are called "cnoidal" waves, because their wave profiles are exactly the square of the Jacobian elliptic function CN(x) with different moduli constant. The two extreme limits are (1) the lower limit $\mathcal{E}/\mathcal{S} \rightarrow 0$ corresponding to a linear sinusoidal wave, and (2) the upper limit of $\mathcal{E}/\mathcal{S} \rightarrow \infty$ corresponding to solitary wave. A cnoid wave train with extremely long wave length can be approximately regarded as a sequence of solitary wave. Following Lighthill (1967), a regime diagram with the amplitude a and the characteristic wave length $\mathcal{L}$ as the two axes can be constructed (see figure 4), which show that the solitary wave is a boundary which separates the natural evolution of a long finite amplitude disturbance into two quite different regimes. Numerical calculation (to be discussed in detail in chapter 3) shows that a point with a small deviation above (below) the solitary wave curve will tend to move up (down) and to the left (right) in figure 4, i.e., the nonequilbrium wave tends to steepen (flatten).

It is well known that the general mathematical analysis of non-linear wave motion divides into two distinct approaches:

(a) Stoke's expansion: development of a linear wave theory, and its subsequent extensions to finite amplitude wave using a regular perturbation expansion in the one small parameter $a/\mathcal{L}$. Fourier analysis is used in this case.

(b) Shallow water theory: development of a time dependent KdV-type equation based on the two small parameter $\mathcal{E}$ = a/H, $\mathcal{S} = (H/\mathcal{L})^2$. The second approach allows us to
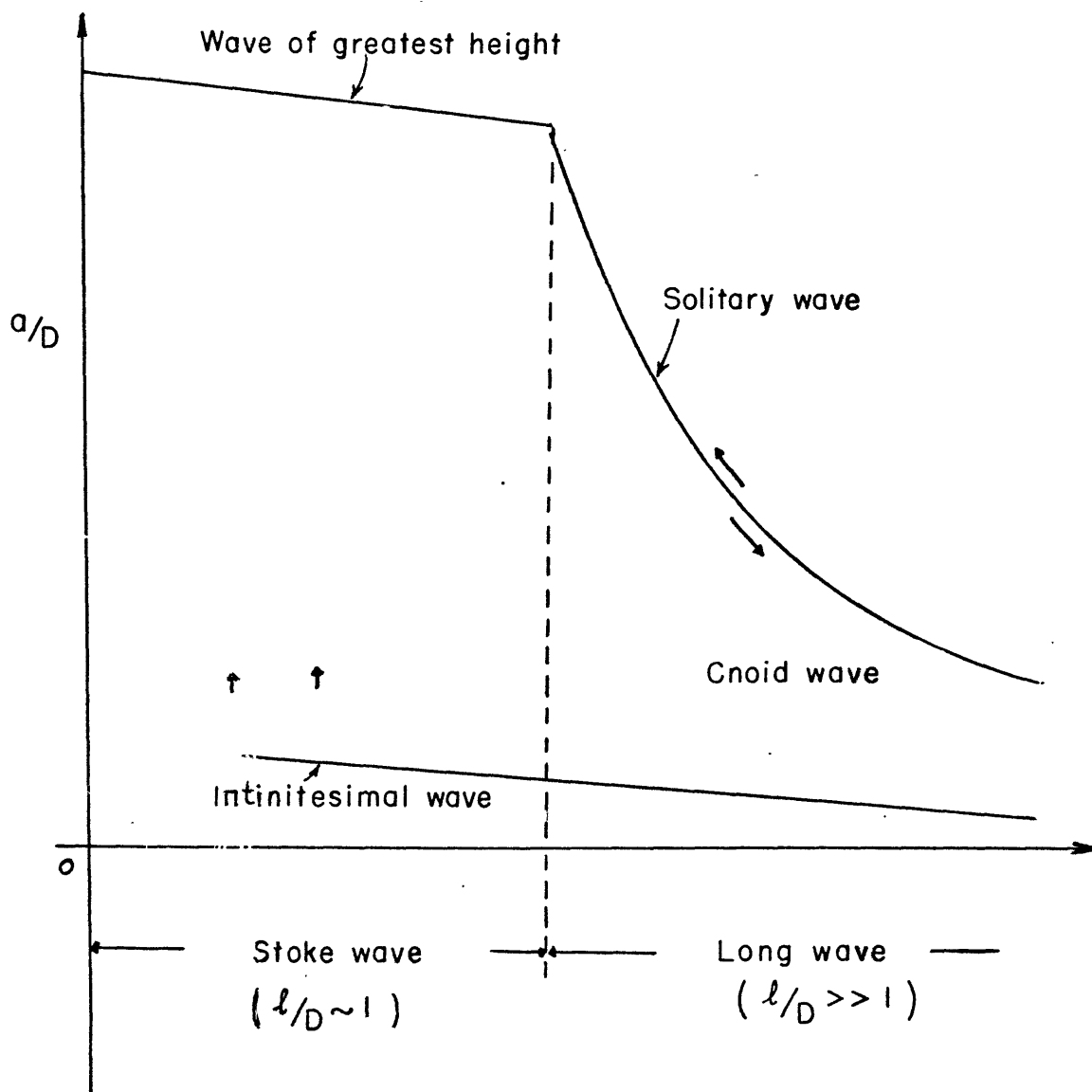
Figure 4 . Numerical results showing that solitary wave is
a boundary of natural evolution on Lighthill's
diagram.

analysis the natural evolution of an arbitrary long dis-

turbance in addition to the wave form solution in case (a).

(c) Since the Stoke's expansion and shallow water theory

are not completely reconciled, we will now compare the

two approaches and discuss their principal differences.

(1)(a) The Stoke's expansion (a) is derived on the small

parameter $a/\mathcal{L}$ and the parameter $(H/\mathcal{L})^2$ is assumed

to be not less than order unity.

(b) Shallow water theory (b) is based on two small para-

meters, $\mathcal{E}$ = a/H and $\mathcal{S}$ = $(H/\mathcal{L})^2$. Note that $a/\mathcal{L}$ =

$a/H \cdot H/\mathcal{L} = \mathcal{E}\mathcal{S}^{1/2}$. If we take the limit $H \rightarrow 0$ for

case (a), we do not obtain solitary or cnoid waves.

(2)(a) To order $(a/\mathcal{L})$, there is no phase velocity change,

due to finite amplitude effect.

(b) To order $(a/H, H^2/\mathcal{L}^2)$, there is a change of phase

velocity.

(3)(a) To order $(a/\mathcal{L})$, a sinusoidal wave will keep symme-

tric wave form.

(b) A sinusoidal wave tends to distort and break.

(4)(b) Can be easily used to treat an initial value problem

for an arbitrarily long disturbance whereas (a) cannot.

(5) Since higher harmonics are generated by nonlinearity

using the Stoke's expansion, it seems necessary to check

for the possibility of "self-interaction", i.e., the

interaction between a wave and its higher harmonics. If

the dispersion relation is $\omega = \omega(k)$, we need

$\omega(2k) - \omega(k) = \omega(k)$ for interaction between a primary wave and its
first harmonic. This is generally impossible for internal and
surface wave (except for capillary-gravity surface waves which have
a special dispersion relation). However, the above resonance con-
dition is almost satisfied in long wave theory due to the fact that
for vanishing wave number, the dispersive curve approaches a straight
line. Mei(1971) has discussed this self interaction mechanics in
shallow water wave theory by means of an analogy with nonlinear
optics.

Since we are primarily interested in the initial value problem,
we will focus our attention on results obtained by the second
approach (b). Utilizing temporal equations of the KdV-type, we will
now examine the interaction between two surface solitary waves.
Zabusky (1967) and Madsen and Mei (1969) have shown using the KdV
equation that significant nonlinear interaction between two solitary
waves occur only near the intersection of the crests. Numerical cal-
culations show that when the solitary wave of large amplitude catch
up with the smaller one, the amplitude of the larger peak decreases as
the smaller one increases its amplitude and then exchange roles such
that the one previously identified as the large peak now becomes the
smaller and vise versa.

Nonlinear effects are understood in a really systematic manner
only for nondispersive waves, and are called amplitude dispersion by
Lighthill (1967). Although the study of the interaction of the fre-
quency dispersion and the amplitude dispersion is only in its begin-
ing stages, the study of nonlinear effects with the parameter

$(a/H)(H^2/\ell^2) \gg 1$ is rather well advanced. Different value of the amplitude in a "long wave" are propagated forward at different speeds. As time goes on, regions of large amplitude, being propagated faster, gradually catch up to regions of low amplitude. However, this catching up cannot proceed to where the higher amplitude actually overtakes the lower, since the amplitude must remain a single valued function of position. Immediately before this happens, a region with very large gradients of pressure, velocity, etc., will be generated which prevent further increase of wave amplitude by the frequency dispersive effects which we neglected in this process. Numerical calculations by Pregrine (1966) show that a wave train will be generated behind in the "front", the bore remaining nonturbulent since it can lose the necessary energy by backward radiation through a finite amplitude wave train. However, there is a maximum amplitude which is defined by the solitary waves. Beyond this, progressive steepening of the wave front to the point of turbulent "bore" formation is unavoidable. This analysis is only a first order approximation, however, since all terms need to be retained in order to obtain a final criterion for wave breaking.

The evolution of large scale variations on a finite amplitude periodic wave has been studied by Whitham (1965). To zeroth order the wave number, frequency, and amplitude satisfy a system of first order quasi-linear differential equations. These equations may be hyperbolic or elliptic. If elliptic, the characteristic velocity will have an imaginary part and instabilities will tend to destroy the coherence of the wave train (such as in deep water wave theory). If hyperbolic, wave properties will develop shocks (such as in shallow water wave theory).

A situation similar to the classical shock problem in gas dynamics

arises in that more shock conditions exist that we actually need. The-

se jump conditions correspond to the conservation of waves, mass, momen-

tum, and energy. The conservation of waves corresponds to the conser-

vation of entropy, which is discarded in gas dynamics by considering

the real physical situation across the shock. However, the situation

seems quite different in water waves. Benjamin (1954, 1956, 1967)

chooses the conservation of waves as one of the shock conditions (al-

though he did not point it out explicity) to analyse a stationary

surface wave train of finite amplitude and permanent form, thus dropping

the conservation of momentum and energy. Real friction or dissipative

process make Benjamin's assumption more realistic in the natural pheno-

mena. However, we will use only the conservation of energy and momentum

in the analysis of wave generation.

C. Long Nonlinear Internal Wave Theory:

Our review of nonlinear wave motion has concerned up to now only

surface wave dynamics in a constant density fluid. It is well known

Benjamin (1966, 1967), Benney (1966) that long nonlinear internal

waves are possible in a density stratified fluid. In analogy to the

classical long wave theory, both Benjamin and Benney used a two para-

meter perturbation expansion method to find a governing equation simi-

lar to the KdV equation. However, Long (1965) pointed out that a third

parameter, $\sigma' = \Delta \bar{\rho} / \bar{\rho}$, is critically important in long nonlinear inter-

nal waves, where $\Delta \bar{\rho}$ is the variation of basic density stratification

over a vertical characteristic length D, $\bar{\rho}$ is the vertically averaged

density, and σ' is its fractional change over the vertical characteristic

length. If σ is the same order or smaller than the nonlinear term

a/D or the dispersive term D^2/ℓ^2, the three parameter perturbation

expansion method should be used. The "inertial" effect due to σ

= 0.1 will be of equal importance as the nonlinear effect due to a

finite amplitude a/D = 0.1; σ of this order are frequently used in

laboratory experiments.

Long only examined stationary waves for the case of constant

Brunt-Vaisala frequency. We will in chapter 3 formally use a three

parameter perturbation expansion approach to find a time dependent

KdV equation for arbitrary stratification and basic shear. We will

then find that this additional term corresponding to $\sigma \neq 0$ tends to

decrease the phase velocity. The physical meaning of this result is

analogous to the frequency effect of the self-mass of a spring in a

simple mass-spring system. We will also find that the nonlinear

effect of internal wave motion is critically related to the basic

density stratification and structure. For typical thermoclines, i.e.,

the density variation of the upper part of the fluid is much greater

than that of the lower part, the nonlinear effect is to steepen

(flatten) an isopycnal depression (elevation). An obvious difference

from surface wave theory is that both an initial elevation and depre-

ssion may become a solitary internal wave corresponding to different

basic density structure while only initial elevations develop into

surface solitary waves. We shall also find that the nonlinear effect

vanishes for a constant Brunt-Vaisala frequency, and that no solitary

waves exist unless we take a second order term of order $\varepsilon\sigma$ into con-

sideration. This conclusion agrees with Long's stationary wave analysis.

2. Development of Model Problem

A. Discussion of Massachusetts Bay Observation:

In order to simplify the complicated situation in Massachusetts
Bay and make a reasonable model to represent the dominant features
which are closely related to the generation of the internal wave trains
observed in Massachusetts Bay, we begin by summarizing Halpern's data
and discuss some possible physical interpretations.

(a) The average time interval between the onset of 29 groups
of high frequency fluctuations observed at station T was
12.4 hours. This strongly suggests that the dominant
driving force is the semi-diurnal tidal flow.

(b) The crests of the surface bands, which are generated by
the internal waves, lie parallel to Stellwagen Bank and
exhibit the same curvature. Thus it seems that the bank
is a "wave source" or, at least, has a significant
influence on these internal wave trains.

(c) Speed measurements recorded at Stellwagen Bank (tempera-
ture measurements at the bank are missing) do not show
the groups of large amplitude high frequency fluctuations.
This means that these internal wave trains have to be
generated somewhere between the bank and station T loca-
ted 9 km west of the bank crest. This rules out a quasi-
steady lee wave mechanism as a wave source.

(d) The large abrupt rise in the mean level of these high fre-
quency temperature oscillations may be related to the fol-
lowing three reasons although, as we will see, only one is

possible in Massachusetts Bay. (1) Nonlinear steepen-
ing of the long semi-diurnal tidal waves: Although the
basic density stratification in Massachusetts Bay will
produce a negative nonlinear effect (see chapter 3), and
will make the warm front steepen, the distance (9 km)
between Stellwagen Bank and station T is too short to
allow a symmetric wave to deform into such a front. (2)
Strong mixing near the bank: This is ruled out by the
fact that the temperature rises at all depths. (3)
Blocking effect: When the tidal current becomes very
weak, the Froude number is very low. It is well known
from the work of Long (1955) that blocking phenomena
occur in a stratified flow for small Froude number.
Thus, shortly before high water, the velocity of tidal
flow decreases to this critical velocity and the lower
part of the water column is then suddenly blocked by
Stellwagen Bank, and only the upper part of the fluid
or warm water is allowed to flow across the bank to
form a sharp warm front. This warm front will be fur-
ther steepened by the negative nonlinear properties
associated to the specific density stratification in
Massachusetts Bay. Although a cold front is also form-
ed, its slope will be decreased by the nonlinear effect,
so that the slope of the cold front will be very small
at station T. The dispersive effect of the cold front
is also decreased, preventing the generation of inter-

nal wave trains. Although we feel that the blocking

effect of Stellwagen Bank is the likely candidate for

creating the warm front, its effectiveness will be

greatly decreased by the three dimensional structure

of the bank. The width of the open end of Massachusetts

Bay is approximately 70 km, where the length of the bank

is approximately 40 km. Thus we expect some cold water

may flow into Massachusetts Bay through these open parts

during the blocking time interval; this may be one of

the reasons why the length of the observed bands is

only 10 km where the length of the bank is almost 40 km.

We will now construct a simple model to simulate some of the most
important factors found in Massachusetts Bay. Our principle goal is
to find the possible wave generating mechanics and not go into details
of its modifications caused by the very complicated situation in Massa-
chusetts Bay. We assume that a symmetric submarine ridge is towed
back and forth periodically in a density stratified fluid in a long
wave tank. The forcing and response are two-dimensional and the fluid
is considered to be essentially inviscid. The major differences
between this model and the tidal flow over Stellwagen Bank are:

(1) Basic velocity shear: It is well known that strong velo-

city shears exist in tidal flow. According to Miles

(1961) and Howard (1961), a sufficient condition for

small amplitude stable motion in parallel stable stra-

tified, inviscid flow is that Richardson number Ri has

to be everywhere greater than $1/4$. Although Ri is

always greater than 1/4 at Massachusetts Bay, Halpern reports that Ri was less than unity and was as low as 0.3 just prior to the initiation of the short-period internal waves. Since this Ri value is a ten-minute average, it may drop to less 1/4 occasionally. Halpern's data indicate that the mean shear is almost perpendicular to the direction of propagation of the internal waves, so that it is unlikely that shear instability plays a significant role in the generation of these internal waves. While the neglect of shear greatly simplifies our laboratory experiments, we will include the influence of velocity shear in the direction of propagation on the nonlinear and dispersive effects in the theoretical analysis.

(2) Three dimensional effect: In our experiments, the ridge occupies the whole width of the wave tank, while Stellwagen Bank obviously does not close the open end of Massachusetts Bay. From Halpern's aerial photographs of the surface bands, these internal waves seem to remain two dimensional for a relatively long distance westward of the bank. However, as mentioned before, the three dimensionality of the real topography reduces the blocking effect of the bank. One evidence is that the length of the observed bands is much smaller than the length of the bank, and their ends were wrinkled and compressed along their axes.

(3) Horizontal variation of mean current: We assume that the "mean current" (relative to the moving ridge) is uniform

in space, while the actual east-west tidal flow in

Massachusetts Bay has to vanish at shore.

(4) The asymmetric shape of Stellwagen Bank: The slope of

the west side of the bank is approximately three times

the slope of the east side of the bank at the same

latitude as station T. The asymmetric slope may be one

of the reasons why the high frequency fluctuation was

absent in the speed measurements 11 km east of the bank.

Since the dispersive effects are proportional to $\delta = (D/\ell)^2$,

the ratio of δ at east side to δ at west side is only

approximately 1/10. This crucially restricts the gene-

ration of internal wave trains.

(5) The change of total depth: We assume the total depth re-

mains constant while the actual tidal amplitude is appro-

ximately 1.5 m in Massachusetts Bay. The phase lag of

high or low water around Massachusetts Bay is approxima-

tely equal to (width of Massachusetts Bay)/(speed of long

wave) $= \dfrac{40 \, km \times 1000}{(9.8 \times 80)^{1/2}} \cong$ 20 min. This value is much

smaller than the period of the tide.

(6) The body force: The horizontal acceleration for the tidal

flow is absent in the experiments, however, it is too

small to be considered.

While a more realistic model could be developed from observational

knowledge of the mean current structure in Massachusetts Bay, we feel

that our simple two-dimensional model should contain most of the fun-

damental physics of the internal wave generation appropriate to Massa-

chusetts Bay. We will now consider the different general flow re-
gimes which are possible in our model problem.

B. General Classification of Flow Regimes:

The properties of fluid motion in an inviscid flow depend on
the scale and amplitude of the motion and on the physical parameters
which characterize the problem. In the previous discussion, we found
that for a given physical system, the ratio of scale and amplitude are
crucially important in determining the fluid behavior. We will now
define several dimensionless numbers, which depend on the relevant
scales, which can be used to classify the flow into several quite
different regimes. Assume that a symmetric ridge is towed periodi-
cally back and forth in a density stratified, inviscid fluid layer
as shown schematically in figure 3 . The relevant dimensional scales
are:

L = the "excursion" of the oscillating ridge,

T = the period of the oscillating ridge,

A = the height of the ridge,

W = the streamwise width of the ridge,

H = the total depth of the layer,

N = the typical Brunt-Vaisala frequency of the fluid,

λ = the wave length,

U = the typical velocity of the moving ridge,

n = internal wave mode number.

In the experiments, the slope of the ridge A/W is almost kept
constant and small enough to avoid significant boundary layer sepa-
ration phenomena. As the ridge is moving, the fluid particles will

be forced to move up and down for L/λ times in a time interval T

with a vertical amplitude $\sim$ A, thus the vertical velocity W can be

scaled as

$$W \sim (L/\lambda)(A/T).$$

Using the equation of continuity, the horizontal velocity of the

fluid can be scaled as

$$u \sim w\frac{\lambda}{H} \sim \frac{A}{H}\frac{L}{T},$$

and the inverse of the square root of Richardson number, R_o, can be

defined as

$$R_o = \frac{du/dz}{N} \sim \frac{u/H}{N} \sim \left(\frac{A}{H}\right)\left(\frac{L}{H}\right)\left(\frac{f}{N}\right),$$

where $f = 2\pi/T$ is the frequency of the oscillating ridge.

It is well known from Miles (1960) that the flow may not keep

stable for $R_o > 2$, so that mixing phenomena are expected for large R_o.

However, potential flow occurs if we keep A/W very small and $U > \frac{NH}{n\pi}$

i.e., U exceeds the phase velocity an internal wave may have. In order

to analyse the blocking effect of the ridge, we have to change the re-

levant horizontal velocity scale from the perturbation velocity u to

the velocity of the ridge U. The internal Froude number Fi is defined

$$F_i = \frac{U}{(g'H)^{1/2}} \sim \left(\frac{L}{H}\right)\left(\frac{f}{N}\right),$$

where g' is the reduced gravity $g\frac{\Delta\rho}{\rho}$. Blocking occurs at very low

Froude number. Since Fi is independent of A, the start of blocking

does not depend on A eventhough the volume of fluid being blocked is

proportional to A·U. In a three dimensional space with A/H, L/H, and

f/N as three orthogonal axes (see figure 5), the wave regime is then bounded by two critical surfaces which represent the critical Richardson number and critical Froude number which separate the blocking and mixing regimes from the wave regime.

The wave regime can be further divided into three subregimes by using a parameter $R_L = L/\lambda$ (1) For $R_L \gg 1$, quasi-steady lee waves arise. This case occurs when the period T of the oscillating ridge is much greater than the period of lee waves, and the acceleration of the ridge can be neglected in the analysis. Note, however, that lee waves do not exist if $U > \dfrac{NH}{n\pi}$, the largest phase velocity an internal wave may have. (2) For $R_L \ll 1$, the ridge is considered to be a classical "wave maker"; the period of the wave is exactly the same as the period of the oscillating ridge. However, the ridge will no longer generate waves if f > N, i.e., the highest frequency an internal wave may have (3) For $R_L \sim 1$, an intermediate case between (1) and (2) arises with lee waves being superposed on long waves. These various regimes are illustrated in figure 5 .

In chapter 3, we will analyse the generation of large amplitude internal waves. This flow belongs in the blocking regime, since for a high ridge blocking produces a very large internal initial distur- bance with a sharp front which evolves into a long nonlinear internal wave train.. In chapter 4, we will analyse "quasi-steady" lee waves. By neglecting the acceleration of the ridge, we can consider the ridge as a moving wave "source" which emits waves along the rays in a t-x diagram. In chapter 5, the mixing regime will be analysed. Here the oscillating ridge is viewed as a "mixer", emitting mixed fluid along
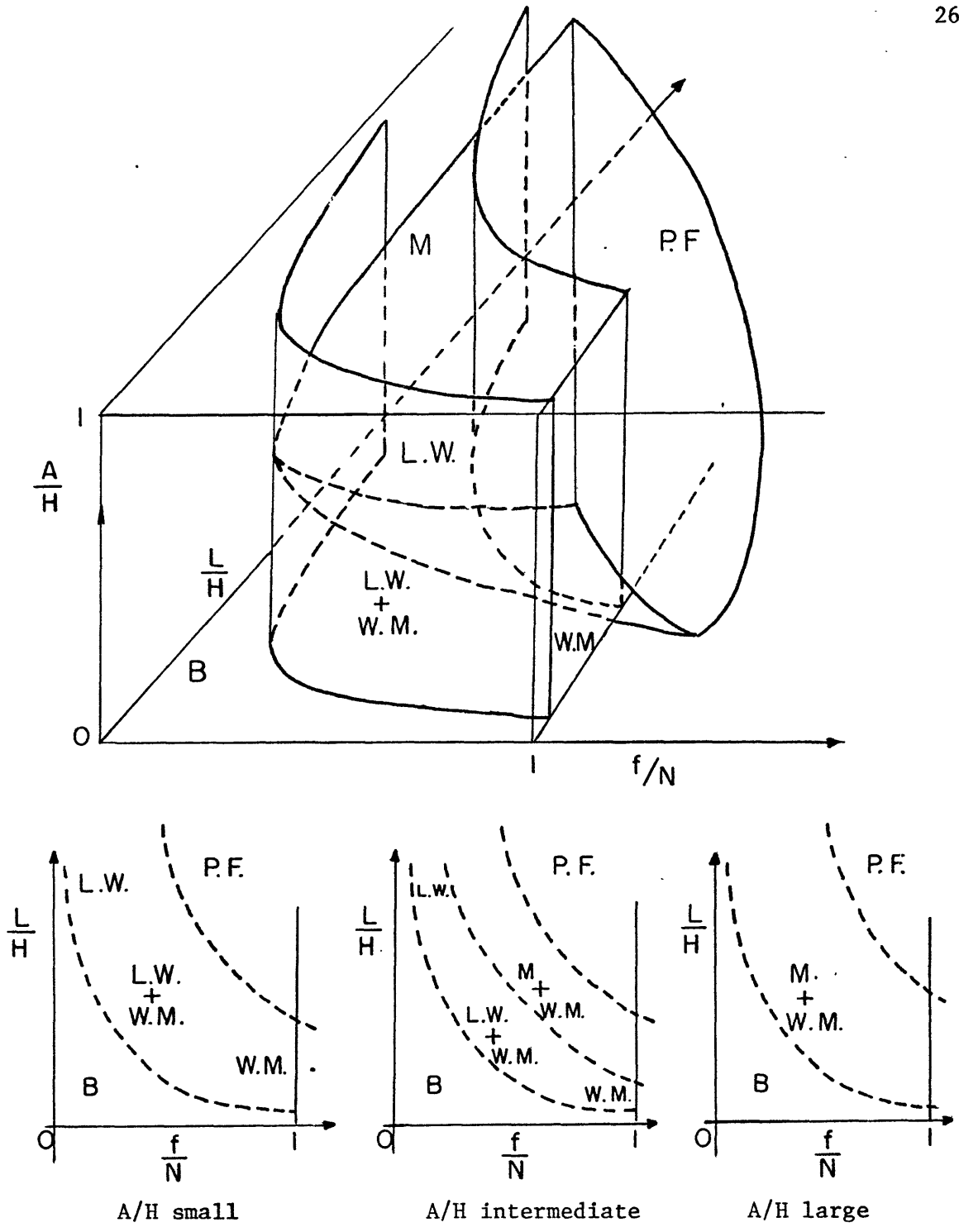
Figure 5 . The classification of regimes: P.F. (potential flow),
M. (mixing), W.M. (wave maker), L.W. (lee waves),
and B. (blocking).

the neutral bouyancy level and causing the unmixed fluid to recir-
culate back to the ridge.

C. Description of Laboratory Experiment:

The two-dimensional inviscid model problem developed in the pre-
ceding section is directly applicable to a simple laboratory experi-
ment. We will now describe the experimental apparatus and procedures.

A rectangular wave tank is used to contain the stratified salt
water; it is 4.9 m long, 20.5 cm wide, and 38.4 cm deep. The tank is
filled using a procedure attributed to Oster (1965). This allowed any
arbitrary but stable basic stratification state to be made. Owing to
the corrosive properties of salt water and the convenience for obser-
vation, two 50 gallon Tygon barrels are used in the filling system.

The filling procedure is essentially the same as used by Cacchione
(1970). Several days before an experiment, the two 50 gallon Tygon
barrels were filled to a predetermined volume with hot water. A pre-
determined amount of salt was added to one barrel and mixed carefully.
After the tank had been cleaned, the ridge and wave absorbers put in
place, and driving system tested, the siphon connecting the two barrels
was primed and the stirrer in the fresh water barrel started. The tank
was then filled from the fresh water barrel. The filling process took
one day to complete. On the next day, vertical profiles of the index
of refraction were taken over several stations using an American optical
Company refractometer model 10402. These profiles were then converted
into specific gravity profiles using the manufacturer's calibration
curves.

A two inch thick screen was placed with an inclination to the side wall at each end of the wave tank (see Phillips et.al., 1968). These screens were used to absorb the internal waves and separate the disturbances caused by the driving wheels on the end walls.

The driving system of the experiment is designed to move the ridge along the bottom of the wave tank. In order to produce "quasi-steady" lee wave trains, the oscillating amplitude and period of the ridge must be much greater than the wave length and period of the lee wave itself. At the same time, we also wanted the motion of the ridge to be relatively smooth, i.e., any occasional irregular motions of the ridge must have time scales and amplitudes much smaller than the period and amplitude of the lee waves. So the drive system has to meet the following primary requirements of

        (1) relatively large, variable "excursion",

        (2) relatively long, variable period,

        (3) reasonably smooth and precise motion.

Since the experiment was designed to get usable data at reasonable cost, we employed wherever possible components left by former students (Cacchione, et.al.) and standard instruments available at the laboratory. In the resulting drive system, the ridge is moved by means of a wire/pully arrangement connected to a precision variable speed gear box assembly (see figure 6 and 7). A small amplitude rectilinear sinusoidal motion device was used to perturb the frequency of oscillator 1, which drives the synchronous motor 1. Motor 2 is driven at constant speed. Both motors are coupled through a differential gear to the
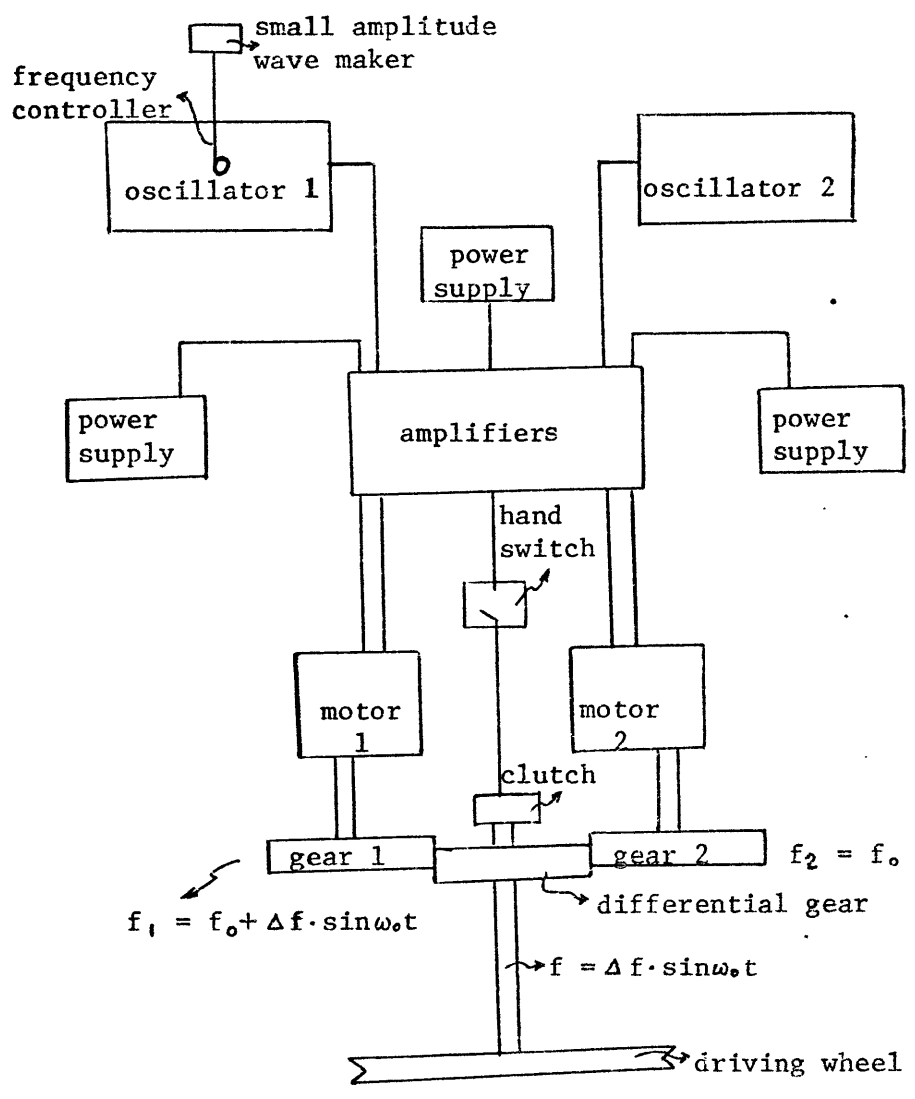
Figure 6 . Drive system.

A - B cross section

string
rubber

Driving wheel

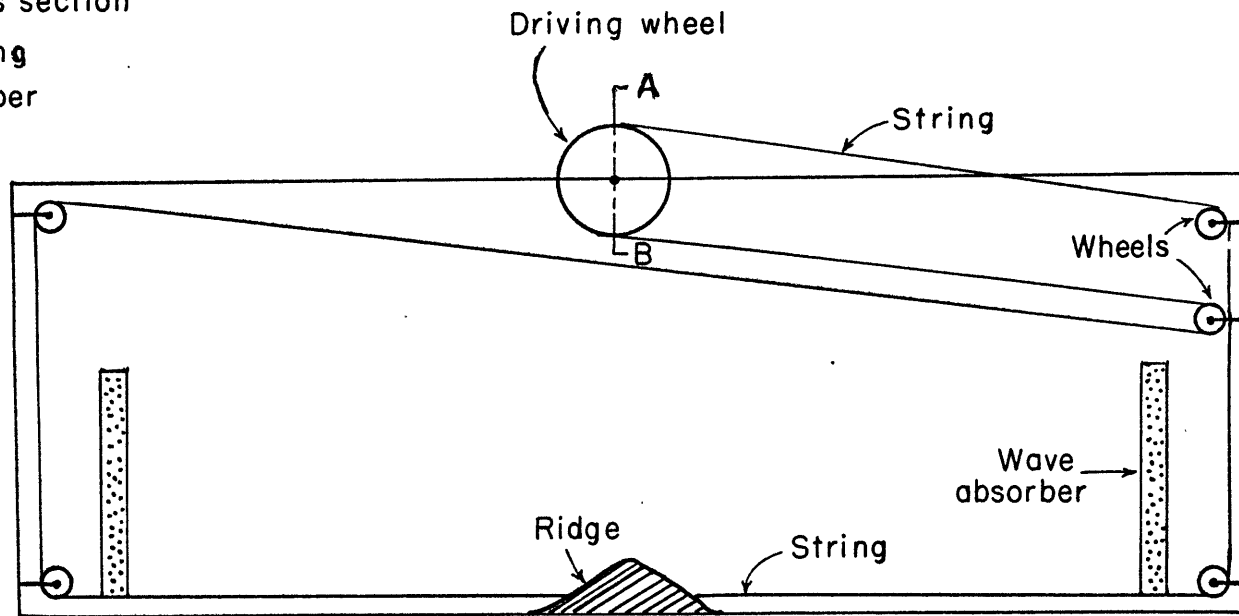A

String

Wheels

Wave absorber

Ridge

String

Figure 7. Schematic cross-section of apparatus, showing wave tank, ridge, wave absorbers, and driving wheel.

drive wheel so that the speed of the latter is only proportional to the perturbation frequency of oscillator 1. Thus "excursion" and period of the oscillating ridge can be changed by varying the amplitude and period of the frequency perturbation of oscillator 1.

The ridge is made by bending thin aluminium sheet into the symmetric shape desired and mounting on a smooth plexiglas plate. The shape of ridge can be approximately expressed by the curve $Ab^2/(x^2 + b^2)$ as shown in figure 8 , where A is the maximum height of ridge, b is a constant. In order to avoid significant friction between the side wall and the ridge, two small wheels were put on each side of the ridge to press against the side walls. The gap between the side and the ridge may produce some unwanted minor disturbances, however, these disturbances were found to die out quickly with distance and to have little influence.

The variations of the properties of the internal disturbances as they propagated away from the ridge were measured with several AC conductivity probes built by Cacchione (1970). The vertical density gradient of the fluid was established using salinity stratification. The temperature variations in the water were found to be small except in thin boundary layer. Since salinity is approximately a linear function of conductivity in the range of salinity values we used, the change of salinity at a point can be approximately evaluated by the change of conductivity. Just before the start of each experiment, the conductivity probes were given static calibrations by raising and lowering them vertically by known increments while recording their output at each level; this gave an updated sensitivity coefficient for each

32.
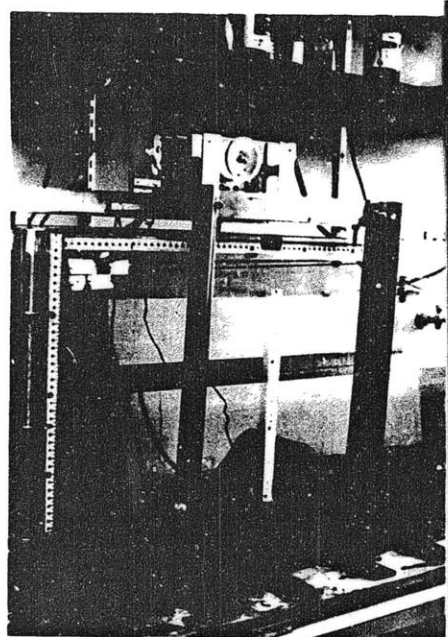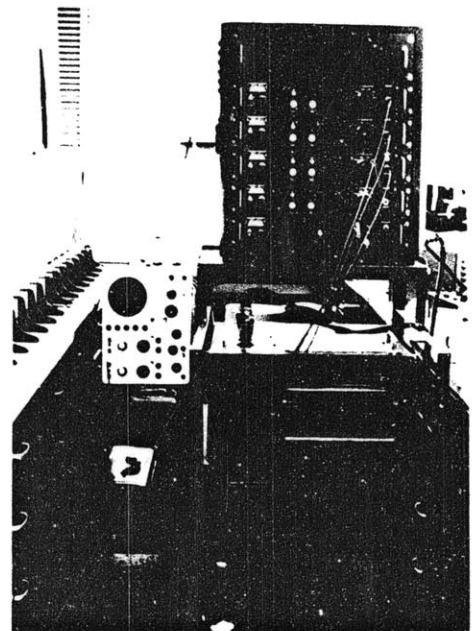
(A)   (B)

Figure 8 . (A) Photography of wave tank, ridge and
            drive wheel. (B) Osciloscope, and
            recorder.

probe. The conductivity fluctuations of the fluid were recorded on a fast 4-channel Sanborn strip chart recorder. Potassium permanganate ($KMnO_4$) was used to make vertical dye streaks to determine the vertical profile of the horizontal velocity field and to make the mixed region visible.

3. Long Nonlinear Internal Waves, Theory and Experiment

A. Development of Theoretical Model:

(1) Basic Derivation of Long Nonlinear Internal Wave Equation.

In analogy to classical long surface wave theory, Benjamin (1954, 1966, 1967) did extensive work on stationary internal waves of finite amplitude and permanent form. Benney (1966) extended Benjamin's work to include the time-dependent properties by introducing a new two parameter expansion method. However, for internal waves, the density perturbation does not always equal the velocity perturbation. In order to make Benney's expansion method suitable for all density stratifications (especially for when the Boussinesq approximation applies), we include a third parameter σ in our analysis, where σ is the fractional change in the basic density over the vertical characteristic length D. In this section, we will use a three parameter expansion method based on the assumption that $\sigma \ll 1$; however, σ may or may not be the same order of magnitude as the nonlinear parameter $\mathcal{E}$ = a/D and the dispersive parameter $\int = D^2/\ell^2$, where a is the amplitude of the internal motion and ℓ is the horizontal characteristic length. Long (1964) studied a stationary case with constant Brunt-Vaisala frequency and found that solitary waves do not exist unless higher order terms are retained in his analysis. Long's solutions will then be a special case in the following analysis.

Assume a shallow water layer of incompressible, inviscid fluid with density ρ . The basic density state is $\bar{\rho}_o(z) = \rho_o(1 + \sigma \bar{\rho}(z))$ where $\sigma = \Delta\rho/\rho_o$, $\Delta\rho$ is the basic density change over the vertical

characteristic length, and f_o is a constant. The two dimensional equations of motion are

$$f(u_t + uu_x + wu_z) = -p_x , \qquad (3.1)$$

$$f(w_t + uw_x + ww_z) = -p_z - gf , \qquad (3.2)$$

$$u_x + w_z = 0 , \qquad (3.3)$$

$$f_t + uf_x + wf_z = 0 . \qquad (3.4)$$

where u is the horizontal velocity, w is the vertical velocity, p is the pressure, g is gravity, and the subscripts x, z, and t represent the derivatives to x, y, and t respectivity. By eliminating the pressure term from equation (3.1) and (3.2), we get the vorticity equation

$$[f(u_t + uu_x + wu_z)]_z - f_x - [f(w_t + uw_x + ww_z)]_x = 0. \quad (3.5)$$

Now we will scale equations (3.3), (3.4), and (3.5) and make all variables dimensionless. Denoting dimensionless variables by prime, we have

$$x = \ell x' , \quad z = Dz' , \quad t = \frac{\ell}{(\sigma g D)^{1/2}} t' ,$$

$$u = \varepsilon (\sigma g D)^{1/2} u' , \quad w = \varepsilon \cdot \frac{D}{\ell} (\sigma g D)^{1/2} w' ,$$

$$f = f_o (1 + \sigma \bar{p}'(z) + \sigma \varepsilon p'(x, z, t)) .$$

The horizontal characteristic length of the dominant structure of the internal disturbance, ℓ, is chosen as the length in which the

deflection of a stream line changes from zero to its maximum value.

D is defined as D = H/nπ , where H is the total depth and n is the mode number. The time scale $\ell/(\sigma g D)^{1/2}$ is the time interval for ℓ to pass a certain point. The vertical velocity scale is $a/(\ell/(\sigma g D)^{1/2})$

$= \varepsilon \frac{D}{\ell} \sqrt{\sigma g \hbar}$. The horizontal velocity scale $\varepsilon (\sigma g \hbar)^{1/2}$ is obtained from the equation of continuity. Experimental data showed that the above scale provided quite good estimates of the magnitudes of the various quantities. Introducing these dimensionless variables into equations (3.3), (3.4), and (3.5) and droping primes, we have

$$\rho_t - \bar{\rho}_z \psi_x + \varepsilon \psi_z \rho_x - \varepsilon \psi_x \rho_z = 0 \; , \tag{3.6}$$

$$\left\{ (1 + \sigma \bar{\rho} + \sigma \varepsilon \rho)(\psi_{zt} + \varepsilon \psi_z \psi_{zx} - \varepsilon \psi_x \psi_{zz}) \right\}_z - \rho_x + \delta \left\{ (1 + \sigma \bar{\rho} + \sigma \varepsilon \rho)(\psi_{xt} + \varepsilon \psi_z \psi_{xx} - \varepsilon \psi_x \psi_{xz}) \right\}_x = 0 \; , \tag{3.7}$$

where ψ is a stream function defined by

$$u = \psi_z \; , \qquad w = -\psi_x \; . \tag{3.8}$$

Assume ε , δ , and σ are all small independent parameters, not necessarily of the same order of magnitude. The boundary conditions are

$$\psi_x = 0 \; , \qquad at \qquad z = 0 \; , \tag{3.9}$$

$$\psi_x = 0 \; , \qquad at \qquad z = n\pi \; . \tag{3.10}$$

Following a procedure similar to Benney's (1966) two parameter expansion method, the stream function ψ and the perturbation density ρ are expanded using three parameters ε , δ , and σ as follows,

$$\psi(x, z, t) = \sum_{i=0}^{\infty} \sum_{j=0}^{\infty} \sum_{k=0}^{\infty} \varepsilon^i \delta^j \sigma^k \psi^{(i,j,k)}(x, z, t) \quad (3.11)$$

$$\rho(x, z, t) = \sum_{i=0}^{\infty} \sum_{j=0}^{\infty} \sum_{k=0}^{\infty} \varepsilon^i \delta^j \sigma^k \rho^{(i,j,k)}(x, z, t) \quad (3.12)$$

The zeroth order solution $\psi^{(0,0,0)}(x, z, t)$ will have a form,

$$\psi^{(0,0,0)}(x, z, t) = A(x, t) \phi^{(0,0,0)}(z) , \quad (3.13)$$

$$A_t = -cA_x , \quad (3.14)$$

where $\phi^{(0,0,0)}(z)$ and C are eigenfunctions and eigenvalues of the follow-ing boundary value problem:

$$\phi_{zz}^{(0,0,0)} - \frac{\bar{\rho}_z}{c^2} \phi^{(0,0,0)} = 0 , \quad 3.15$$

$$\phi^{(0,0,0)}(0) = \phi^{(0,0,0)}(n\pi) = 0 .$$

In order to make the first order functions $\psi^{(1,0,0)}(x, z, t)$, $\psi^{(0,1,0)}(x, z, t)$, and $\psi^{(0,0,1)}(x, z, t)$ also separable, equation (3.14) must be modified to the following form

$$A_t = -cA_x + \varepsilon r A A_x + \delta s A_{xxx} + \sigma g A_x \quad (3.16)$$

with

$$\psi^{(1,0,0)}(x, z, t) = A^2 \phi^{(1,0,0)}(z) , \quad (3.17)$$

$$\psi^{(0,1,0)}(x, z, t) = A_{xx} \phi^{(0,1,0)}(z) , \quad (3.18)$$

$$\psi^{(0,0,1)}(x, z, t) = A \phi^{(0,0,1)}(z) , \quad (3.19)$$

where the functions $\phi^{(1,0,0)}_{(\hat{z})}$, $\phi^{(0,1,0)}_{(\hat{z})}$, and $\phi^{(0,0,1)}_{(\hat{z})}$ and the constants r , s, and q are obtained by solving the following boundary value problems for r,

$$\phi^{(1,0,0)}_{\hat{z}\hat{z}} - \frac{\bar{\rho}_{\hat{z}}}{c^2}\,\phi^{(1,0,0)} = \frac{r}{c}\,\phi^{(0,0,0)}_{\hat{z}\hat{z}} + \frac{1}{c}\,\phi^{(0,0,0)}_{\hat{z}}\phi^{(0,0,0)}_{\hat{z}\hat{z}} - \frac{1}{c}\,\phi^{(0,0,0)}\phi^{(0,0,0)}_{\hat{z}\hat{z}\hat{z}}$$

$$\phi^{(1,0,0)}(0) = \phi^{(1,0,0)}(n\pi) = 0 \;, \tag{3.20}$$

for s,

$$\phi^{(0,1,0)}_{\hat{z}\hat{z}} - \frac{\bar{\rho}_{\hat{z}}}{c^2}\,\phi^{(0,1,0)} = \frac{2s}{c}\,\phi^{(0,0,0)}_{\hat{z}\hat{z}} - \phi^{(0,0,0)} \tag{3.21}$$

$$\phi^{(0,1,0)}(0) = \phi^{(0,1,0)}(n\pi) = 0 \;,$$

and for q,

$$\phi^{(0,0,1)}_{\hat{z}\hat{z}} - \frac{\bar{\rho}_{\hat{z}}}{c^2}\,\phi^{(0,0,1)} = \frac{2q}{c^2}\,\phi^{(0,0,0)}_{\hat{z}\hat{z}} - \left(\bar{\rho}\,\phi^{(0,0,0)}_{\hat{z}}\right)_{\hat{z}} \tag{3.22}$$

$$\phi^{(0,0,1)}(0) = \phi^{(0,0,1)}(n\pi) = 0 \;.$$

The eigenvalue problem (3.15) yields an infinite set of eigenfunctions $\phi^{(0,0,0)}_{n}(\hat{z})$ and eigenvalues c_n^2 . The constants r, s, and q must take unique values if the boundary value problems (3.20), (3.21), and (3.22) are to have solutions. Corresponding to each mode ($\phi^{(0,0,0)}_{n}$, Cn), it is found by suitable integrations that

$$r = \frac{\displaystyle\int_0^{n\pi} \bar{\rho}_{\hat{z}\hat{z}}\,\phi^{(0,0,0)\,3}_{n}\,d\hat{z}}{\displaystyle\int_0^{n\pi} \bar{\rho}_{\hat{z}}\,\phi^{(0,0,0)\,2}_{n}\,d\hat{z}} \;, \tag{3.23}$$

$$S = + \frac{G_n}{2} \frac{\int_0^{n\pi} \phi_n^{(0,0,0)^2} dz}{\int_0^{n\pi} \bar{\rho}_z \phi_n'^{(0,0,0)^2} dz} \quad , \qquad (3.24)$$

$$q = - \frac{G_n^3}{2} \frac{\int_0^{n\pi} \bar{\rho} \phi_z^{(0,0,0)^2} dz}{\int_0^{n\pi} \bar{\rho}_z \phi_n^{(0,0,0)^2} dz} \quad . \qquad (3.25)$$

The sign and magnitude of the constants r, s, and q are very important in the generating mechanics of long nonlinear internal waves. It is obvious that r = 0, i.e., the nonlinear effect vanishes identically, if the density stratification is linear with z. However, as long as the density stratification is stable ($\bar{\rho}_z > 0$), both s and q keep the same sign and non-zero value.

In general, data obtained in experimental work correspond directly to the displacement of the stream line η rather than to the stream function ψ . It is thus useful to establish the relation between the two functions. To first order approximation, the function η and ψ are

$$\eta(x, z, t) = A\eta^{(0,0,0)}(z) + \varepsilon A^2 \eta^{(1,0,0)}(z) + \int A_{xx} \eta^{(0,1,0)}(z) + \sigma A_x \eta^{(0,0,1)}(z) \quad (3.26)$$

$$\psi(x, z, t) = A\phi^{(0,0,0)}(z) + \varepsilon A^2 \phi^{(1,0,0)}(z) + \int A_{xx} \phi^{(0,1,0)}(z) + \sigma A_x \phi^{(0,0,1)}(z) ,$$

$$\qquad (3.27)$$

where the function A(x, t) satisfies equation (3.16).

ψ and η can be related by using the vertical velocity ,

$$-\frac{\partial \psi}{\partial x} = w = \frac{\partial \eta}{\partial t} + (\bar{u}(z) + \varepsilon u)\frac{\partial \eta}{\partial x} \quad \text{at} \quad z = z_0 + \eta \quad (3.28)$$

where $\bar{u}(z)$ is the basic velocity shear. Introducing (3.26), and (3.27)
into (3.28) and using a Taylor series expansion, we get

$$\phi^{(0,0,0)} = (c - \bar{u})\eta^{(0,0,0)}, \qquad (3.29)$$

$$\phi^{(1,0,0)} = (c-\bar{u})\eta^{(1,0,0)} - r\eta^{(0,0,0)} - \frac{3}{2}\eta^{(0,0,0)}\phi_z^{(0,0,0)} - \frac{1}{2}u_z\eta^{(0,0,0)^2}, \quad (3.30)$$

$$\phi^{(0,1,0)} = (c-\bar{u})\eta^{(0,1,0)} - s\eta^{(0,0,0)}, \qquad (3.31)$$

$$\phi^{(0,0,1)} = (c-\bar{u})\eta^{(0,0,1)} - q\eta^{(0,0,0)}. \qquad (3.32)$$

If $\bar{u}(z) = 0$ (the influences of shear will be analysed later), the
zeroth order relation between ψ and η is simply

$$\psi^{(0,0,0)} = c\eta^{(0,0,0)}$$

Introducing this relation into (3.23), (3.24), and (3.25), we find that we
need only to multiple the nonlinear coefficient r by a factor C
to change $\psi^{(0,0,0)}$ directly to $\eta^{(0,0,0)}$.

Now the problem is how to determine the function A(x, t) from
experimental or field data of the form η(x, z, t). From (3.26), we
get

$$A(x, t) = \frac{\eta(x, t, z_0)}{\eta^{(0,0,0)}(z_0)} + O(\varepsilon, \delta, \sigma) \qquad (3.33)$$

where $\eta^{(o,o,o)}_{(z)}$ can be calculated by equation (3.15) from the basic

stratification, and the point $z = z_o$ is the depth at which the measure-

ments are made. Although $\frac{\partial A}{\partial t}$ and $\frac{\partial A}{\partial x}$ are both zeroth order terms

in equation (3.16), the combination $(\frac{\partial}{\partial t} + C \frac{\partial}{\partial x})A$ is correct to

first order, thus the introduction of (3.33) into equation (3.16) will

only produce a second order error, which is allowed in our first order

analysis. It is convenient and causes no loss of generality to put

$\eta^{(o,o,o)}_{(z_o)} = 1.$ We then have

$$\eta_t + C\eta_x - \varepsilon r \eta \eta_x + \delta s \eta_{xxx} - \sigma q \eta_x = 0. \qquad (3.34)$$

For a wave solution of the form $\eta = \eta(x - C_p t)$ where C_p is the phase

velocity, we have

$$C_p = C - \varepsilon r \eta + \delta s \frac{\eta'''}{\eta'} - \sigma q.$$

Thus the nonlinear effect will increase (decrease) the phase speed if

the sign of the product term $r \cdot \eta$ is negative (positive). This proper-

ty is very important in the determination of the steepening or flatten-

ing of an initial disturbance. For a typical seasonal thermocline in

the ocean in which the most temperature variation occurs in the upper

half of the water column, the coefficient of the nonlinear term r is

positive. Thus a warm front or a depression of the stream line will

be steepened, and vice versa. From (3.25), we find that the coefficient

q is always positive, thus the role of this inertial term is simply

to decrease the phase velocity. The constant s is always positive.

However, whether the phase speed is increased or decreased depends on

the sign of η'''/η'. For a sinusoidal wave, the dispersive effect

is always to decrease the phase speed.

Three conservative quantities which correspond to mass, momentum, and energy can be derived from equation (3.34). These conservation equations can be written in the following form

$$\frac{\partial P_m}{\partial t} + \frac{\partial Q_m}{\partial x} = 0 \quad , \qquad m = 1, 2, 3 \qquad (3.36)$$

where

$$P_1 = \eta \quad , \quad Q_1 = (c - \sigma \delta)\eta - \frac{r\varepsilon}{2}\eta^2 - s\delta \eta_{xx} \quad ,$$

$$P_2 = \frac{1}{2}\eta^2 \quad , \quad Q_2 = \frac{1}{2}(c - \sigma \delta)\eta^2 - \frac{1}{3} r\varepsilon \eta^3 - s\delta(\eta \eta_{xx} - \frac{1}{2}\eta_x^2) \quad ,$$

$$P_3 = \frac{1}{3}\eta^3 - \frac{s\delta}{r\varepsilon}\eta_x^2 \quad , \quad Q_3 = \frac{1}{3}(c - \sigma\delta)\eta^3 - \frac{r\varepsilon}{4}\eta^4 - s\delta$$

$$\left(\eta^2 \eta_{xx} - \frac{2}{r\varepsilon}\eta_t \eta_x\right) - \frac{s^2\delta^2}{r\varepsilon}\eta_{xx}^2 \quad .$$

It is obvious that an infinite sequence of conservation equations can be obtained, however, the complexity of the derivation increases rapidly with increasing m. These conservative quantities are very useful in theoretical analsis or numerical calculation. For a disturbance with η and its derivatives vanishing at $x = x_1$ and x_2, or a periodic disturbance with wave length $\lambda = x_2 - x_1$, we have

$$\frac{\partial}{\partial t} \int_{x_1}^{x_2} \eta \, dx = 0 \quad , \qquad (3.37)$$

$$\frac{\partial}{\partial t} \int_{x_1}^{x_2} \eta^2 \, dx = 0 \quad , \qquad (3.38)$$

$$\frac{\partial}{\partial t} \int_{x_1}^{x_2} \left(\eta^3 - \frac{3S}{\Gamma \varepsilon} \eta_x^2 \right) dx = 0 \qquad (3.39)$$

Equations (3.37) and (3.38) can be easily used to check the accuracy of numerical predictions of the natural evolution of an localized or periodic disturbance.

(2) Discussion of Boussinesq Approximation

Most studies of internal motion in a weakly stratified fluid use the Boussinesq approximation which neglects density variations in the inertial terms of the equations of motion. After careful scaling for these variables, we find that the parameter δ appears only in the inertial terms of the vorticity equation (3.7). Since δ is an independent parameter, use of the Boussinesq approximation in a first order expansion is equivalent to the assumption that δ is a second order parameter, and in a second order expansion that δ is a third order parameter, and so on. By putting $\delta = 0$ in the first order expansion, our results agree with Benjamin's (1966) analysis of stationary finite amplitude internal waves in a Boussinesq fluid.

(3) Discussion of Modifications due to Inclusion of Basic Shear $\bar{u}(z)$.

In this section the influences of the basic shear on the nonlinear and dispersive terms will be analysed. Assume there is no singular point ($\bar{u}(z) = C$) and the Richardson number Ri is greater that 1/4 everywhere in the fluid layer. The order of magnitude of $\bar{u}(z)$ is $\sqrt{\delta g D}$ For simplicity, we will only consider the case for the Boussinesq approximation, i.e., when $\delta = 0$. Following a similar procedure, equation (3.15), (3.20), and (3.21) are modified to the following form

$$\phi_{\bar{z}\bar{z}}^{(0,0,0)} - \left(\frac{\bar{P}_{\bar{z}}}{U^2} + \frac{\bar{U}_{\bar{z}\bar{z}}}{U}\right)\phi^{(0,0,0)} = 0 \quad,$$

$$\phi_{\bar{z}\bar{z}}^{(1,0,0)} - \left(\frac{\bar{P}_{\bar{z}}}{U^2} + \frac{\bar{U}_{\bar{z}\bar{z}}}{U}\right)\phi^{(1,0,0)} = \frac{1}{2U^2}\left[r\left(-2U\phi_{\bar{z}}^{(0,0,0)} + \right.\right.$$

$$\bar{U}_{\bar{z}\bar{z}}\,\phi^{(0,0,0)}\right) - 2U\phi_{\bar{z}}^{(0,0,0)}\phi_{\bar{z}\bar{z}}^{(0,0,0)} + 2U\phi^{(0,0,0)}\phi_{\bar{z}\bar{z}\bar{z}}^{(0,0,0)}$$

$$\left.+ \phi^{(0,0,0)}\left(\bar{U}_{\bar{z}}\,\phi^{(0,0,0)} - \bar{U}_{\bar{z}\bar{z}\bar{z}}\,\phi^{(0,0,0)}\right)\right], \qquad (3.40)$$

$$\phi_{\bar{z}\bar{z}}^{(0,1,0)} - \left(\frac{\bar{P}_{\bar{z}}}{U^2} + \frac{\bar{U}_{\bar{z}\bar{z}}}{U}\right)\phi^{(0,1,0)} = -\frac{2S}{U}\phi_{\bar{z}\bar{z}}^{(0,0,0)} + \frac{S\bar{U}_{\bar{z}\bar{z}}}{U^2}\phi^{(0,0,0)} - \phi^{(0,0,0)},$$

$$(3.41)$$

$$r = \frac{\int_0^{n\pi}\frac{\phi^{(0,0,0)^3}}{U}\left(\frac{\bar{P}_{\bar{z}}}{U^2} + \frac{\bar{U}_{\bar{z}\bar{z}}}{U}\right)_{\bar{z}} d\bar{z} + \int_0^{n\pi}\frac{\phi^{(0,0,0)^2}}{2U^2}\left(\bar{U}_{\bar{z}}\phi_{\bar{z}\bar{z}}^{(0,0,0)} - \bar{U}_{\bar{z}\bar{z}\bar{z}}\phi^{(0,0,0)}\right)d\bar{z}}{\int_0^{n\pi}\frac{\phi^{(0,0,0)^2}}{U^2}\left(\frac{\bar{P}_{\bar{z}}}{U} + \frac{1}{2}\bar{U}_{\bar{z}\bar{z}}\right)d\bar{z}}$$

$$(3.42)$$

$$S = \frac{-\frac{1}{2}\int_0^{n\pi}\phi^{(0,0,0)^2}\,d\bar{z}}{\int_0^{n\pi}\frac{\phi^{(0,0,0)^2}}{U^2}\left(\frac{\bar{P}_{\bar{z}}}{U} + \frac{1}{2}\bar{U}_{\bar{z}\bar{z}}\right)d\bar{z}} \qquad (3.43)$$

where $U \equiv \bar{u}(z) - C.$

Since r and s are very complicated functions of $\bar{u}(z)$, we will
compute several examples to illustrate the effects shear $\bar{u}(z)$ has on
the nonlinear and dispersive term. The coefficients r, s, c, and
$Z_{max.}$ (where $Z_{max.}$ is the position of the maximum of the eigenfunction
$\phi_1^{(o,o,o)}(z)$) have been calculated and listed in table 1 for the several
typical velocity and density profiles shown in figure 9 . These ex-
amples indicate that profiles with the magnitude of speed increasing
upward gives a negative nonlinear coefficient and vice versa, whereas
$\bar{u}(z)$ which is symmetric in z about the mid-depth gives zero contri-
bution to r.

(4) Special Case of Two Layer Density Model

We now examine the modifications to the general theory caused
by a discontinuous two layer density field. Let $\rho = \rho_o + \Delta\rho$ in
$0 \leqslant z \leqslant h_1$ and $\rho = \rho_o$ in $h_1 \leqslant z \leqslant h_1 + h_2 = \pi$. The only possible inter-
nal long wave for a two layer system is the first mode which has a
maximum vertical displacement at the interface. Equation (3.15)
becomes

$$\phi_{zz}^{(o,o,o)} = 0 \qquad\qquad (3.44)$$

in each layer separately, and the solution satisfying the boundary
condition $\phi^{(o,o,o)}(o) = \phi^{(o,o,o)}(\pi) = 0$ and continuity at the interface
$z = h_1$ is

$$\phi^{(o,o,o)} = z/h_1 \quad , \qquad 0 \leqslant z \leqslant h_1 \quad , \qquad (3.45)$$

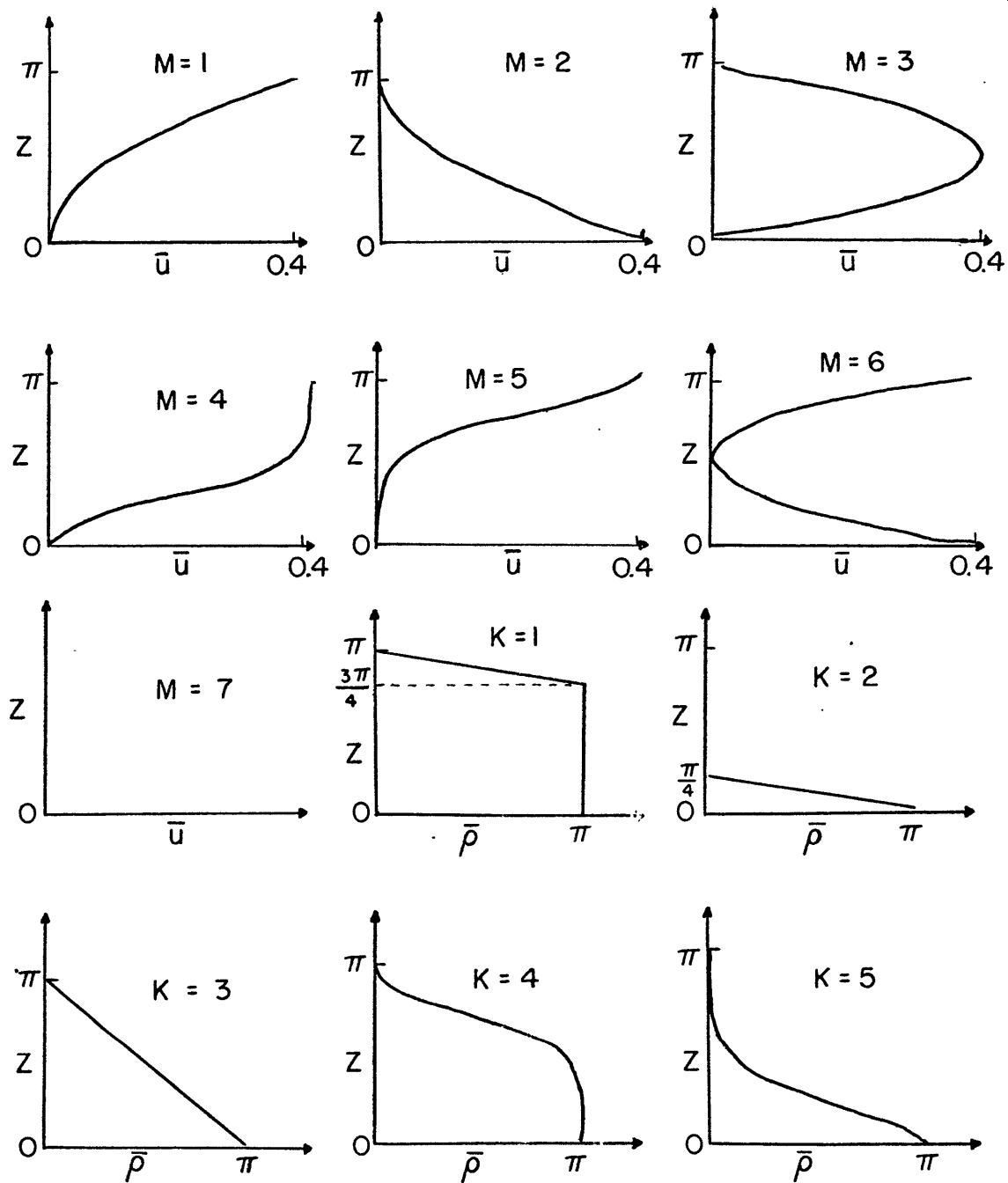$$\phi^{(o,o,o)} = (\pi - z)/h_2 \quad , \qquad h_1 \leqslant z \leqslant \pi \qquad (3.46)$$

Figure 9 . Several typical velocity profiles $\bar{u}(z)$ (M=1 to 7)
and density profiles $\bar{\rho}$ (z)(K=1 to 5) which are
used to calculate the coefficients r and S in table 1 .

$\bar{u}(z)$ (M)	$\bar{\rho}(z)$ (K)	$C_o\ (\sqrt{\sigma gD})$	$Z_{Max.}$ (H)	r	s
1	1	1.16	0.80	-2.43	0.23
1	2	0.88	0.20	2.56	0.24
1	3	1.17	0.52	-0.17	0.53
1	4	1.35	0.64	-0.85	0.51
1	5	1.21	0.38	0.87	0.53
2	1	0.88	0.80	-2.56	0.24
2	2	1.16	0.20	2.43	0.23
2	3	1.17	0.48	0.17	0.53
2	4	1.21	0.62	-0.87	0.53
2	5	1.35	0.36	0.85	0.51
3	1	0.98	0.80	-2.75	0.14
3	2	0.98	0.20	2.75	0.14
3	3	1.21	0.50	0.00	0.35
3	4	1.32	0.64	-0.91	0.36
3	5	1.33	0.36	0.91	0.36
4	1	1.23	0.80	-2.53	0.18
4	2	0.93	0.20	2.76	0.17
4	3	1.27	0.54	-0.19	0.41
4	4	1.46	0.66	-0.88	0.41
4	5	1.30	0.36	0.95	0.42
5	1	1.17	0.80	-2.37	0.25
5	2	0.88	0.20	2.53	0.27
5	3	1.17	0.54	-0.16	0.57
5	4	1.35	0.64	-0.80	0.54
5	5	1.20	0.38	0.84	0.57
6	1	1.14	0.78	-2.37	0.32
6	2	1.14	0.22	2.37	0.32
6	3	1.23	0.50	-0.00	0.68
6	4	1.35	0.64	-0.82	0.64
6	5	1.35	0.38	0.82	0.64
7	1	0.85	0.80	-2.54	0.21
7	2	0.85	0.20	2.54	0.21
7	3	1.00	0.50	0.00	0.50
7	4	1.12	0.64	-0.87	0.49
7	5	1.12	0.38	0.87	0.49

Table 1 . Numerical calculations of the coefficients of r, S, C , and $Z_{max.}$ using several typical velocity profiles and density profiles in figure 9 .

Since equation (3.44) is homogeneous, we can set $\phi^{(o,o,o)}(h_1) = 1$ with no loss of generality.

The phase velocity C can be easily found by considering the two-layer system as a continuously stratified fluid in the limit that $\Delta \rightarrow 0$ where Δ is the thickness of the interface over which the density variation occurs. Then we may take the limit of equation (3.15) at the interface

$$\lim_{\Delta \to 0} \int_{h_1 - \Delta}^{h_1 + \Delta} \left[\phi_{zz}^{(o,o,o)} - \frac{\bar{p}}{c^2} \phi^{(o,o,o)} \right] dz = 0$$

to get

$$\lim_{\Delta \to 0} \left[\phi_z^{(o,o,o)} - \frac{\bar{p}}{c^2} \phi^{(o,o,o)} \right]_{h_1 - \Delta}^{h_1 + \Delta} + \lim_{\Delta \to 0} \int_{h_2 - \Delta}^{h_1 + \Delta} \frac{\bar{p}}{c^2} \phi_z^{(o,o,o)} \, dz = 0$$

Since $\bar{p}$ and $\phi_z^{(o,o,o)}$ are finite functions, the integral term vanishes as $\Delta \to 0$. This implies that the quantity $(\phi_z^{(o,o,o)} - \frac{\bar{p}}{c^2} \phi^{(o,o,o)})$ must be continuous across the interface (continuity of pressure). Introducing (3.45) and (3.46) into the above relation yields

$$C = (h_1 h_2)^{1/2}. \tag{3.47}$$

The constants r, s, and q can be calculated using (3.23), (3.24), (3.25), (3.45), and (3.46). After a little manipulation, we have

$$r = \frac{\int_0^\pi \bar{f}_{zz}\, \phi^{(0,0,0)^3}\, dz}{\int_0^\pi \bar{f}_z\, \phi^{(0,0,0)^2}\, dz} = \frac{3}{2}\frac{(h_1-h_2)}{h_1 h_2}, \qquad (3.48)$$

$$s = +\frac{c}{2}\frac{\int_0^\pi \phi^{(0,0,0)^2}\, dz}{\int_0^\pi \bar{f}_z\, \phi^{(0,0,0)^2}\, dz} = \frac{-1}{6}(h_1 h_2)^{1/2}, \qquad (3.49)$$

$$q = -\frac{c^3}{2}\frac{\int_0^\pi \bar{f}\, \phi_z^{(0,0,0)^2}\, dz}{\int_0^\pi \bar{f}_z\, \phi^{(0,0,0)^2}\, dz} = \frac{1}{2} h_2^{3/2} h_1^{1/2}. \qquad (3.50)$$

From (3.48) it is obvious that r is positive if $h_1 > h_2$. This implies that a depression will be steepened ahead of its peak if $h_1 > h_2$, and an elevation will be steepened ahead of its peak if $h_1 < h_2$. The non-linear effect vanishes exactly if $h_1 = h_2$. Since q is always positive, the internal effect of $\Delta\rho$ tends to decrease the phase velocity. The constant s is always positive: however, the phase velocity variation due to the dispersive effect depends on the sign of η'''/η'. For a sinusoidal wave, the dispersive effect always decreases the phase velocity.

(5) Derivation of a Second Order KdV Equation

The governing equation (3.16) derived earlier is a valid approxi-mation correct to first order only. In order to increase the valid time interval of prediction for an initial value problem, we need to calculate the second order terms in this asymptotic expansion.

Equation (3.16) is thus modified into the following form

$$A_t = -cA_x + \varepsilon \Gamma A A_x + \delta S A_{xxx} + \sigma \beta A_x + \varepsilon^2 \lambda_1 (A^3)_x + \delta^2 \lambda_2 A_{xxxxx}$$

$$+ \sigma^2 \lambda_3 A_x + \varepsilon \sigma \lambda_4 A A_x + \varepsilon \delta (\lambda_5 A A_{xxx} + \lambda_6 A_x A_{xx}) + \delta \sigma \lambda_7 A_{xxx} \quad (3.51)$$

and

$$\varepsilon^2 : \quad \psi^{(2,0,0)} = A^3 \phi^{(2,0,0)}(z) , \qquad (3.52)$$

$$\delta^2 : \quad \psi^{(0,2,0)} = A_{xxxx} \phi^{(0,2,0)}(z) , \qquad (3.53)$$

$$\sigma^2 : \quad \psi^{(0,0,2)} = A \phi^{(0,0,2)}(z) , \qquad (3.54)$$

$$\varepsilon \delta : \quad \psi^{(1,1,0)} = A A_{xx} \phi_1^{(1,1,0)}(z) + A_x^2 \phi_2^{(1,1,0)}(z) \qquad (3.55)$$

$$\varepsilon \sigma : \quad \psi^{(1,0,1)} = A^2 \phi^{(1,0,1)}(z) , \qquad (3.56)$$

$$\delta \sigma : \quad \psi^{(0,1,1)} = A_{xx} \phi^{(0,1,1)}(z) , \qquad (3.57)$$

where the functions $\phi^{(2,0,0)}$, $\phi^{(0,2,0)}$, $\phi^{(0,0,2)}$, $\phi_1^{(1,1,0)}$, $\phi_2^{(1,1,0)}$, $\phi^{(1,0,1)}$, and $\phi^{(0,1,1)}$ and the constants λ_1, λ_2, λ_3, λ_4, λ_5, λ_6, and λ_7 are obtained by solving the following boundary value problems.

For $\phi^{(2,0,0)}$ and $\lambda_1 : 0 (\varepsilon^2)$

$$\phi_{zz}^{(2,0,0)} - \frac{\bar{P}_z}{c^2} \phi^{(2,0,0)} = \frac{1}{3c^2} \left[6 c \lambda_1 \phi_{zz}^{(0,0,0)} - 4 \Gamma^2 \phi_{zz}^{(0,0,0)} \right.$$

$$\left. - 4 \Gamma \phi_z^{(0,0,0)} \phi_{zz}^{(0,0,0)} + 3 \Gamma \phi^{(0,0,0)} \phi_{zzz}^{(0,0,0)} - \phi_z^{(0,0,0)2} \phi_{zz}^{(0,0,0)} \right.$$

$$\phi_z^{(0,0,0)}\phi^{(0,0,0)}\phi_{zz}^{(0,0,0)} + \frac{1}{2}\phi^{(0,0,0)}\phi_{zz}^{(0,0,0)^2} - \frac{1}{2}\phi^{(0,0,0)^2}\phi_{zzzz}^{(0,0,0)}$$

$$+2C\,\phi_z^{(1,0,0)}\phi_{zz}^{(0,0,0)} + 8\Gamma C\,\phi_{zz}^{(1,0,0)} + 4C\,\phi_z^{(0,0,0)}\phi_{zz}^{(1,0,0)}$$

$$-2C\,\phi^{(0,0,0)}\phi_{zzz}^{(1,0,0)} - 4C\,\phi^{(1,0,0)}\phi_{zzz}^{(0,0,0)}\Big], \qquad (3.58)$$

$$\phi^{(2,0,0)}(0) = \phi^{(2,0,0)}(n\pi) = 0.$$

For $\phi^{(0,2,0)}$ and $\lambda_2 : o(\int^2)$

$$\phi_{zz}^{(0,2,0)} - \frac{\bar{P}_z}{C^2}\phi^{(0,2,0)} = \frac{1}{C^2}\Big\{2\lambda_2 C\,\phi_{zz}^{(0,0,0)} - S^2\phi_{zz}^{(0,0,0)}$$

$$+2SC\big(\phi^{(0,0,0)} + \phi_{zz}^{(0,1,0)}\big) - C^2\phi^{(0,1,0)}\Big\}, \quad (3.59)$$

$$\phi^{(0,2,0)}(0) = \phi^{(0,2,0)}(n\pi) = 0.$$

For $\phi^{(0,0,2)}$ and $\lambda_3 : o(\sigma^2)$

$$\phi_{zz}^{(0,0,2)} - \frac{\bar{P}_z}{C^2}\phi^{(0,0,2)} = \frac{1}{C^2}\Big\{2\lambda_3 C\,\phi_{zz}^{(0,0,0)} + 2\int C\big(\bar{P}\phi_z^{(0,0,0)}\big)_z$$

$$+2\int C\,\phi_{zz}^{(0,0,1)} - C^2\big(\bar{P}\phi_z^{(0,0,1)}\big)_z + \int^2\phi_{zz}^{(0,0,0)}\Big\}, \quad (3.60)$$

$$\phi^{(0,0,2)}(0) = \phi^{(0,0,2)}(n\pi).$$

For $\phi^{(1,0,1)}$ and $\lambda_4 : o(\varepsilon\sigma)$

$$\phi_{z\bar{z}}^{(1,0,1)} - \frac{\bar{p_{\bar{z}}}}{c^2}\phi^{(1,0,1)} = \frac{1}{2c^2}\left\{ 2\lambda_4 c\,\phi_{z\bar{z}}^{(0,0,0)} + 4\Gamma c\left(\bar{p}\,\phi_{\bar{z}}^{(0,0,0)}\right)_{\bar{z}} \right.$$

$$+ 4\Gamma c\,\phi_{z\bar{z}}^{(0,0,1)} - 4\Gamma g\,\phi_{z\bar{z}}^{(0,0,0)} + 4g\,c\,\phi_{z\bar{z}}^{(1,0,0)}$$

$$- 2g\,\phi_{\bar{z}}^{(0,0,0)}\phi_{z\bar{z}}^{(0,0,0)} + 2g\,\phi^{(0,0,0)}\phi_{z\bar{z}\bar{z}}^{(0,0,0)} - c\,\bar{p}_{z\bar{z}}\phi^{(0,0,0)}\phi_{\bar{z}}^{(0,0,0)}$$

$$- 2c^2\bar{p}_{\bar{z}}\,\phi_{\bar{z}}^{(1,0,0)} + 2c\,\bar{p}_{\bar{z}}\,\phi_{\bar{z}}^{(0,0,0)^2} - 2c\,\bar{p}_{\bar{z}}\,\phi^{(0,0,0)}\phi_{z\bar{z}}^{(0,0,0)}$$

$$- 2c^2\bar{p}\,\phi_{z\bar{z}}^{(1,0,0)} + 2\bar{p}c\,\phi_{\bar{z}}^{(0,0,0)}\phi_{z\bar{z}}^{(0,0,0)} - 2\bar{p}c\,\phi^{(0,0,0)}\phi_{z\bar{z}\bar{z}}^{(0,0,0)}$$

$$+ 2c\,\phi_{\bar{z}}^{(0,0,1)}\phi_{z\bar{z}}^{(0,0,0)} + 2c\,\phi_{\bar{z}}^{(0,0,0)}\phi_{z\bar{z}}^{(0,0,1)} - 2c\,\phi^{(0,0,1)}\phi_{z\bar{z}\bar{z}}^{(0,0,0)}$$

$$- 2c\,\phi^{(0,0,0)}\phi_{z\bar{z}\bar{z}}^{(0,0,1)} - c^3\phi_{\bar{z}}\,\phi_{z\bar{z}\bar{z}}^{(0,0,0)} + c^3\phi_{z\bar{z}}^{(0,0,0)^2}\left.\right], \qquad (3.61)$$

$$\phi^{(1,0,1)}(0) = \phi^{(1,0,1)}(n\pi).$$

For $\phi_1^{(1,1,0)}$ and $\lambda_5 = o(\varepsilon\delta)$

$$\phi_{1zz}^{(1,1,0)} - \frac{\bar{p}_2}{c^2}\phi_1^{(1,1,0)} = \frac{1}{c^2}\left\{2\lambda_5 C\phi_{zz}^{(0,0,0)} + 4rs\,\phi_{zz}^{(0,0,0)}\right.$$

$$+ 4Sc\,\phi_{zz}^{(1,0,0)} - 2S\phi_z^{(0,0,0)}\phi_{zz}^{(0,0,0)} - 2C\phi^{(0,1,0)}\phi_{zzz}^{(0,0,0)}$$

$$+ S\phi^{(0,0,0)}\phi_{zzz}^{(0,0,0)} + 4rc\,\phi_{zz}^{(0,1,0)} + 4rc\,\phi^{(0,0,0)}$$

$$+ 2C\phi_z^{(0,0,0)}\phi_{zz}^{(0,1,0)} + 2C\phi^{(0,0,0)}\phi_z^{(0,0,0)} - 2C^2\phi^{(1,0,0)}\Big\},$$

$$\tag{3.62}$$

$$\phi^{(1,1,0)}(0) = \phi_1^{(1,1,0)}(n\pi).$$

For $\phi_2^{(1,1,0)}$ and $\lambda_6 : 0 \ (\mathcal{E}\delta)$

$$\phi_{2zz}^{(1,1,0)} - \frac{\bar{p}_2}{c^2}\phi_2^{(1,1,0)} = \frac{1}{2c^2}\left\{2\lambda_6 C\phi_{zz}^{(0,0,0)} - c^2\phi_{1zz}^{(1,1,0)}\right.$$

$$+ \frac{\bar{p}_2}{c^2}\phi_1^{(1,1,0)} - 2rs\,\phi_{zz}^{(0,0,0)} + 4rc\,\phi_{zz}^{(0,1,0)} + S\phi^{(0,0,0)}\phi_{zzz}^{(0,0,0)}$$

$$+ 4rc\,\phi^{(0,0,0)} - 2C\phi^{(0,0,0)}\phi_{zzz}^{(0,1,0)} - 2C\phi^{(0,0,0)}\phi_z^{(0,0,0)}$$

$$+ 2C\phi_z^{(0,1,0)}\phi_{zz}^{(0,0,0)}\Big\}, \tag{3.63}$$

where $\phi_1^{(1,1,0)}$ in the right side of equation (3.63) can be eliminated from equation (3.62), and

$$\phi_2^{(1,1,0)}(o) = \phi_{12}^{(1,1,0)}(n\pi).$$

For $\phi^{(0,1,1)}$ and $\lambda_7 = o(\delta\sigma)$

$$\phi_{\bar{z}\bar{z}}^{(0,1,1)} - \frac{\bar{p}_{\bar{z}}}{c^2}\phi_{\cdot}^{(0,1,1)} = \frac{1}{c^2}\left\{2\lambda_7 C \phi_{\bar{z}\bar{z}}^{(0,0,0)} + 2SC(\bar{p}\phi_{\bar{z}}^{(0,0,0)})_{\bar{z}}\right.$$

$$+ 2SC\phi_{\bar{z}\bar{z}}^{(0,0,1)} + 2gC\phi_{\bar{z}\bar{z}}^{(0,1,0)} + 2gC\phi^{(0,0,0)} + 2gS\phi_{\bar{z}\bar{z}}^{(0,0,0)}$$

$$\left. - C^2(\bar{p}\phi_{\bar{z}}^{(0,1,0)})_{\bar{z}} - C^2\phi^{(0,0,1)} - C^2\bar{p}\phi^{(0,0,0)}\right](3.64)$$

$$\phi^{(0,1,1)}(o) = \phi^{(0,1,1)}(n\pi).$$

The constants λ_1, λ_2, λ_3, λ_4, λ_5, λ_6, and λ_7 are given by

$$\lambda_1 = \frac{1}{6C\int\phi_{\bar{z}}^{(0,0,0)2}}\left[4\Gamma^2\int\phi_{\bar{z}}^{(0,0,0)2} - 10\Gamma\int\phi^{(0,0,0)}\phi_{\bar{z}}^{(0,0,0)}\right.$$

$$\phi_{\bar{z}\bar{z}}^{(0,0,0)} + \int\phi_{\bar{z}}^{(0,0,0)4} - 2\int\phi^{(0,0,0)2}\phi_{\bar{z}\bar{z}}^{(0,0,0)2}$$

$$-3\int\phi^{(0,0,0)}\phi_{\bar{z}}^{(0,0,0)2}\phi_{\bar{z}\bar{z}}^{(0,0,0)} - 2C\int\phi_{\bar{z}}^{(0,0,0)2}\phi_{\bar{z}}^{(1,0,0)}$$

$$+8\Gamma c\int\phi^{(0,0,0)}\phi_{\bar{z}\bar{z}}^{(1,0,0)} - 6c\int\phi^{(0,0,0)}\phi_{\bar{z}}^{(0,0,0)}\phi_{\bar{z}\bar{z}}^{(1,0,0)}$$

$$+4\int \phi_{\bar z}^{(0,0,0)}\phi^{(1,0,0)}\phi_{2\bar z}^{(0,0,0)} + 4C\int \phi^{(0,0,0)}\phi_{\bar z}^{(1,0,0)}\phi_{2\bar z}^{(0,0,0)}\Big],$$

$$(3.65)$$

$$\lambda_2 = \frac{1}{2C\int \phi_{\bar z}^{(0,0,0)2}}\left[S^2\int \phi_{\bar z}^{(0,0,0)2} + 2CS\int \phi^{(0,0,0)2} \right.$$

$$\left. + 2SC\int \phi^{(0,0,0)}\phi_{2\bar z}^{(0,1,0)} - C^2\int \phi^{(0,0,0)}\phi^{(0,1,0)} \right],$$

$$(3.66)$$

$$\lambda_3 = \frac{1}{2C\int \phi_{\bar z}^{(0,0,0)2}}\left[2gC\int \phi^{(0,0,0)}\phi_{\bar z}^{(0,0,1)} \right.$$

$$\left. + C^2\int \bar\rho\,\phi_{\bar z}^{(0,0,1)}\phi_{\bar z}^{(0,0,0)} - 2gC\int \bar\rho\,\phi_{\bar z}^{(0,0,0)2} - g^2\int \phi_{\bar z}^{(0,0,0)2} \right],$$

$$(3.67)$$

$$\lambda_4 = \frac{1}{2C\int \phi_{\bar z}^{(0,0,0)2}}\left[4\Gamma C\int \phi^{(0,0,0)}\phi_{2\bar z}^{(0,0,1)} - 4\Gamma C\int \bar\rho\,\phi_{\bar z}^{(0,0,0)2} \right.$$

$$+ 4\Gamma g\int \phi_{\bar z}^{(0,0,0)2} + 4gC\int \phi^{(0,0,0)}\phi_{2\bar z}^{(1,0,0)} + 2g\int \phi_{\bar z}^{(0,0,0)3}$$

$$+ C\int \bar\rho_{\bar z}\,\phi^{(0,0,0)2}\phi_{\bar z}^{(0,0,0)} + 2C\int \bar\rho_{\bar z}\,\phi^{(0,0,0)}\phi_{\bar z}^{(0,0,0)2}$$

$$+ 2C^2\int \bar\rho\,\phi_{\bar z}^{(0,0,0)}\phi_{\bar z}^{(1,0,0)} - 2C\int \bar\rho\,\phi_{\bar z}^{(0,0,0)3} + 2C\int \bar\rho\,\phi^{(0,0,0)2}\phi_{2\bar z\bar z}^{(0,0,0)}$$

$$+ 2C\int \phi^{(0,0,0)}\phi_{\bar z}^{(0,0,1)}\phi_{2\bar z}^{(0,0,0)} + 2C\int \phi^{(0,0,0)}\phi_{\bar z}^{(0,0,0)}\phi_{2\bar z}^{(0,0,1)}\Big)$$

$$(3.68)$$

$$-2C\int \phi^{(0,0,0)}\phi^{(0,0,1)}\phi_{zzz}^{(0,0,0)} - 2C\int \phi^{(0,0,0)2}\phi_{zzz}^{(0,0,1)}$$

$$+C^3\int \phi_z^{(0,0,0)2}\phi_{zz}^{(0,0,0)} + 2C^3\int \phi^{(0,0,0)}\phi_{zz}^{(0,0,0)2}\Big] \qquad (3.68)$$

$$\lambda_5 = \frac{1}{2C\int \phi_z^{(0,0,0)2}}\Big[4Sc\int \phi^{(0,0,0)}\phi_{zz}^{(1,0,0)} - 4rs\int \phi_z^{(0,0,0)2}$$

$$+2S\int \phi_z^{(0,0,0)3} - 2C\int \phi^{(0,0,0)}\phi^{(0,1,0)}\phi_{zzz}^{(0,0,0)} + 4rc\int \phi^{(0,0,0)}\phi_{zz}^{(0,1,0)}$$

$$+4rc\int \phi^{(0,0,0)2} - 2C\int \phi^{(0,0,0)}\phi_z^{(0,0,0)}\phi_{zz}^{(0,1,0)}$$

$$+2C\int \phi^{(0,0,0)2}\phi_z^{(0,0,0)} - 2C^2\int \phi^{(0,0,0)}\phi^{(1,0,0)}\Big], \qquad (3.69)$$

$$\lambda_6 = \frac{1}{2C\int \phi_z^{(0,0,0)2}}\Big[2rs\int \phi_z^{(0,0,0)2} + 4rc\int \phi^{(0,0,0)}\phi_{zz}^{(0,1,0)}$$

$$+S\int \phi^{(0,0,0)2}\phi_{zzz}^{(0,0,0)} + 4rc\int \phi^{(0,0,0)2} - 2C\int \phi^{(0,0,0)2}\phi_z^{(0,0,0)}$$

$$+4C\int \phi^{(0,0,0)}\phi_z^{(0,0,0)}\phi_{zz}^{(0,1,0)} + 2C\int \phi^{(0,0,0)}\phi_z^{(0,1,0)}\phi_{zz}^{(0,0,0)}\Big], \qquad (3.70)$$

$$\lambda_7 = \frac{1}{2C\int \phi_z^{(0,0,0)2}}\Big[2Sc\int \phi^{(0,0,0)}\phi_{zz}^{(0,0,1)} - 2Sc\int \bar{p}\,\phi_z^{(0,0,0)2}$$

$$+2\tfrac{g}{b}c\int \phi^{(0,0,0)}\phi_{zz}^{(0,1,0)} + 2\tfrac{g}{b}c\int \phi^{(0,0,0)2} + C^2\int \bar{p}\,\phi_z^{(0,1,0)}\phi_z^{(0,0,0)}$$

$$-2\tfrac{g}{b}S\int \phi_z^{(0,0,0)2} - C^2\int \phi^{(0,0,0)}\phi^{(0,0,1)} - C^2\int \bar{p}\,\phi^{(0,0,0)2}\Big]. \qquad (3.71)$$

B. <u>Numerical Analysis and Comparison with Experiment</u>;

(1) Generation of Long Nonlinear Internal Waves from a Front

We have already pointed out that the finite amplitude internal wave trains observed in Massachusetts Bay may be generated from the blocking front formed by the semidiurnal tidal flow near Stellwagen Bank. From the experimental results shown in figure $/$ and 2, it is obvious that the nonlinear effect plays a very important role in the wave generating mechanism. However, we will now illustrate that dispersion rather than nonlinearity plays the major role, with the latter just increasing or decreasing dispersion. In this section we will solve equation $(3./6)$ numerically to explore influences of dispersion and nonlinearity on wave generation.

In the classical theory of bores, the energy cannot be conserved across the bore front due to dissipation at the turbulent front. Lemoine (1948) tried to use linear wave theory to test the possibility that a stationary wave train behind a bore front could radiate the necessary energy away from the front and thus avoid a turbulent front. His results showed that the amplitude of the wave train needed to be so large that the assumption of linear theory is violated. In their theory of stationary wave trains on a bore, Benjamin and Lighthill (1954) examined in detail the constraints for which a finite amplitude long wave train is possible to exist behind a bore front. They showed that the necessary condition for a stationary cnoid wave train on a weak bore is that either the energy or the momentum or both of them cannot be kept constant across the front. On the other hand, for

nonstationary conditions, both energy and momentum can be conserved across the front which seems more reasonable for a smooth nonturbulent bore of inviscid fluid. In addition, we can even find out how these waves are generated from a front by solving the suitable initial value problem. The surface wave KdV equation has been solved numerically by many authors (Peregrine [1966], Zabusky and Kruskal [1965], Mei, Madsen, and Savage [1970]). For internal waves, the basic density stratification may change the sign of the coefficient of the nonlinear term. Since the form of the governing internal KdV equation remains indentical to the surface wave equation, we will use the same general numerical method as Peregrine (1966).

In order to calculate the constants r, s, and q we have to solve the following boundary value problem

$$\phi_{zz} + f(c, z)\phi = 0 \tag{3.72}$$

with boundary conditions $\phi(o) = \phi(H) = 0$,
where C is the eigenvalue, ϕ is the corresponding eigenfunction, and f(c, z) is an arbitrary function. The solution was found using the following second-order finite-difference approximation,

$$\frac{\phi_{i+1} - 2\phi_i + \phi_{i-1}}{\Delta z^2} + f(c, z_i)\phi_i = 0 \tag{3.73}$$

$$\phi_1 = 0 \tag{3.74}$$

$$\phi_N = 0 \tag{3.75}$$

where $z_i = \Delta z(i-1)$, $i = 1, \ldots, N$, $\Delta z = H/(N-1)$, and $\phi_i = \phi(z_i)$.

Equation (3.72) is homogeneous so that we may assume that the eigenfunction is known at one point between the two boundaries. The method we used is to give an arbitrary value to ϕ_2 and an initial value C_T for the eigenvalue C. Then we can calculate $\phi_3 \ldots, \phi_N$ using (3.73) and (3.74). If ϕ_N does not satisfy equation (3.75), the calculation is repeated with a new value of C_T until convergence is reached.

The accuracy of the eigenfunction is improved by decreasing and reducing the convergence criteria on $\phi_N = 0$. Since here we are primarily interested in the first mode, introducing the first mode solutions into (3.23), (3.24), and (3.25) allows the constants r, s, and q to be found numerically. However, higher modes do make minor contributions in the initial disturbance and introduce some error to this initial value problem.

The governing equation (3.34) may be changed into several different forms, since the higher order terms in (3.34) may be manipulated using the following zeroth order relation

$$\eta_t + C\eta_x = 0 \quad (\mathcal{E}, \int).$$

Such modifications introduce a second order error which can be neglected in our first order approximation. We then change (3.24) into the following form

$$\eta_t + C_0 \eta_x + R\eta\eta_x + S\eta_{xxt} = 0, \qquad (3.76)$$

where $C_0 = C - \sigma'q$, $R = -\varepsilon\Gamma$, and $S = \int S/C$. The following second-order finite-difference analog to (3.76) is used

$$\frac{\eta(i, j+1) - \eta(i, j)}{\Delta t} + (C_0 + R\eta(i,j)) \frac{[\eta(i+1, j+1) - \eta(i+1, j+1)}{4\Delta x}$$

$$+\eta(i+1, j) - \eta(i-1, j)] + \frac{S}{\Delta x^2 \Delta t} (\eta(i+1, j+1) - 2\eta(i, j+1)$$

$$+ \eta(i-1, j+1) - \eta(i+1, j) + 2\eta(i, j)$$

$$- \eta(i-1, j)) = 0, \qquad (3.77)$$

where $\eta(i, j) = \eta([i-1]\Delta x, [j-1]\Delta t)$. Gaussian elimination is used to calculate $\eta(i, j+1)$ using $\eta(i, j)$ and the boundary values $\eta(1, j+1)$ and $\eta(N, j+1)$. The integrating range in space is chosen large enough so that the boundary values remain almost constant over the period of integration. Furthermore, the integrating range translates with speed C_0, thus, saving computing time. The above numerical procedure is mainly intended to be applied to initial value problems. For boundary value problems, equation (3.76) can be changed to the following form

$$\eta_x + \frac{1}{C_o}\eta_t - \frac{R}{C_o}\eta\eta_t - \frac{S}{C_o^2}\eta_{ttx} = 0 . \qquad (3.78)$$

This equation (3.78) has the same form as equation (3.76) with the inter-change the independent variables x and t ; thus, our numerical proce-dure used for initial value problems may also be used in boundary value problems.

The accuracy of this numerical procedure can be checked by the following ways:

(1) Conservation of η (this requirement is due to equation (3.37)),

(2) Conservation of η^2 (this requirement is due to equation (3.38)),

(3) Special case (a solitary wave is an exact stationary solution to equation (3.78), therefore, there will be no change in η if the initial condition is a solitary wave). The numerical results were essentially independent of any decrease in the time and space intervals Δt and ΔX.

Since our governing KdV equation is based on an asymptotic ex-pansion in several small parameters, we must check if the initial conditions and time interval of prediction we chose are compatible with this approximate equation. The following requirements are necessary.

(1) The initial disturbance must propagate in the +x direction only with positive phase velocity C_o .

(2) The dominant structure of the initial disturbance must satisfy the long wave approximation.

(3) Since the magnitudes of the terms neglected in this equation are of order ε^2, $\varepsilon\delta$, and δ^{-2}, the accumulated error may become a magnitude of order unity after a time interval of $1/\varepsilon^2$ or $1/\delta^2$. However, there will be no significant change in the initial disturbance before a time interval $1/\varepsilon$. Thus the "usable" time range of this equation is $1/\varepsilon \leqslant t < 1/\varepsilon^2$. For internal waves in a continuously stratified fluid, the initial disturbance may consist of infinite modes. Although the experimental data showed that the first mode is the dominant one, the misrepresentation of the higher modes may introduce some additional error into our prediction.

The only stationary solution of the KdV equation with no motion at infinity is the solitary wave with its nonlinear term exactly balancing the dispersive term such that the shape of wave remains constant. The phase speed of the solitary wave is greater than the long wave speed. The typical KdV equation is

$$\eta_t + C_0 \eta_x + R \eta \eta_x + S \eta_{xxx} = 0, \tag{3.79}$$

and the solitary wave solution $\eta(x - ct)$ is

$$\eta = R\eta_0 \operatorname{sech}^2\left\{ (R\eta_0/12S)^{1/2}(x-ct) \right\}, \tag{3.80}$$

$$C = C_0 + R\eta_0/3, \tag{3.81}$$

where R = 3/2, S = -1/6 for surface wave.

Now we will analyse the nonlinear and dispersive effects in the generation of long nonlinear internal waves from an internal front. The variations of the nonlinear and dispersive effects due to different basic density and velocity profiles are represented by the different combinations of R and S. The front structure consists of two different levels connected by one half of a solitary wave profile with R = S = 1 and $\eta_\circ$ = 0.2.

(A) Varying R with S = 1: The numerical calculations (shown in figure 10) show that

(1) The phase speed of the crest of the leading wave is increased as R is increased.

(2) The amplitude of the crest of the leading wave becomes larger and its width becomes shorter and the slope of the front increases as R is increased.

(3) More wave crests are generated as R is increased.

Figure 11. shows that trajectories of the leading wave crest for different R, and figure 12 shows that growth rates of the leading wave crest for different R. While the phase speed of the leading wave crest increases with increasing R and keeps almost constant with time except initially, the growth rate of the amplitude of the leading wave crest increases with R and decreases with time.

(B) Varying S with R = 1: The numerical calculations (shown in figure 13) show that
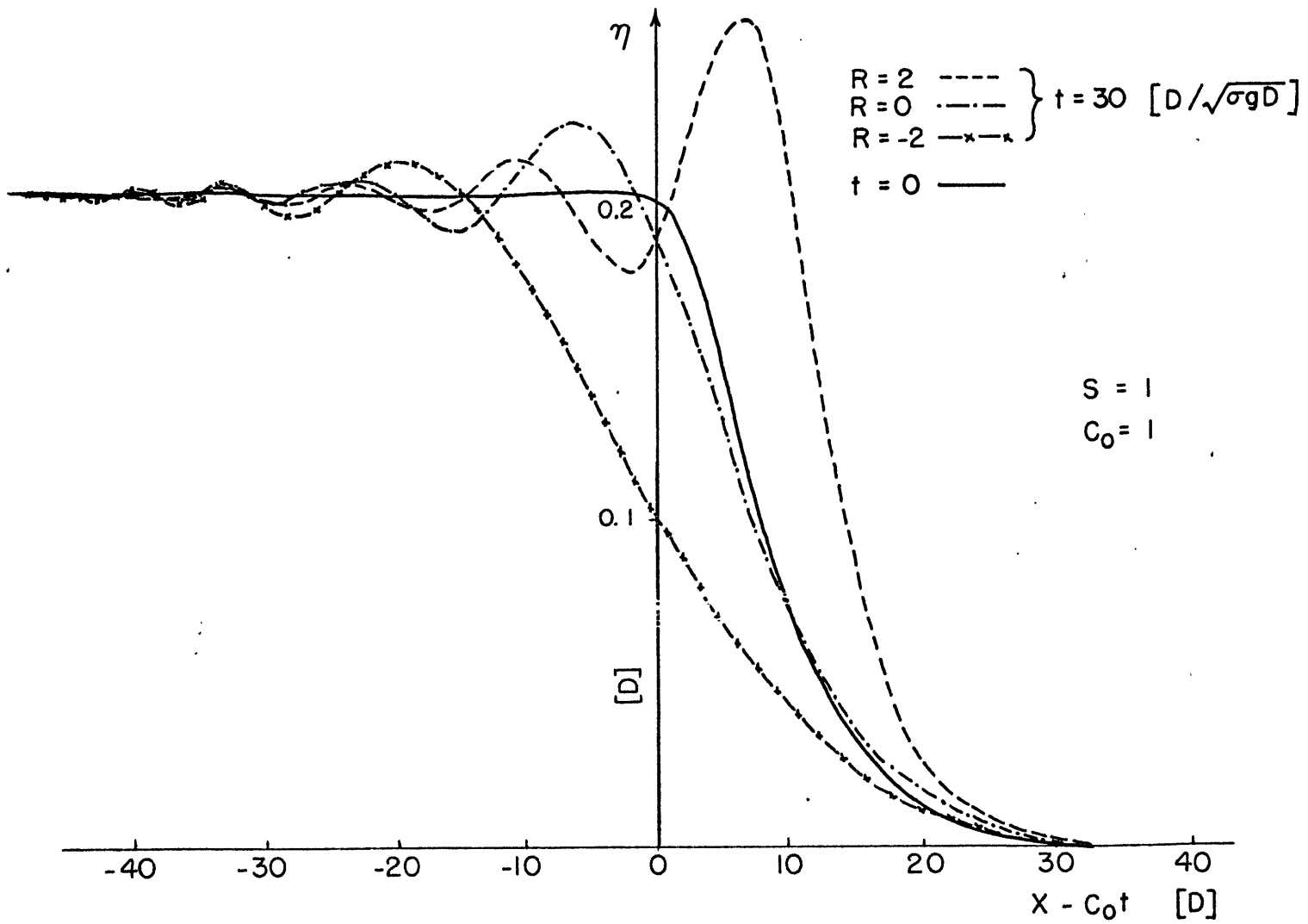
(1) The phase speed of the crest of the leading wave is

Figure *10*. Numerical example illustrating the nonlinear effect on the generation of long waves on a front.

Figure //. The trajectory of the peak of the leading wave for different R.
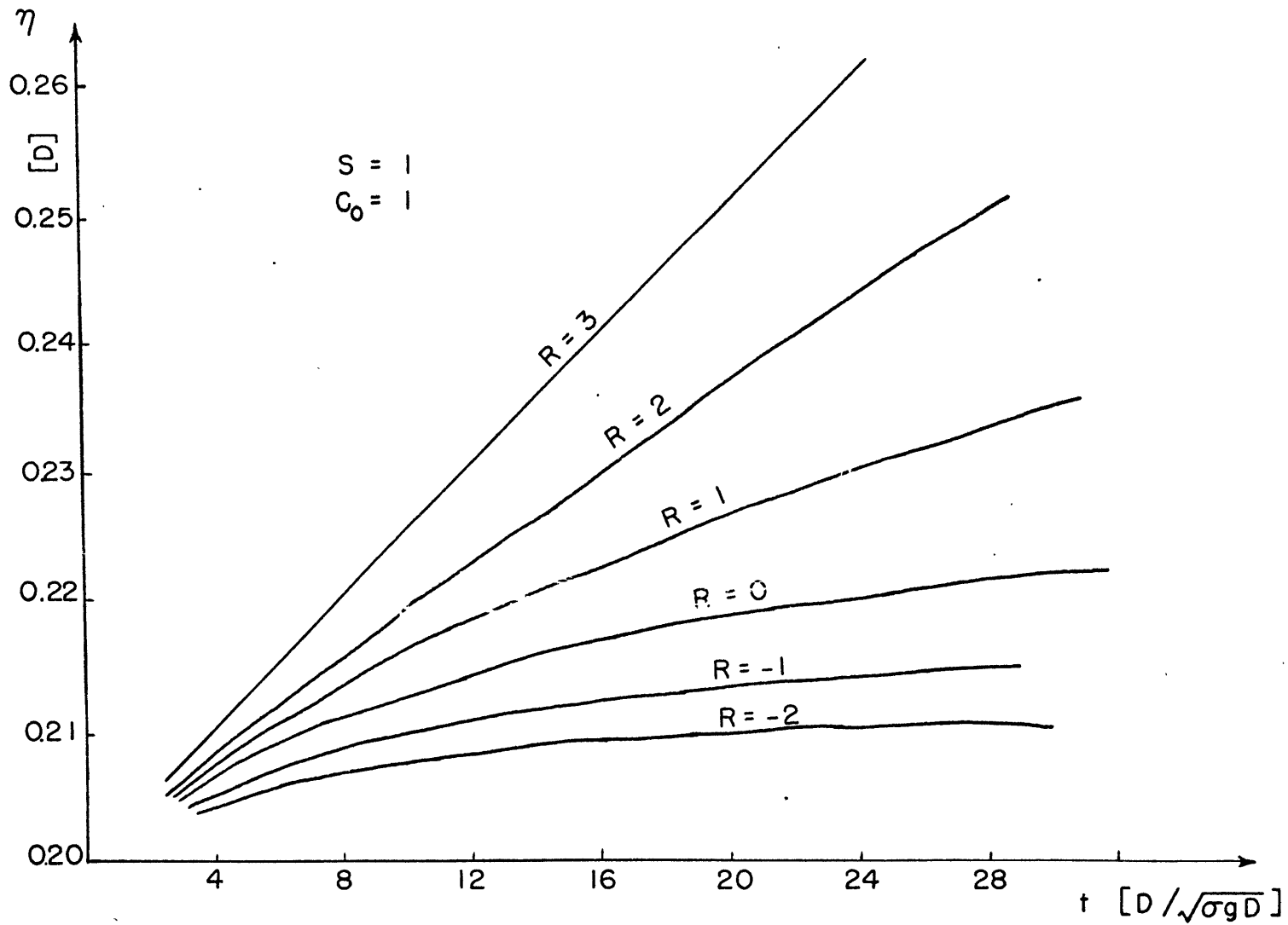
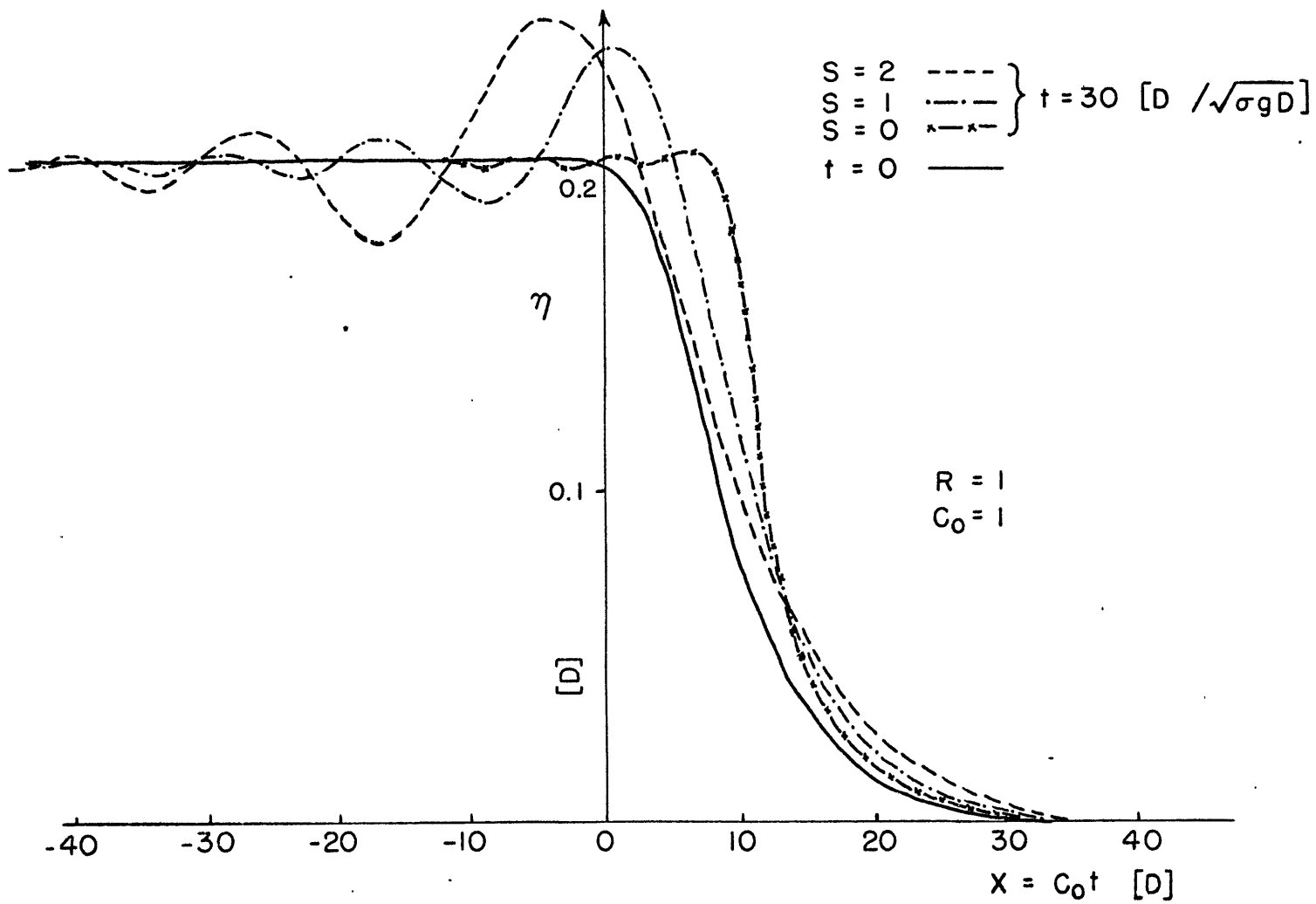Figure /2. The growth of the amplitude of the leading wave for different R.

Figure /3. Numerical example illustrating the dispersive effect on the generation of long waves on a front.

decreased as S is increased.

(2) The amplitude of the crest of the leading wave becomes

large and its width becomes shorter as S is increased.

Waves are not observed when S = 0, thus corresponding

to Airy's theory.

(3) More wave crests are generated as S is increased.

Figure 14 shows the trajectories of the leading wave crest for diffe-

rent S, and figure 15 shows the growth rates of the amplitude of the

leading wave crest for different S. Here the phase speed of the

leading wave crest decreases with increasing S and increases with time,

while the growth rate of the amplitude of the leading wave crest in-

creases with increasing S for small S and then keeps almost constant.

The wave length (defined by the distance between the leading two wave

crests) increases with time in both (A) and (B).

As an aside to this section, it is interesting to observe nume-

rically how the solitary wave adjusts itself if there is a small de-

viation from the exact solution. The purpose of this investigation

is to find whether the solitary wave is a boundary which separates

two different regions of evolution of an isolated long disturbance or

if the initial disturbance tends to evolve into a steady solitary wave

profile. Two cases are analysed.

In the first case, corresponding to a decreased nonlinear effect,

the wave amplitude decreases gradually and the wave length increases,

with some small waves being formed behind the main peak. In the second

case corresponding to an increased nonlinear terms, a reverse trend is

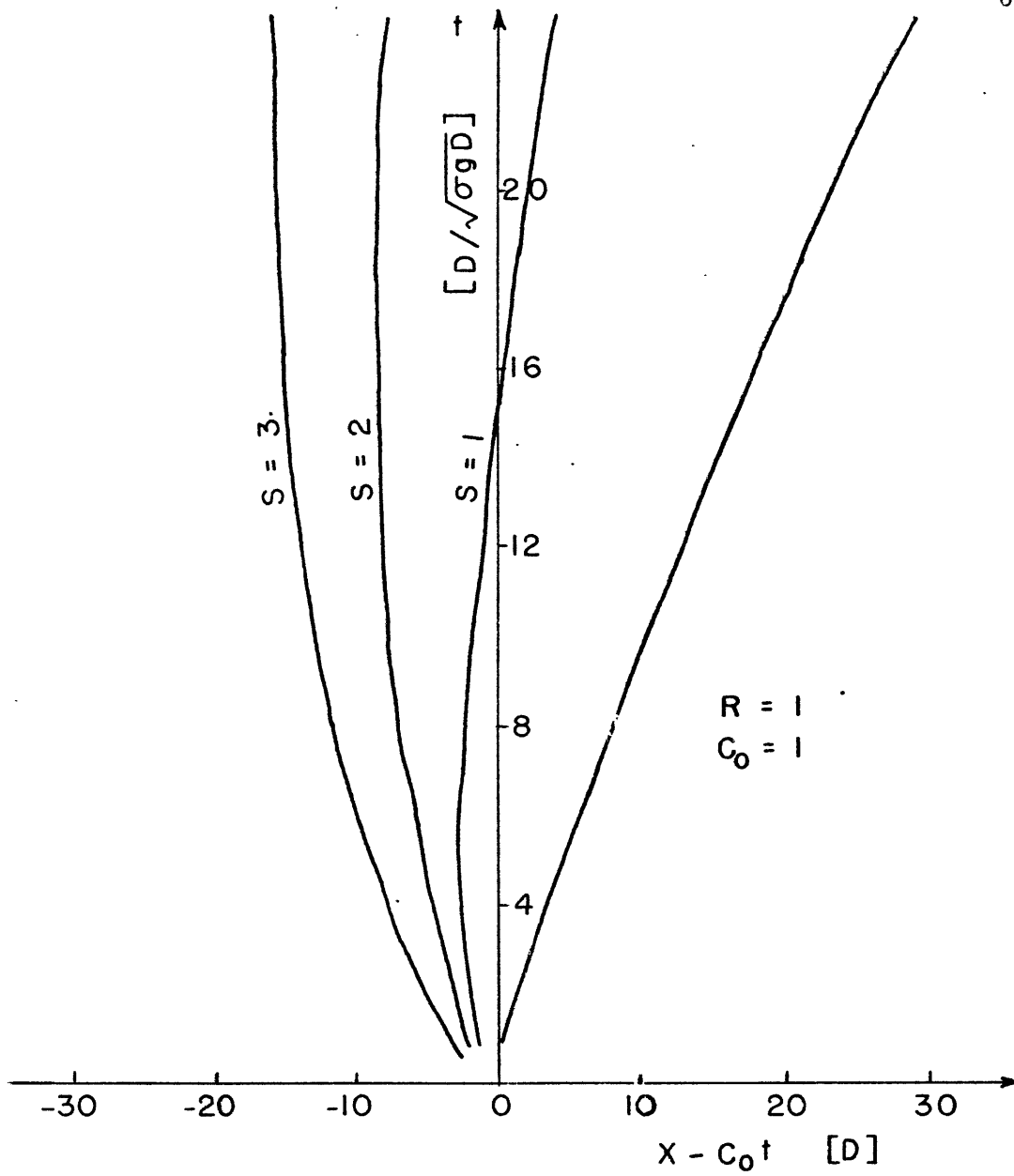shown (figure 4). Thus, the solitary wave clearly plays an important

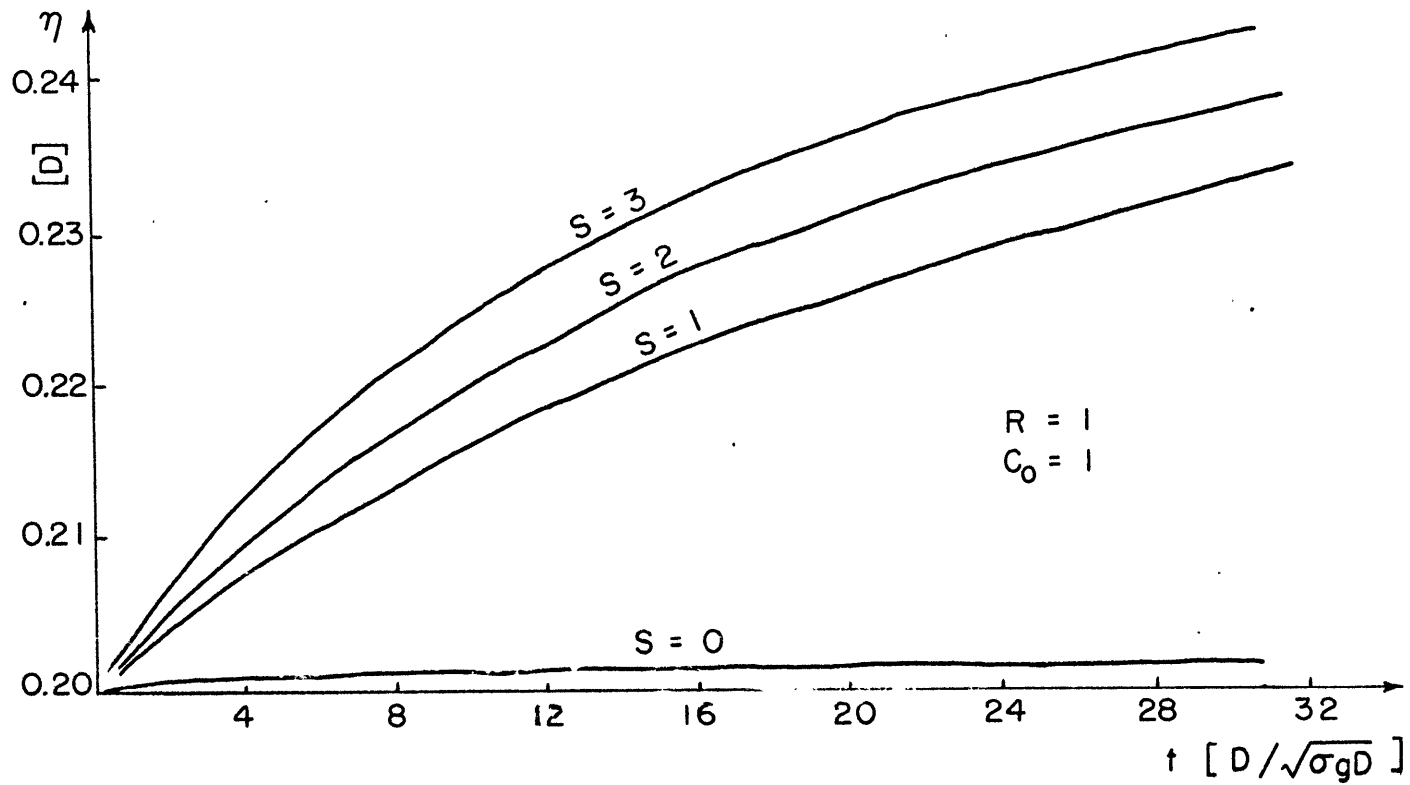Figure 14. The trajectory of the peak of the leading wave with different S.

Figure /5. The growth of the amplitude of the leading wave for different S.

role in the natural evolution of certain long disturbances.

(2) Comparison of numerical solution with laboratory results.

In the four laboratory experiments to be discussed here, the appropriate physical dimensions as shown in figure 3 are: A = 6.5 cm, W = 17 cm, L = 10 cm, RA = 60 cm, AB = 51 cm, BC = 38 cm, T = 36 sec, H = 13.5 cm, σ = 0.00274 for experiments 1 and 2, and σ = 0.00165 for experiments 3 and 4.

Experiment 1: moving the ridge toward the probes for one half period of a sinusoidal path. The numerical calculations shown in figure 16 correspond to the laboratory observations shown in figure 1. Both illustrate the generation of a long nonlinear internal wave train from an initial elevation of the isopycnal surfaces. In these figures and those which follow, we choose to compare the numerically predicted isopycnal surface elevation with that infered from direct conductivity measurements using the lowest order relationship,

$$\eta(t) = \frac{C^*(t) - \bar{C}^*}{d\bar{C}^*/d\bar{z}} , \qquad (3.82)$$

where $\bar{C}^*$ and $d\bar{C}^*/dz$ are the average value and gradient of conductivity at the the depth of the probe. In our laboratory experiment, the conductivity of the saline fluid increase monotonically with depth. In Massachusetts Bay, density in the seasonal thermocline is primarily determined by the temperature field with the mean temperature decreasing with depth. To facilitate direct comparison of our results with Halpern's temperature observations, we plot our streamline elevation
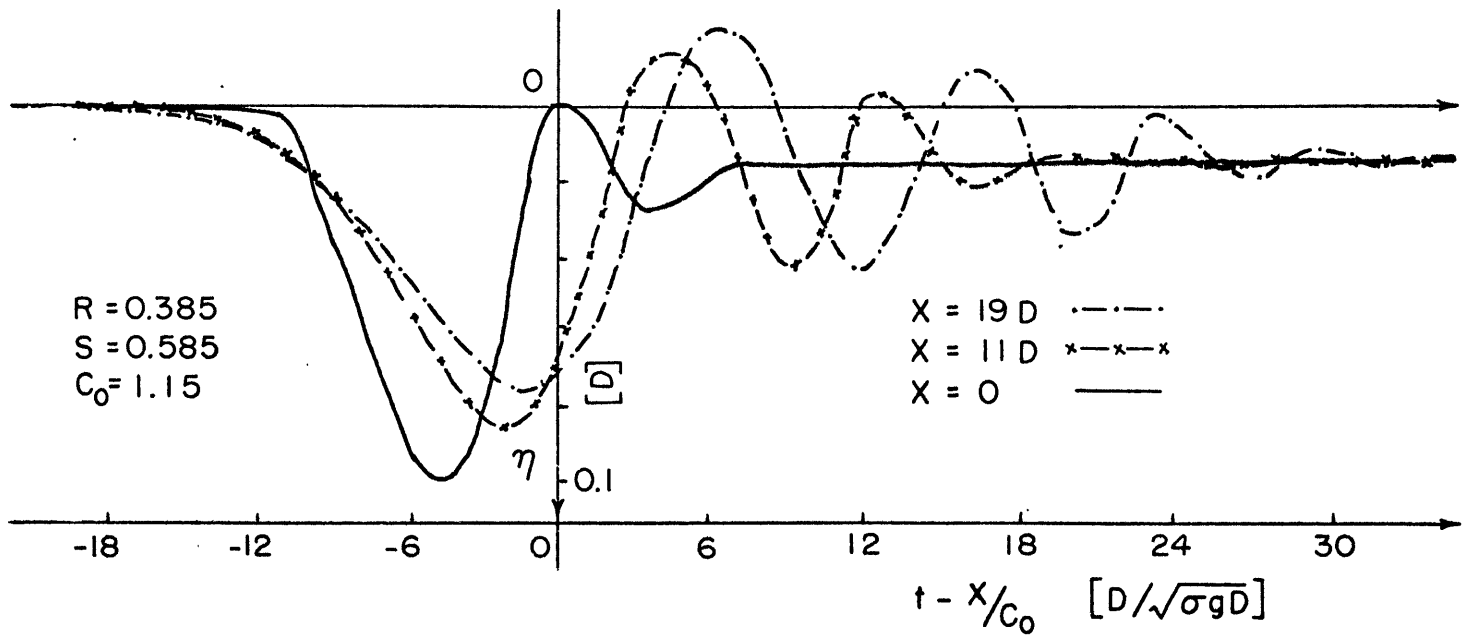
R = 0.385
S = 0.585
C_0 = 1.15

X = 19 D ·—·—·
X = 11 D ×—×—×
X = 0 ————

$t - X/C_0$ $[D/\sqrt{\sigma gD}]$

Figure 16. Numerical results corresponding to experiment 1.

results with the positive $+\eta$ direction downwards. These plots are then identical to temperature measurements if we had indeed used temperature to stratify our laboratory system.

Experiment 2: moving the ridge away from the probes for one half period of a sinusoidal path. Both the numerical prediction in figure 17 and the laboratory results in figure 2 show the generation of a solitary type wave from an initial depression of the isopycnal surfaces.

Experiment 3: moving the ridge for one complete period of a sinusoidal path. If we choose the maximum point of the streamline elevation in the experimental results (see in figure 18) as the begining point of a "warm front", the "thermal" record looks similar to the warm front observed in Massachusetts Bay. An internal wave train is generated on this "warm front". Figure 19 illustrates the numerical calculations corresponding to the experimental results, which show the growth of the leading waves.

Experiment 4: moving the ridge for several periods. The experimental results and numerical results (see figure 20 and 21 respectively) show that several waves are generated on the initial periodic disturbance.

Comparison of the experimental and numerical results indicate relatively good agreement between observed and predicted phase speed and wave period (see table 2 for comparisons for experiments 3 and 4). However, the data also shows a general drift due to the probes themselves in addition to some net mass transport which may change the basic density structure.
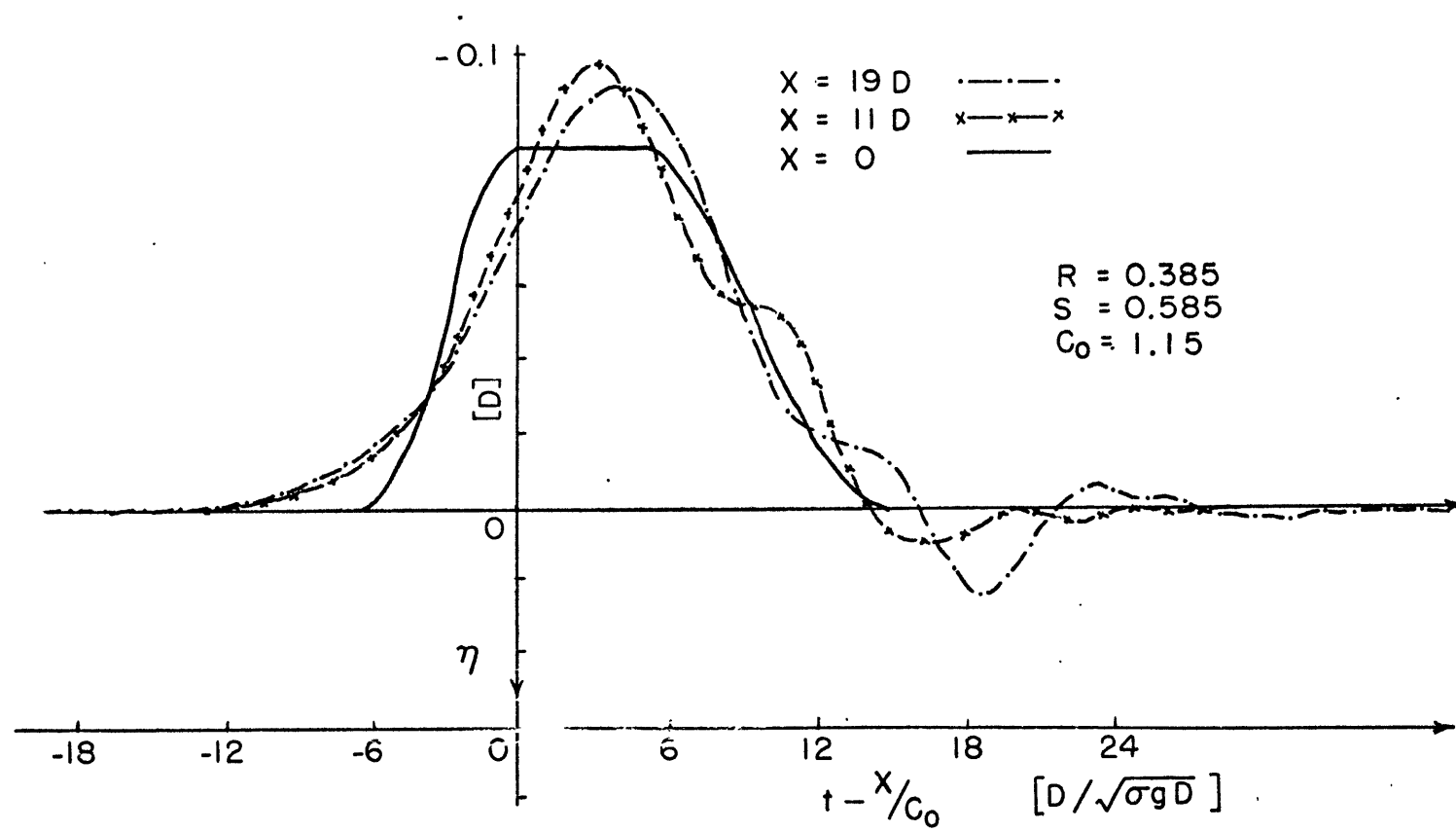
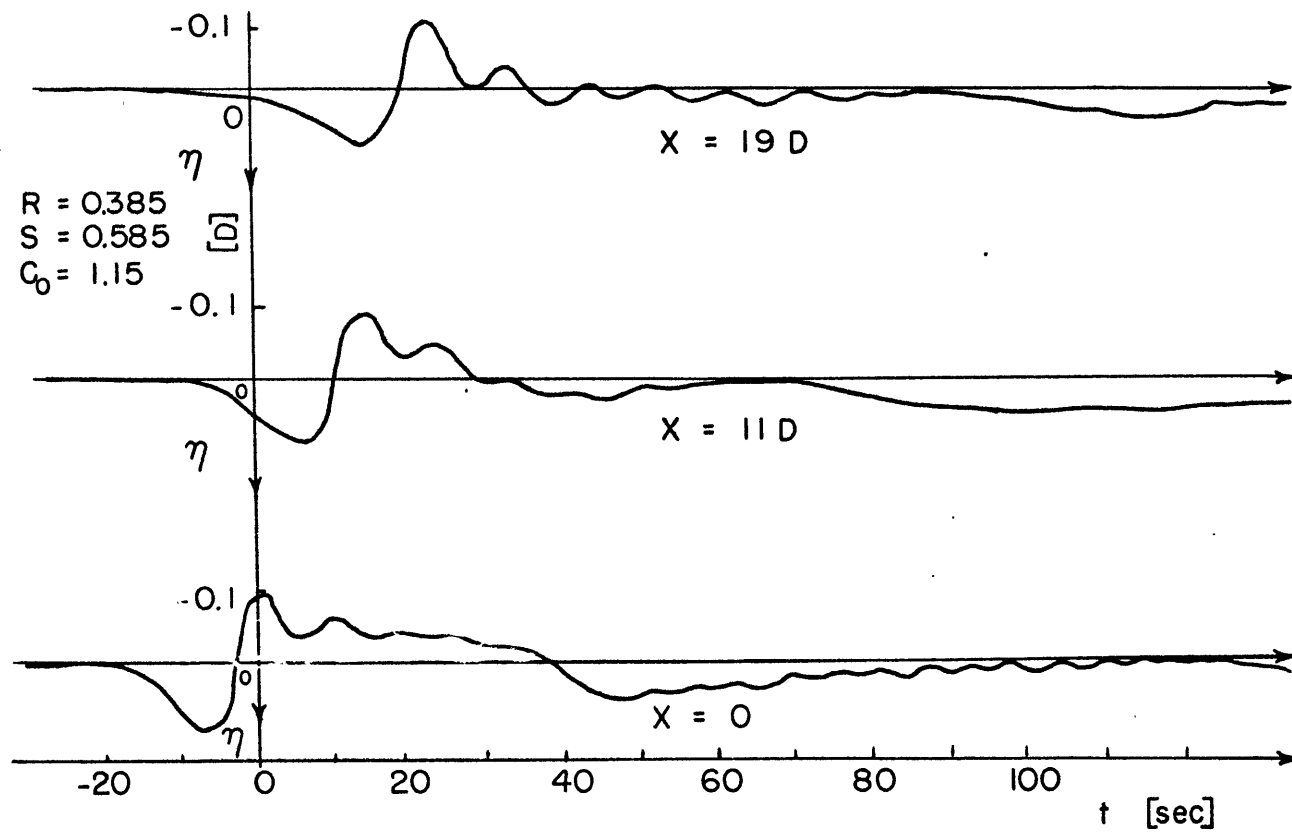Figure /7. Numerical results corresponding to experiment 2.

Figure /8 . Results of experiment 3 showing the generation of waves by moving the ridge for one completely period of a sinusoidal path.
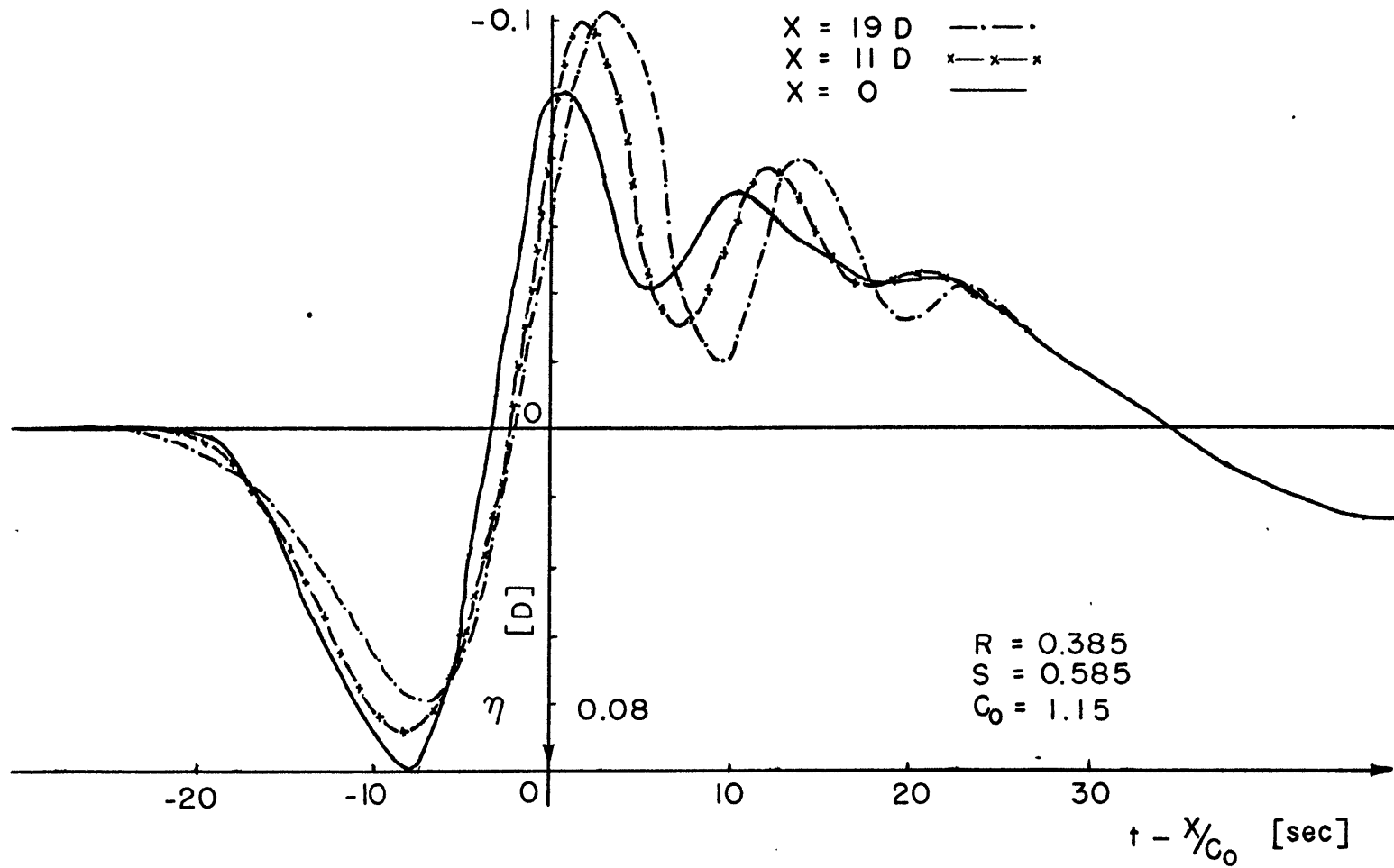
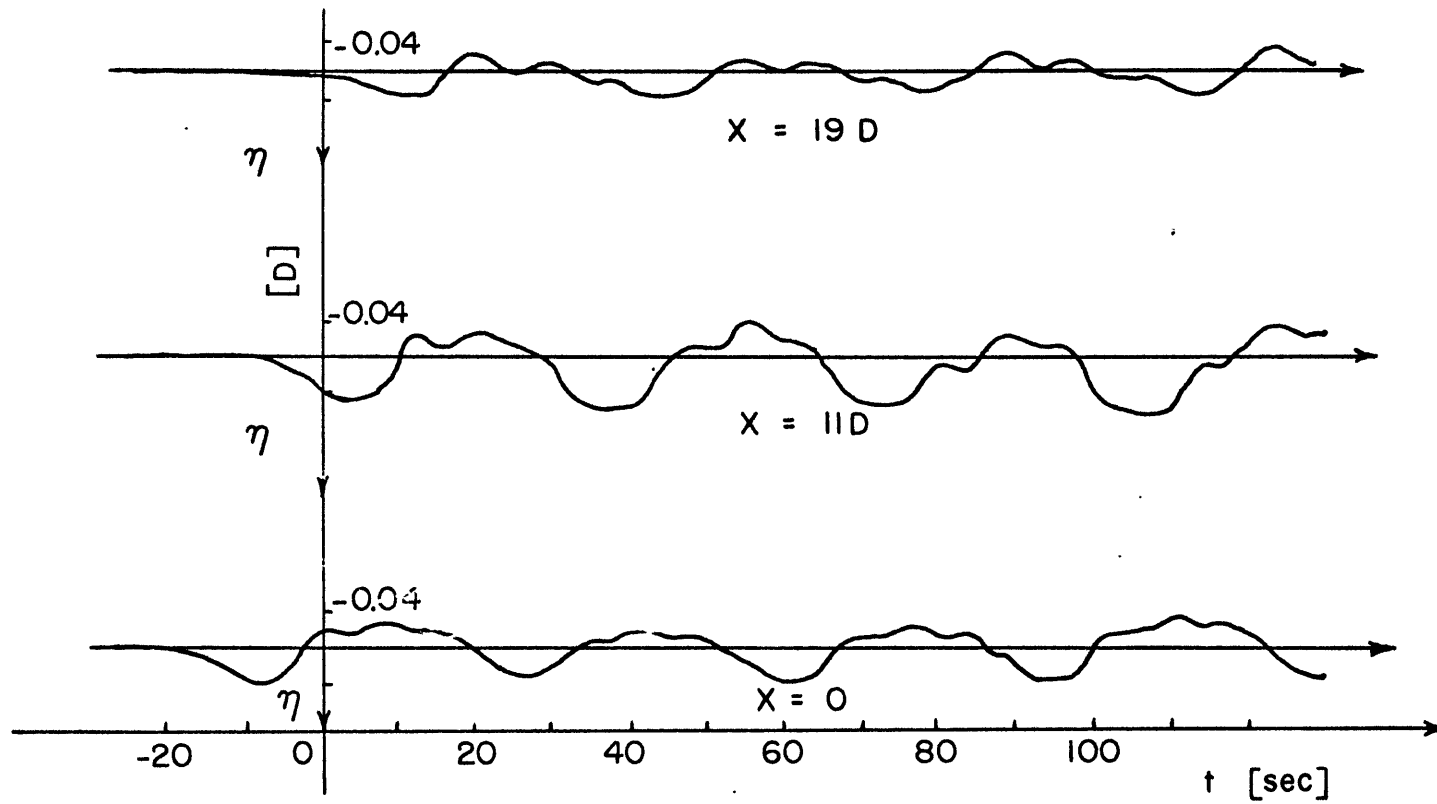Figure 19. Numerical results of experiment 3.

Figure 20. Results for experiment 4 showing the generation of wave trains
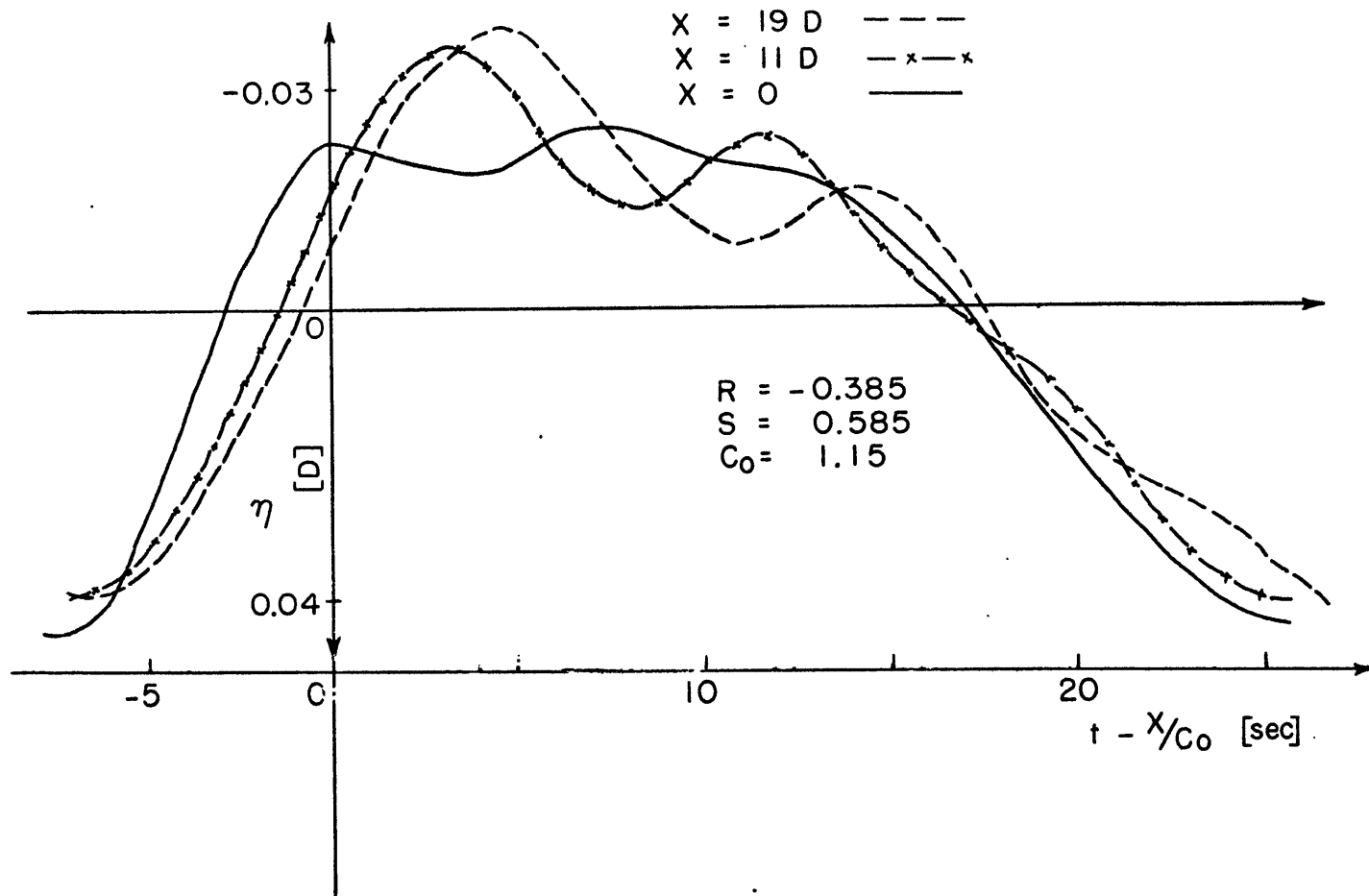by moving the ridge for several periods.

Figure 2| . Numerical results corresponding to experiment 4 .

The experimental results show that the internal disturbances

are mainly first mode due to the following reasons. (1) The higher

modes have a phase speed much smaller than the velocity of the lead-

ing wave, and thus cannot catch up the frontal region in which we are

interested. (2) The horizontal particle position as determined by

dye streaks appeared to be quite asymmetric with depth. (3) Conduc-

tivity measurements are coherent at different depths, indicating that

the vertical velocity at different depth are in phase. (4) Good

agreement shown in table 2 between the experimental results and nume-

rical results (based on the assumption that the lowest mode is the

only energetic mode). Experiment 1 and 2 clearly demonstrate the

influence of nonlinearity on the generation of waves. An additional

numerical example is shown in figure 22 to demonstrate the nonlinear

effect by constrasting predictions made from identical initial con-

ditions but with nonlinear coefficients of opposite sign.

	Phase Velocity*	Wave Period**	Wave Length
Experiment 1	2.0 cm/sec.	11 sec.	22 cm.
Numerical Result	2.3 cm/sec.	12 sec.	27.6 cm.
Experiment 3	3.5 cm/sec.	10 sec.	35.0 cm.
Numerical Result	3.8 cm/sec.	10 sec.	38.0 cm.

Table 2.

* The propagating velocity of the leading wave peak.

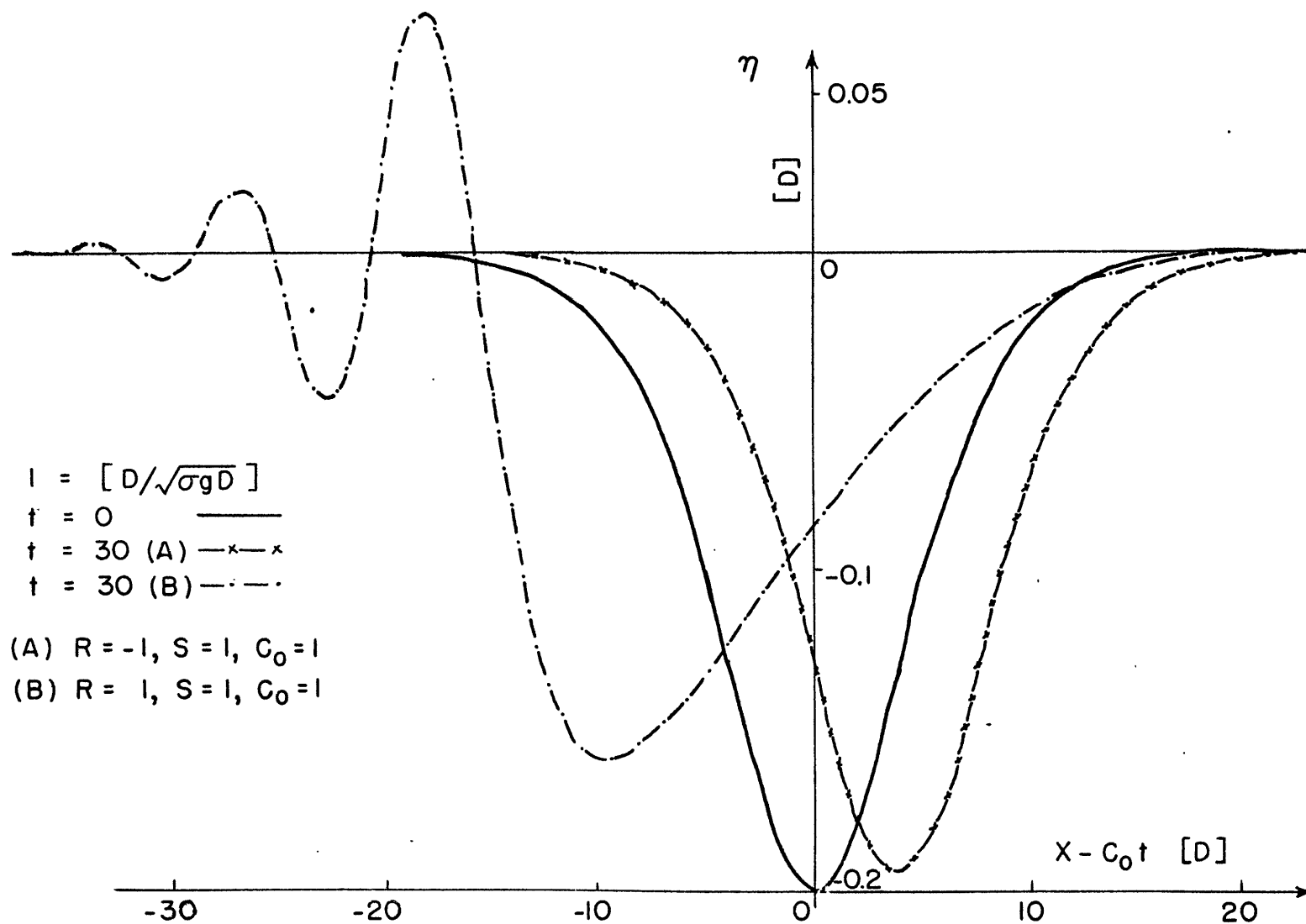** The time interval between the first and second wave peaks.

Figure 22. Numerical example illustrating the influence of nonlinear effect; (A) Nonlinear effect balances dispersive effect. (B) Reversing the sign of nonlinear effect causes wave train to be generated.

The discrepancy in the phase speed between the experimental and numerical results may be partially explained by the following reasons. (1) The initial condition used in the numerical calculation is obtained by approximately matching several sinusoidal curve to the experimental trace measured at probe A in a way that the first derivative is continuous. The resulting error will influence the phase speed through the dispersive effect. (2) Due to truncation error, η (see equation (3.37)) is not exactly conserved; the percentage error grows with time, i.e., 5.1% at probe B, and 8.8% at probe C (experiment 1); 1.5% at probe B, and 2.7% at probe C (experiment 3). (3) Accurate measurement of the density profile was quite difficult due to the relative precision of the refractometer, the smallness of the vertical density gradient, and the small depth of the fluid layer. The estimated error in C_p could be at least $\pm$ 5%. (4) Although viscous forces do not change the phase speed in linear wave theory, viscous damping by decreasing the wave amplitude influences the phase speed through the nonlinear effect. Since the wave amplitudes generated in the laboratory experiments are typically small, i.e., $a/D \sim 0.1$, viscous damping is probably negligible. (5) The neglect of higher order terms in the governing equation.

(3) Generation of wave trains in Massachusetts Bay.

The generation of a wave train from an initial front has already been discussed. However, the situation in Massachusetts Bay is quite different. First, the boundary conditions can not be considered constant as in the previous cases, thus periodic boundary conditions must be used and periodic solutions sought. However, in order to save computing time, we are going to calculate only the most interesting region, i.e., the region around the front. Second, the amplitudes of the front and waves are so large (almost 10 m), and the vertical characteristic length D is only 15 m (almost all variation of basic density occurs in the upper 15 m of the total depth in Massachusetts Bay), that the nonlinear parameter $\varepsilon = \dfrac{10\,m/2}{15\,m} \sim 0.33$ The dispersive parameter $\delta = (D/\ell)^2$ changes from 1/600 at Stellwagen Bank to 0.1 at station T while the characteristic horizontal length ℓ changes from 400 m to 50 m. This decrease in ℓ is caused by the nonlinear steepening of the front.

Since the nonlinear parameter ε is so large, order (ε^2) terms must be added to the governing KdV equation,

$$\eta_t + C_o\eta_x + \varepsilon \Gamma \eta \eta_x + \delta S \eta_{xxx} + \varepsilon^2 \lambda_1 \eta^2 \eta_x = 0. \qquad (3.83)$$

The generation of wave trains in Massachusetts Bay can be mainly divided into two stages (1) The nonlinear parameters ε and ε^2 are initially both much greater than the dispersive parameter δ , so that during the initial period of nonlinear steepening of the blocking

front, we may neglect dispersion and deal instead with the appro-

ximate balance

$$\eta_t + (C_0 + \gamma\varepsilon\eta + \lambda_1\varepsilon^2\eta^2)\frac{\partial\eta}{\partial x} = 0. \qquad (3.84)$$

Equation (3.84) implies that η will keep constant following the

characteristic velocity $\frac{dx}{dt} = C_0 + \gamma\varepsilon\eta + \lambda_1\varepsilon^2\eta^2.$ Thus the

dispersive parameter must increase quickly with time.   (2) When the

dispersive parameter δ becomes comparable to ε^2 , new waves start

to form.   Then $(D/\ell)^2 = \varepsilon^2$ implies $\ell \sim 50$ m and the length of the

front is approximately 100 m.   At this stage $(t = T_0)$, we have to

solve the initial value problem numerically.   The finite difference

analogy to equation (3.83) is obtained by adding to equation (3.75) the

nonlinear term proportional to ε^2.

Since the cold front will be flattened by the nonlinear effect

and does not lead to wave generation, we will only analyse the region

around the warm front.   For $t = T_0 + 42$ min., waves have already been

formed behind the front (figure 23).   If permanent waves are formed

at the front, the only solution is a solitary wave.   Assuming the waves

at Massachusetts Bay are solitary internal waves, the following table

shows the nonlinear effect on phase velocity.

	Long Wave Speed	Dispersive Effect + Nonlinear Effect	Wave Speed
Solitary Wave	0.41 m/sec.	+0.12 m/sec.	0.53 m/sec.
Linear Wave (Halpern's)	0.41 m/sec.	-0.06 m/sec.	0.35 m/sec.
Observation (Mass. Bay)	——	——	0.88 ± 0.22 m/sec.

For the wave length, linear wave theory gives 158 m corresponding

to Halpern's observation of 200 m. The numerical calculation for the

second stage shows that the "wave length" is 172 m (figure 23), however,

it is well known that these solitary waves will gradually separate

away from each other (Pregrine, 1966), so it is only a matter of time

($\sim$ 52 min.) for the "wave length" to become 200 m. This implies

that the distance between station T and the point (corresponding to

$t = T_o$) is approximately (42 min. + 52 min.) x 60 sec/min x 0.53 m/sec

$\approx$ 4 km. Another numerical result shown in figure 24 shows the gene-

ration of waves from a periodic disturbance similar in shape to that

observed in Massachusetts Bay.

The relevant parameters (see figure 5) in Massachusetts Bay are

A/H = 0.63, L/H = 106, f/N = 0.0073, and Fi = 0.26. The nonlinear

coefficient R = -2.1, the dispersive coefficient S = 0.72, and the

long wave speed C = 1.14. All calculations presented in this section

are based on the mean density structure observed in Massachusetts Bay

in July, 1966 by Halpern (1971). The observed density profile and its

corresponding first mode zero order eigenfunction $\phi_1^{(o,o)}(z)$ are shown
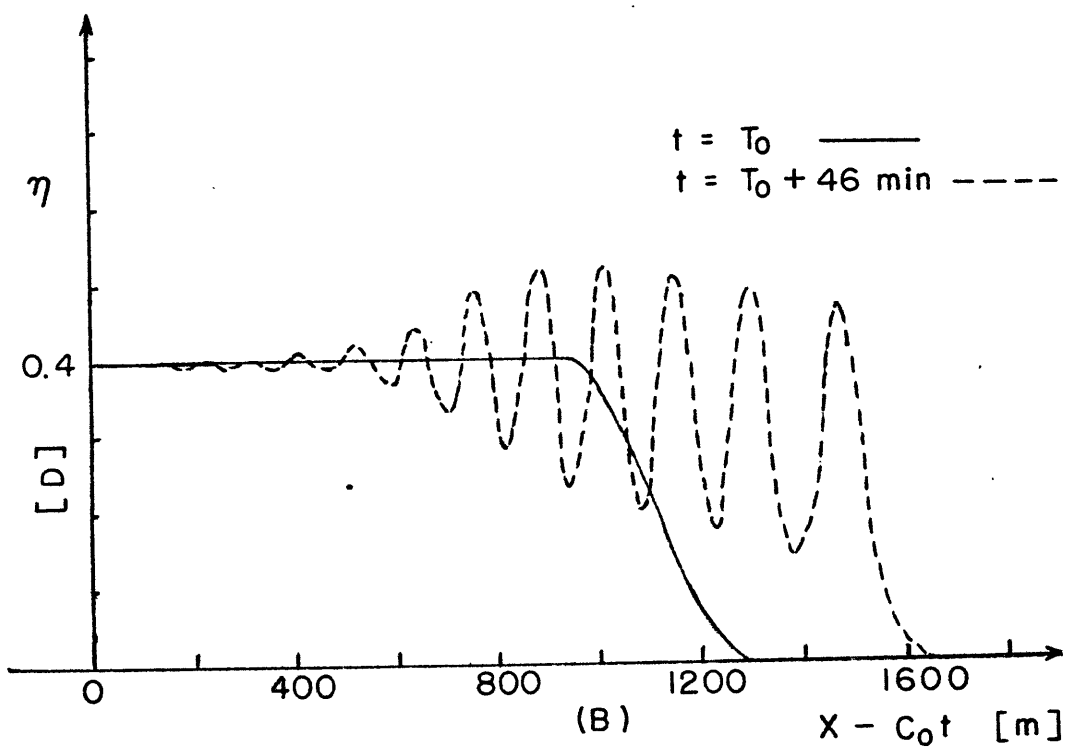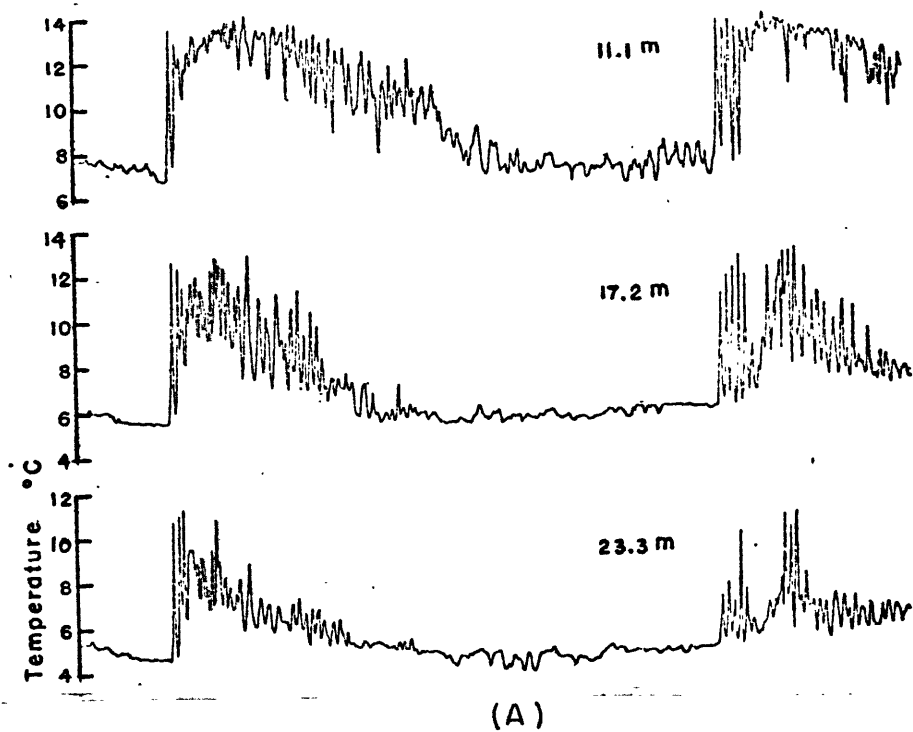
in figure 25.

Figure 23. (A) Temperature measurements at Massachusetts Bay
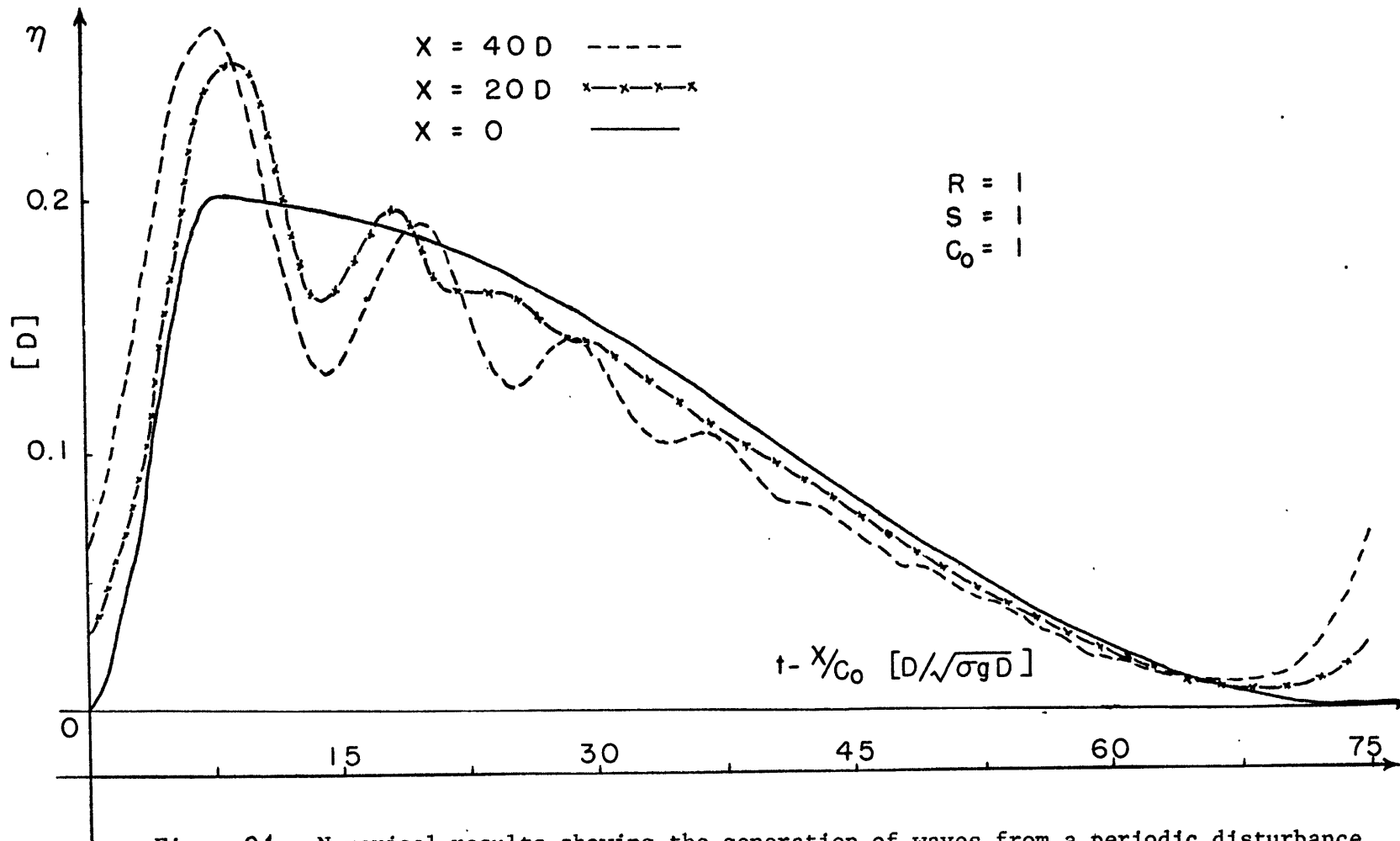(Halpern, 1971). (B) Numerical results corres-
ponding to (A).

Figure 24. Numerical results showing the generation of waves from a periodic disturbance similiar in shape to that observed in Massachusetts Bay.

0.5   0.9

(0,0)

$\phi_1(Z)$

Z [m]

Z ⊥ 60

$Z_{max.}$ 40

20

0

(B)

23.0   24.0   25.0

$\bar{\rho}(Z)$ $(10^{-3}\,gm/cm^3)$
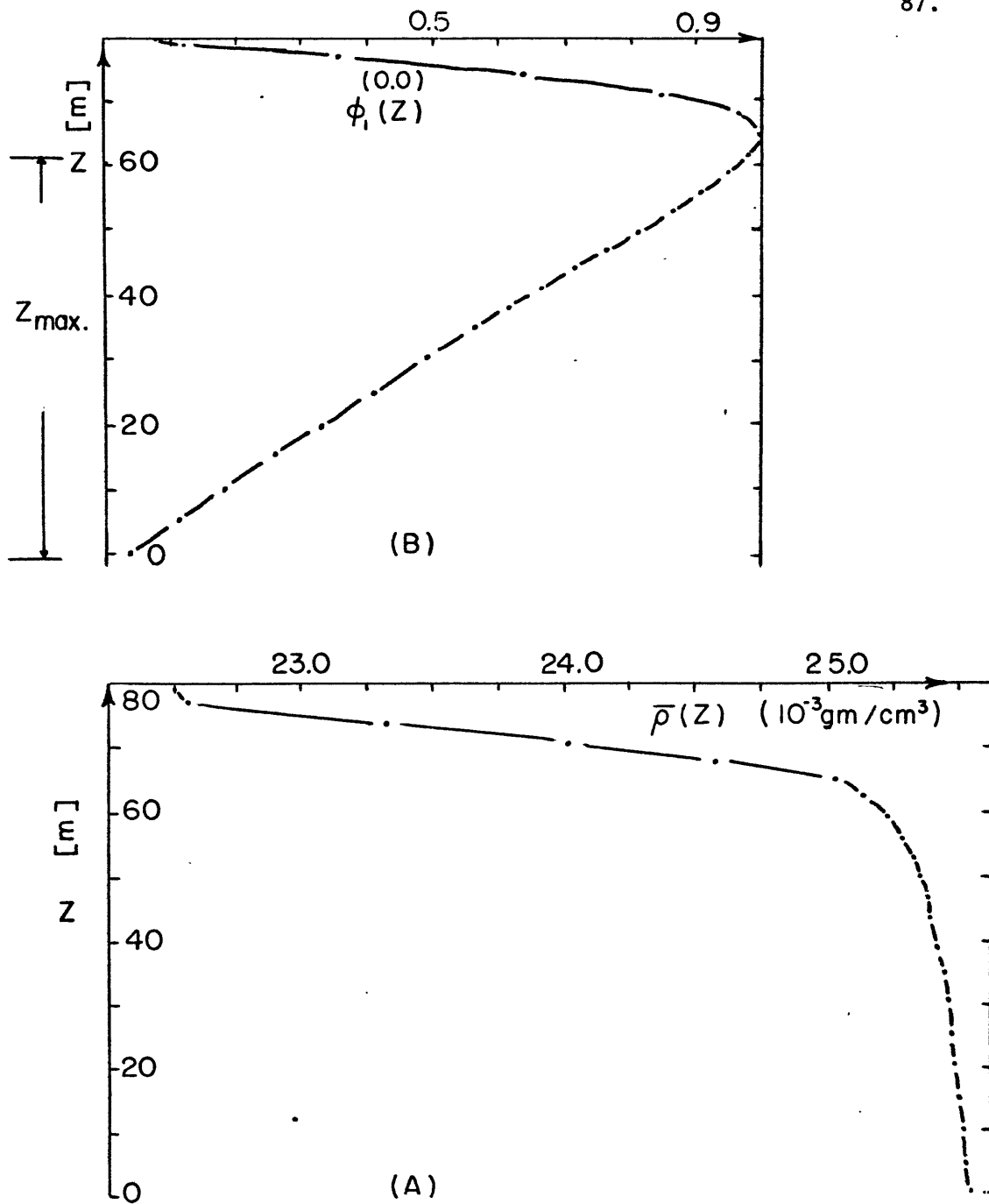
80

60

Z [m]

40

20

0

(A)

Figure 25. (A) Summer density structure at Massachusetts Bay
measured by Halpern (1971). (B) The zero order
first mode eigenfunction, $\phi_1^{(0,0)}(z)$, corresponding
to density structure shown in (A).

4. Quasi-steady Lee Waves

The essential assumption of the quasi-steady approximation is that parameters characterizing the waves are slowly varying over a characteristic wave period. If this variation is slow enough then the waves must locally closely approximate periodic plane waves. The basic range of appliability of the quasi-steady approximation then depends on how accurately real waves systems correspond to periodic plane waves locally.

We assume that a low, smooth ridge is towed horizontally with a volocity U(t) in a density stratified fluid layer. The equations of motion and continuity are when transformed into a coordinate system moving with the ridge,

$$\frac{\partial}{\partial t}(u + U) + (u + U)\frac{\partial u}{\partial x} + w\frac{\partial u}{\partial z} = -\frac{\partial p}{\partial x} , \qquad (4.1)$$

$$\frac{\partial}{\partial t}w + (u + U)\frac{\partial w}{\partial x} + w\frac{\partial w}{\partial z} = -\frac{\partial p}{\partial z} - \rho' g , \qquad (4.2)$$

$$\frac{\partial \rho'}{\partial t} + (u + U)\frac{\partial \rho'}{\partial x} + w\frac{\partial(\bar{\rho} + \rho')}{\partial z} = 0 , \qquad (4.3)$$

$$\frac{\partial u}{\partial x} + \frac{\partial w}{\partial z} = 0 . \qquad (4.4)$$

The above system can also be transformed into the system (x', z', t) which is fixed in relation to the mean current U(t), using the following transformation

$$x' = x - \int_{t_o}^{t} U(\theta)\, d\theta$$

$$z' = z$$

$$t' = t$$

$$\longrightarrow \quad \begin{cases} \dfrac{\partial}{\partial x} = \dfrac{\partial}{\partial x'} \quad , \\[2mm] \dfrac{\partial}{\partial z} = \dfrac{\partial}{\partial z'} \quad , \\[2mm] \dfrac{\partial}{\partial t} = \dfrac{\partial}{\partial t'} - U(t)\dfrac{\partial}{\partial x} \ , \end{cases}$$

(4.5)

So that the governing equations become in this system moving with the mean current,

$$\frac{\partial U}{\partial t'} + \frac{\partial u}{\partial t'} + u\frac{\partial u}{\partial x'} + w\frac{\partial u}{\partial z} = -\frac{\partial p}{\partial x'} \ , \qquad (4.6)$$

$$\frac{\partial w}{\partial t} + u\frac{\partial w}{\partial x'} + w\frac{\partial w}{\partial z'} = -\frac{\partial p}{\partial z'} - \rho'g \ , \qquad (4.7)$$

$$\frac{\partial \rho'}{\partial t} + u\frac{\partial \rho'}{\partial x} + w\frac{\partial (\rho' + \bar{\rho})}{\partial z} = 0 \ , \qquad (4.8)$$

$$\frac{\partial u}{\partial x'} + \frac{\partial w}{\partial z'} = 0 \ . \qquad (4.9)$$

After this transformation, we see that the only difference introduced by a non-steady mean current is the addition of the body force $\dfrac{\partial U(t)}{\partial t}$. Thus if $\dfrac{\partial U(t)}{\partial t}$ is neglected by assumption of the quasisteady approximation, we can treat the time dependent current as locally steady at any instant. For convenience in the following ray theory analysis, we will consider our coordinate system to be fixed

with respect to the mean current. However, we can and will easily transform our results back into the system fixed with respect to the ridge using transformation (4.5), since this latter coordinate system more easily describes the field measurement in which the ridge is at a fixed position.

It is well known from linearized wave theory that the wave number k and frequency ω will change according to certain conservation relations. Assume ω and k are derived from a phase function ϕ by the following equations,

$$\omega = -\frac{\partial \phi}{\partial t} \quad , \qquad k = \frac{\partial \phi}{\partial x} . \qquad (4.10)$$

The wave parameters ω and k must satisfy the dispersion relationship

$$\omega = \Omega \left(k(x, t), f(x, t) \right) \qquad (4.11)$$

where $f(x, t)$ is a parameter involving the local properties of the medium. The variation of ω and k are then governed by the following two equations,

$$\frac{d\omega}{dt} = \frac{\partial \Omega}{\partial f} \cdot \frac{\partial f}{\partial t} \quad , \qquad (4.12)$$

$$\frac{dk}{dt} = -\frac{\partial \Omega}{\partial f} \cdot \frac{\partial f}{\partial x} \quad , \qquad (4.13)$$

where $\frac{d}{dt} = \frac{\partial}{\partial t} + C_g \frac{\partial}{\partial x}$, and C_g is the group velocity, defined by

$$C_g = \frac{\partial \Omega}{\partial k} .$$

It is well known that the energy of a wave packet is affected by interaction with a non-uniform mean flow. Guided by earlier work by

Whitham (1965), Bretherton and Garrett (1967, 1968) have proved that
for a wave packet in a moving and/or time dependent medium, the
quantity E/ω' satisfies the following conservation equation

$$\frac{d}{dt}\left(\frac{E}{\omega'}\right) + \frac{E}{\omega'} \cdot \frac{\partial}{\partial x} \cdot C_g = 0 \; ,$$

where $\omega' = \omega - kU$ is the frequency of the waves measured in a frame
of reference moving with the local mean velocity U of the medium.
The wave energy density E is also measured in this frame of referen-
ce.

For quasi-steady internal waves in a time-dependent mean current
U(t), the dispersion relation is simply

$$\omega = \Omega \equiv k\, U(t) + \omega_0(k). \qquad\qquad (4.14)$$

Introducing (4.14) into (4.13), we have

$$\frac{\partial k}{\partial t} + \left(C_g + U(t)\right)\frac{\partial k}{\partial x} = 0 \; , \qquad\qquad (4.15)$$

where $C_g = \frac{\partial}{\partial k}\,\omega_0(k)$. Equation (4.15) implies that k is constant
following the characteristic line $\frac{dx}{dt} = C_g + U(t)$, where ω
will change according to

$$\frac{\partial \omega}{\partial t} + \left(C_g + U(t)\right)\frac{\partial \omega}{\partial x} = k\, U_t \; . \qquad\qquad (4.16)$$

We now multiply (4.15) by U(t) and substract from (4.16) to get

$$\frac{\partial(\omega - kU)}{\partial t} + \left(C_g + U\right)\frac{\partial}{\partial x}\left(\omega - kU\right) = 0 \; . \qquad (4.17)$$

This result (4.17) implies that the quantity $(\omega - kU)$ rather than ω

is conserved along the characteristic $\frac{dx}{dt} = C_g + U$. Thus, along

the characteristic line $\frac{dx}{dt} = C_g + U$, equation (4.15) and (4.17)

show that the energy density will remain the same as if there is no

mean current U(t), so if a energy density peak curve is formed in the

frame fixed with the mean current U(t), it will also occur in the frame

fixed with the ridge.

It is well known that a stationary internal wave train may be

generated on the lee side of a submarine ridge in a steady, density

stratified mean current (Long [1953, 1954, 1955], Yih [1966]). How-

ever, we do not know the evolution of the flow when the mean current

starts from rest. In this chapter we will analyse some simple time-

dependent phenomena of lee waves with the assumption that the time

derivative of the mean current is so small that the equivalent body

force term in equation (4.6), $\partial U/\partial t$, can be entirely neglected.

We then consider the lee waves as "quasi-steady" and treat the mean

current as steady at any instant. The application of this "quasi-

steady" analysis may be useful in explaining the internal wave trains

generated by a low submarine ridge in a tidal flow, since the tidal

period is generally much longer than the lee wave period. We choose

to examine lee waves generated by a low ridge, since a high ridge

prevents lee waves from propagating over the ridge and may cause

waves to break.

Since the acceleration of the mean current is neglected in our

analysis, ray theory can be used to interpretate these quasi-steady

lee waves. Linear theory predicts that the wave energy propagates

with the group velocity. In the experiments we find that the number

of lee waves gradually increases as the ridge starts to move, indicating that energy gradually propagates away from the ridge by means of these quasi-stationary waves. Since the phase velocity of the lee waves is identical to the velocity of the ridge, we conclude that the lee wave group velocity must be smaller than the phase velocity. However, we will now show that this is a general property of internal waves. In a x - t diagram, the moving ridge can be treated as a wave source which emits energy, with the energy propagating away from the ridge along rays whose slope equals the lee wave group velocity. The variation of the distance between two adjacent rays is proportional to the inverse of the energy density in space; thus, the formation of an energy density peak is quite possible as the lee wave group velocity decreases in time.

The dispersion relationship for linearized internal waves in a linearily stratified fluid contained between two horizontal rigid boundaries is

$$\omega^2 = \frac{k^2 N^2}{k^2 + \frac{n^2 \pi^2}{H^2}} \; , \qquad\qquad (4.18)$$

where N is the constant Brunt-Vaisala frequency, H is the total depth, n is the vertical mode number, and ω and k are the wave frequency and wave number. The phase velocity is

$$C_p = \frac{\omega}{k} = \frac{NH}{n\pi} \left(1 - \frac{\omega^2}{N^2} \right)^{1/2} . \qquad\qquad (4.19)$$

and group velocity is

$$C_g = \frac{\partial \omega}{\partial k} = \frac{NH}{n\pi} \left(1 - \frac{\omega^2}{N^2}\right)^{3/2}. \tag{4.20}$$

Since ω is always smaller than N for internal waves, the maximum magnitude of C_p and C_g is $NH/n\pi$ (corresponding to the longest wave). From (4.19) and (4.20), we have

$$C_g = C_p \left(1 - \frac{\omega^2}{N^2}\right) \leqslant C_p. \tag{4.21}$$

This relationship means that the group velocity of an internal mode is always smaller than the phase velocity, the equal sign applying only in the limit of infinite wave length.

For lee waves, we have an additional relationship

$$\omega = kU, \tag{4.22}$$

where U is the velocity of the moving ridge. From (4.19) and (4.22), we can solve for the two unknowns, k and ω , finding that

$$k = \pm \left(\frac{N^2}{U^2} - \frac{n^2\pi^2}{H^2}\right)^{1/2}, \tag{4.23}$$

$$\omega = \left(N^2 - \frac{n^2\pi^2 U^2}{H^2}\right)^{1/2}. \tag{4.24}$$

where the (-) sign is for negative U and (+) sign is for positive U. Thus, both the period and the wave length increase as the velocity U increases. The maximum U, however, has to be smaller than $NH/n\pi$ in order to keep both k and ω real, since no wave may propagate in phase with a ridge moving faster than the maximum internal wave phase

speed. Introducing (4.24) into (4.20) then yields

$$C_g = \frac{n^2 \pi^2 U^3}{N^2 H^2} \ . \qquad (4.25)$$

Equation (4.25) implies that the wave energy propagates in space with a velocity proportional to the cubic of U, and that the wave energy propagates away from the ridge with the velocity C_E ,

$$C_E = C_p - C_g = C_p \cdot \frac{\omega^2}{N^2} = U \left(1 - \frac{n^2 \pi^2 U^2}{N^2 H^2} \right) . \qquad (4.26)$$

$C_E = 0$ for extremely long waves, and the energy begins to accumulate around the ridge. However, this is also where lee wave theory breaks down.

The wave energy propagates in x - t space along the characteristic lines

$$X = \int_0^{t_0} U(\theta) d\theta + \frac{n^2 \pi^2 U^3(t_0)}{N^2 H^2} (t - t_0), \qquad (4.27)$$

where t_0 is the time at which the wave is generated at the wave source (the moving ridge). In our reference frame fixed with the mean current, these characteristic lines are simple straight lines. For simplicity, we write (4.27) in the following form

$$X = X_s(t_0) + C_g(t_0) \cdot (t - t_0), \qquad (4.28)$$

where $x_s = \int_0^{t_0} U(\theta)\,d\theta$ is the position of the moving ridge. Differentiating (4.28) with respect to t_0 we have

$$\frac{\partial t}{\partial t_0} = \frac{-C_g \cdot U - (x - x_s)\frac{\partial C_g}{\partial t_0}}{C_g^2} + 1 \qquad (4.29)$$

Here we treat t as a dependent variable and x, and t_0 as independent variables. Note that $U = \frac{\partial x_s}{\partial t_0}$. The energy density E is defined as

$$E \cdot \Delta x = E_0 \cdot \Delta x_s , \qquad (4.30)$$

where $E_0 \cdot \Delta x_s$ is the total energy emitted by the wave source as it moves a distance Δx_s. Equation (4.30) is a simple relationship of energy conservation. Since the energy travels along the rays, we may assume that E is the energy contained between two adjacent rays separated by a distance Δx. Since

$$\frac{\Delta x_s}{\Delta x} = \frac{U(t_0) \cdot \Delta t_0}{C_g(t_0) \cdot \Delta t} , \qquad (4.31)$$

conservation of energy requires

$$E = E_0 \cdot \frac{U(t_0)}{C_g(t_0)} \cdot \frac{\Delta t_0}{\Delta t} . \qquad (4.32)$$

In the limit as $\Delta t \to 0$, we may use (4.29) to obtain

$$\lim_{\substack{\Delta t \to 0 \\ \Delta t_0 \to 0}} E = E_0 \cdot \frac{U(t_0) \cdot C_g(t_0)}{C_g^2(t_0) - C_g(t_0)U(t_0) - (x-x_s)\frac{\partial C_g}{\partial t_0}} \qquad (4.33)$$

The curve of the energy density peak is obtained by setting the denominator of (4.33) at zero. If x_p and t_p denote the $x - t$ position of the energy density peak, then

$$x_p = x_s + \frac{C_g^2 - U C_g}{\partial C_g / \partial t_o} \quad , \tag{4.34}$$

Using (4.11), we have

$$t_p = t_o + \frac{C_g - U}{\partial C_g / \partial t_o} \quad . \tag{4.35}$$

By eliminating t_o from (4.34) and (4.35), we may arrive at a single equation for x_p and t_p, but in general the procedure is not easy. Since $U > C_g$ for internal waves and the formation of the energy density peak is possible only when the rays are convergent $(\frac{\partial C_g}{\partial t_o} < o)$, $x_p > x_s$ and $t_p > t_o$ always. For lee waves, we introduce (4.25) into (4.34) and (4.35) to get

$$x_p = x_s + \frac{n^2 \pi^2}{3 N^2 H^2} \cdot \frac{U^2(U^2-1)}{\partial U / \partial t_o} \quad , \tag{4.36}$$

$$t_p = t_o + \frac{1}{3U} \cdot \frac{(U^2-1)}{\partial U / \partial t_o} \quad . \tag{4.37}$$

If $U = \sin \omega_o t_o$,

$$x_s = \int_{\pi/2}^{t_o} \sin \omega_o \theta \, d\theta = \frac{-1}{\omega_o} \cos \omega_o t_o .$$

We then have

$$X_p = X_s - \frac{\eta^2 \pi^2}{6\omega_0 N^2 H^2} \sin 2\omega_0 t \sin \omega_0 t , \qquad (4.38)$$

$$t_p = t_0 - \frac{1}{3\omega_0} \cot \omega_0 t_0 . \qquad (4.39)$$

A typical curve of the energy density peak is shown in figure 26. From (4.38), it is obvious that no energy density peak is observed if the distance of the observation site from the mean location of the ridge is greater than x_s.

Now we will analyze the envelope of the lee wave trains that are found far away from the ridge. The amplitude of the waves when they are generated, i.e., the energy density E_0 at $x = x_s$, is assumed known. Using linearized theory and the Boussinesq approximation, we have

$$\nabla^2 \psi - \beta \psi_z + \frac{\beta g}{U^2} \psi = 0 , \qquad (4.40)$$

where ψ is the perturbation stream function, U is the steady velocity of the mean current, and the density is $\rho = \rho_0 (1 - \beta z)$. The second term in (4.39) is ordinarily very small. If the vertical length scale is H, the ratio of the second term to the last term is $O(U^2/gH) \approx \varepsilon^2 \sigma$ where ε is the nonlinear parameter and σ is the fractional change in mean density over H. By neglecting the second term and putting $\beta g = N^2$, we have
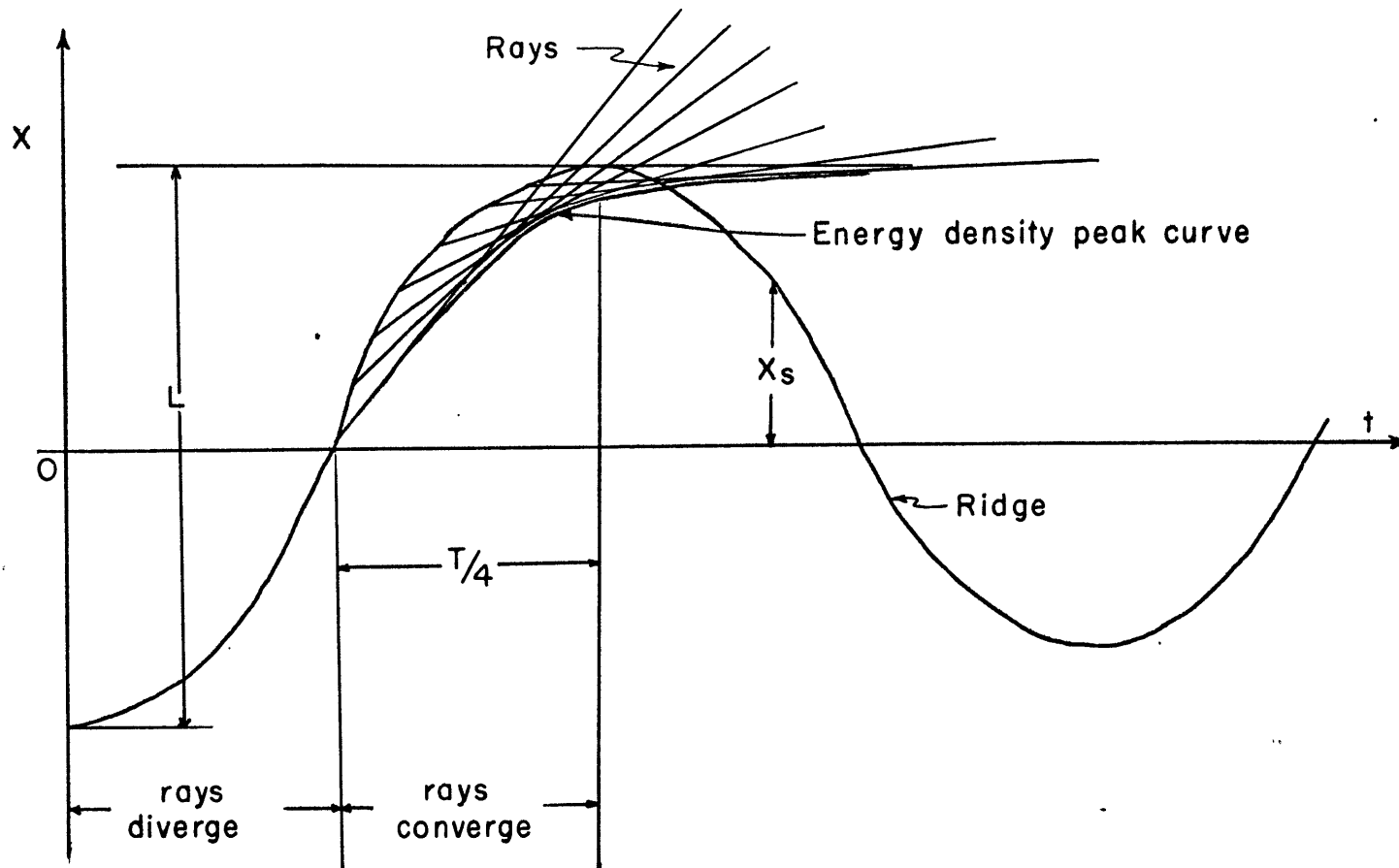
Figure 26. The rays and the energy density peak curve generated by a quasi-steady, periodic moving ridge.

$$\nabla^2 \psi + \frac{N^2}{U^2} \psi = 0. \tag{4.41}$$

Since $\psi = U\eta$, where η is the deflection of stream line, (4.41) can be transformed into the following form:

$$\nabla^2 \eta + \frac{N^2}{U^2} \eta = 0. \tag{4.42}$$

The boundary conditions are

$$\eta = 0 \qquad at \quad z = H, \tag{4.43}$$

$$\eta = \frac{a^2 b}{a^2 + x^2} \qquad at \quad z = 0. \tag{4.44}$$

Using the standard Fourier transform theory, we get

$$\eta = \frac{ab}{2\pi} \int_{-\infty}^{+\infty} e^{-|k|a} \cdot \frac{\sin \left[\left(\frac{N^2}{U^2} - k^2 \right)^{1/2} (z - H) \right]}{\sin \left[\left(\frac{N^2}{U^2} - k^2 \right)^{1/2} H \right]} \cdot e^{ikx} dk. \tag{4.45}$$

The disturbance generated by the moving ridge comprises the near field, which fades rapidly away from the "source", and the far field, which consists of an internal gravity wave. These wave solutions are due to the contributions from the poles of the integral (4.45) on the real axis of k. These poles are

$$k = k_n = \pm \left(\frac{N^2}{U^2} - \frac{n^2 \pi^2}{H^2} \right)^{1/2} , \qquad n = 1, \ldots \ldots, m,$$

101.

where m is the largest integer such that k remains real. These poles which satisfy the lee wave dispersion relation (4.23) give rise to the following contributions,

$$\eta_n = (-1)^n \cdot i\, a b \cdot e^{-|k_n|/a} \cdot e^{i k_n x} \cdot \sin \frac{n\pi}{H}(z - H), \quad n = 1, 2 \cdots m.$$

$$(4.46)$$

Thus, for a fixed vertical mode number n, the wave amplitude $\eta_o(t)$ increases as U(t) increases according to

$$\eta_o(t) \sim e^{-(\frac{N^2}{U^2} - \frac{n^2\pi^2}{H^2})^{1/2} \cdot a}$$

$$(4.47)$$

Equation (4.47) shows that for an arbitrary mode n, the amplitude approaches zero as the mean current U(t) approaches zero. However, for a constant U(t), the amplitude increases with the mode number n. In the limit $U(t) \rightarrow 0$, infinite modes may be generated by the moving ridge, however, the amplitude $\eta_o(t)$ approaches zero in this limit, because there is no energy to supply the generating mechanism. Our experimental results show that the internal waves generated by a low oscillatory ridge are mainly of the first mode. Thus at a fixed observation station well away from the ridge, we find that these internal wave trains are characterized by a relatively large amplitude first wave followed by several of decreasing size (figure 27, 28 & 29).

In a field experiment, the observation is made at a station fixed relative to the submarine ridge. Thus, in the x - t diagram, the position of the observation station is $X_o'(t_o) = X_s(t_o) + X_o$,
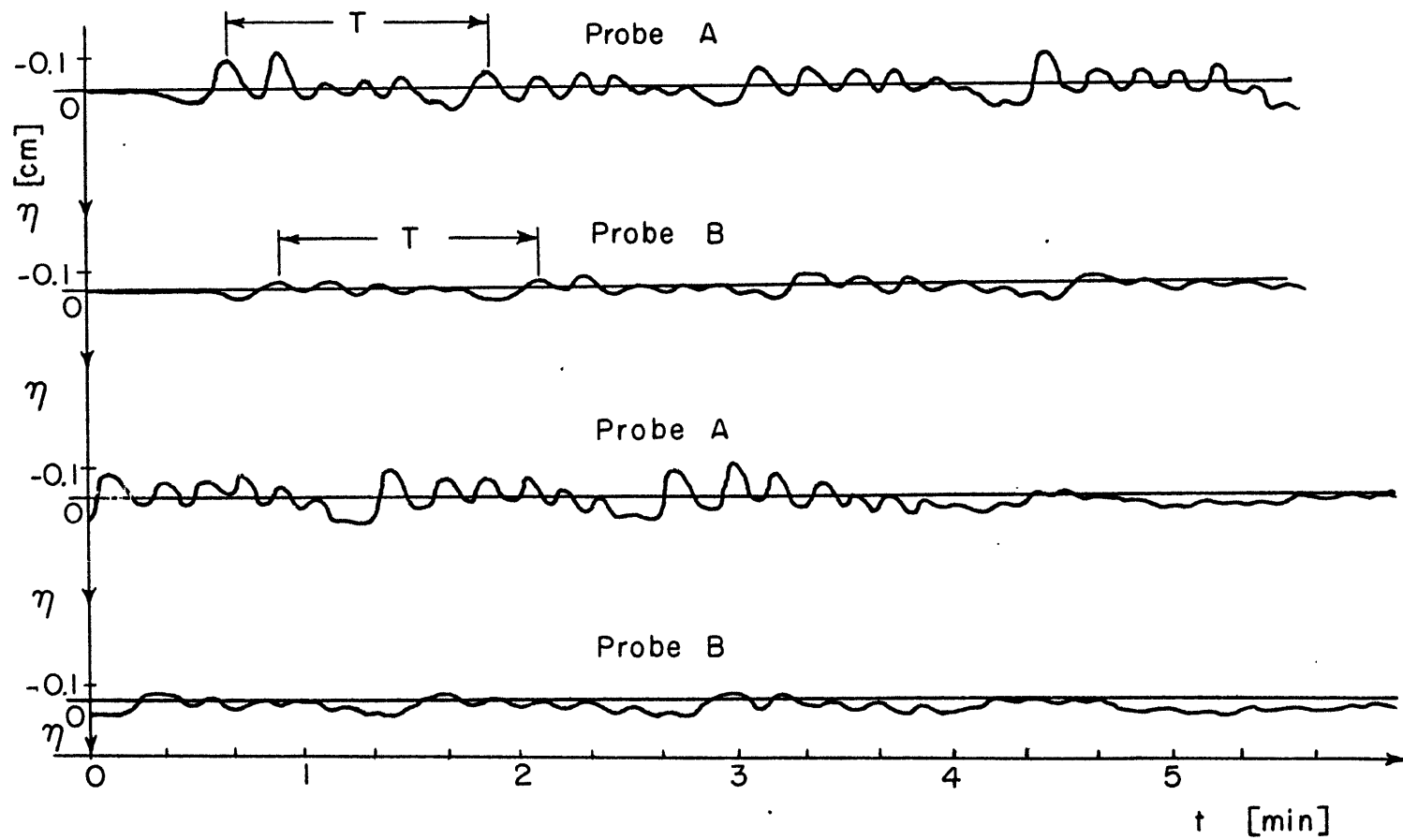
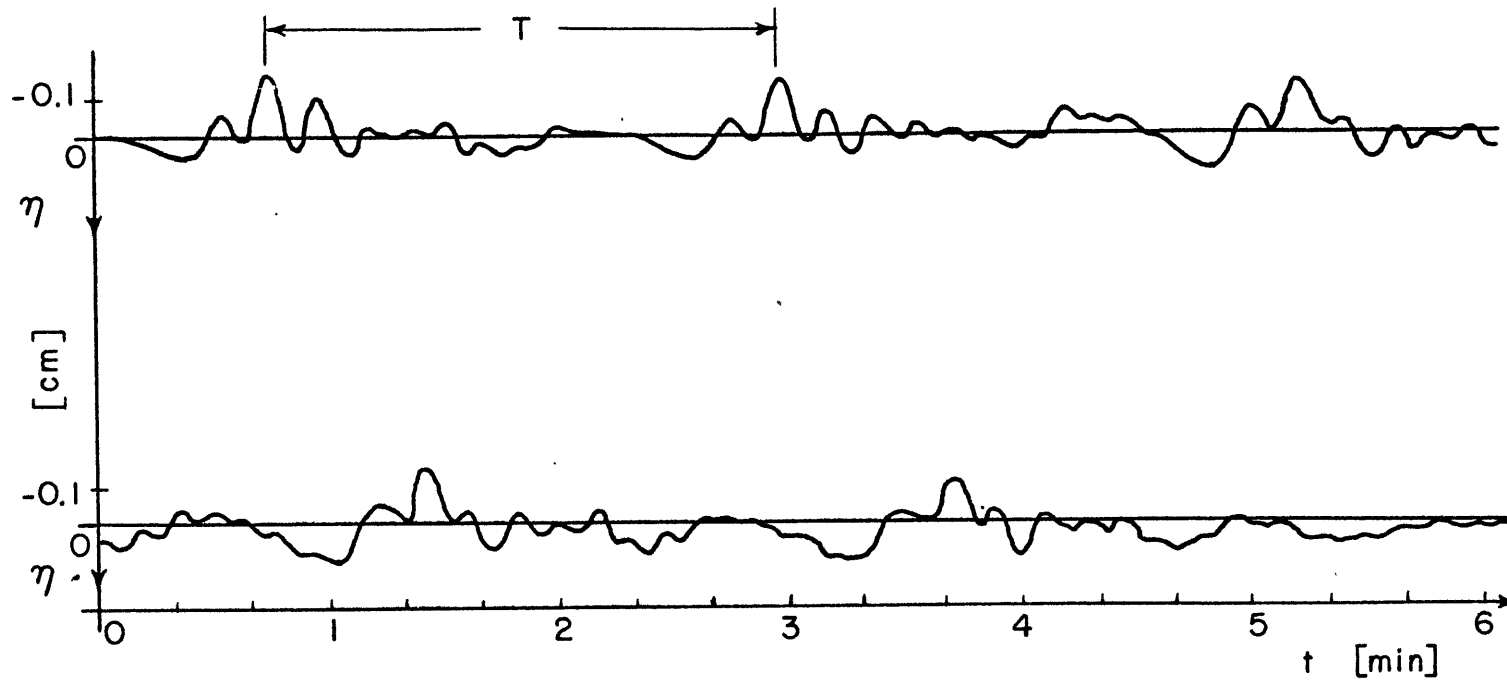Figure 27. Quasi-steady lee wave trains: RA = 57.5 cm, L = 55 cm, T = 76 sec, N = 0.1 cycle/sec, A = 2.3 cm, W = 12.5 cm, and H = 12.5 cm.

Figure 28. Longer period quasi-steady lee wave trains: RA = 60 cm, L = 100 cm, T = 135 sec, N = 0.1 cycle/sec, A = 2.3 cm, W = 12.5 cm, and H = 12.5 cm. Lower record is simple a continuation of upper record.
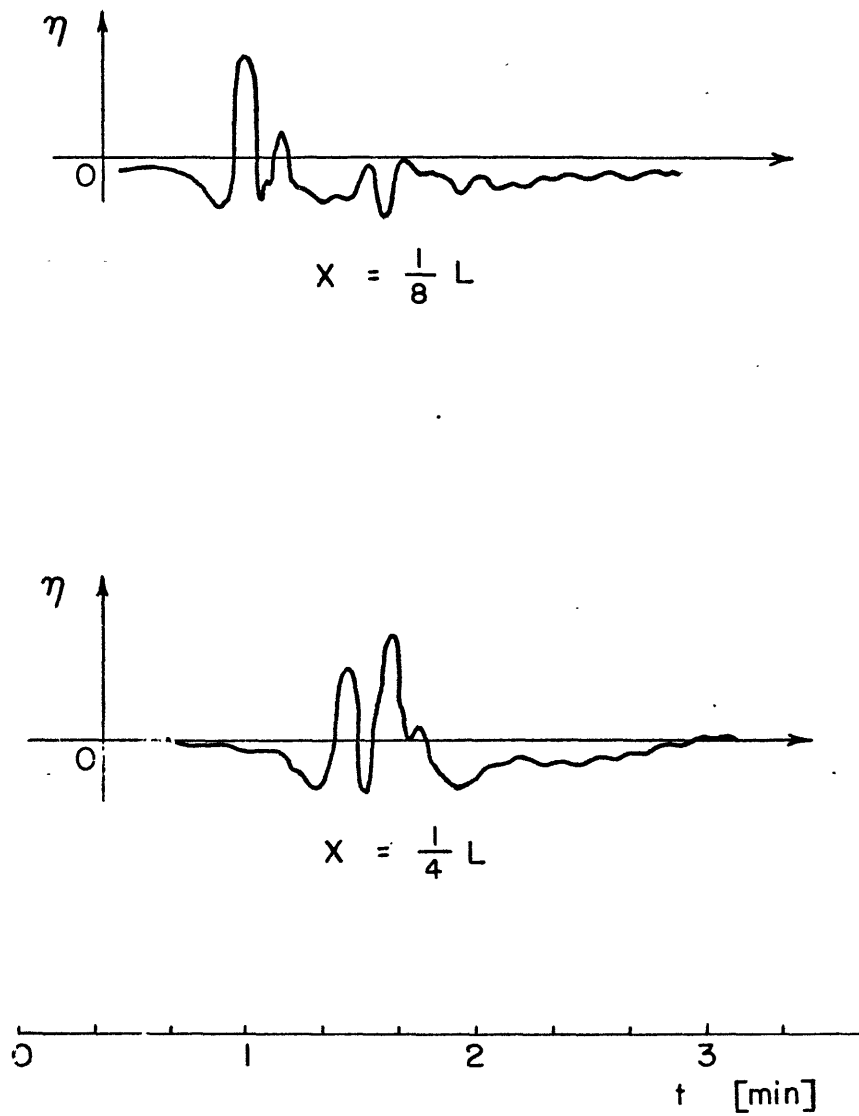
Figure 29. Measurements of the displacement of streamline at
the energy density peak curve at x = 1L/8 and
x = 1L/4 corresponding to figure 26.

where x_0 is the constant distance between the ridge and the station.

This curve intersects the rays at some different points instead of

at the points which correspond to the previous analysis for a station

fixed in relation to the mean current. The frequency difference due

to the relative motion of the reference frame is simply $kU(t)$, where

k is the wave number, which is invariant in a time-dependent mean

current $U(t)$. Part of the energy will be reflected as these waves

propagate across the ridge. For a low smooth ridge, the transmission

coefficient is approximately one, as can be shown using W.K.B.

approximation (Bremmer [1951]).

During the experiments on quasi-steady lee wave generation,

mixing was observed around the moving ridge. Although the mixing

process was generally weak, its accumulative effect was appreciable.

The influence of the mixed fluid was seen not only around the ridge

but also at a distance from the ridge. In order to separate mixing

from internal wave phenomena, a "mixer" was made using a high ridge

which moved horizontally over a short excursion at a high frequency

f_o ($f_o > N$). The mixed fluid was found to flow horizontally away

from the "mixer" along its neutral buoyancy level like a horizontal

wedge, causing the unmixed fluid to flow back in two shear layers

at the top and the bottom of the ridge, as shown in figure 30, and to

increase the mixing process near the ridge. These shear layers

delineated the density difference which could be observed from the

salinity conductivity probes (see figure 31).

The energy source of this system came from the moving ridge

(or mean current in the ocean). This energy was transfered to the

fluid by increasing the potential energy through mixing (Turner,

1966). The density discontinuity along the interface between the

mixed and unmixed fluid generated a pressure gradient (Mei, 1969)

which pushed the mixed fluid away from the mixing "source". The

walls of the tank force a vertical and horizontal recirculation of

the unmixed fluid as required by continuity of mass.

The fluid motion may be classified by the following regions,

the interior region, the mixing region, and the shear layer zone,

as shown in figure 30. We will now examine these different

(A)

(B)

Ridge   Mixed fluid   Shear layer

η_0

Neutral
level

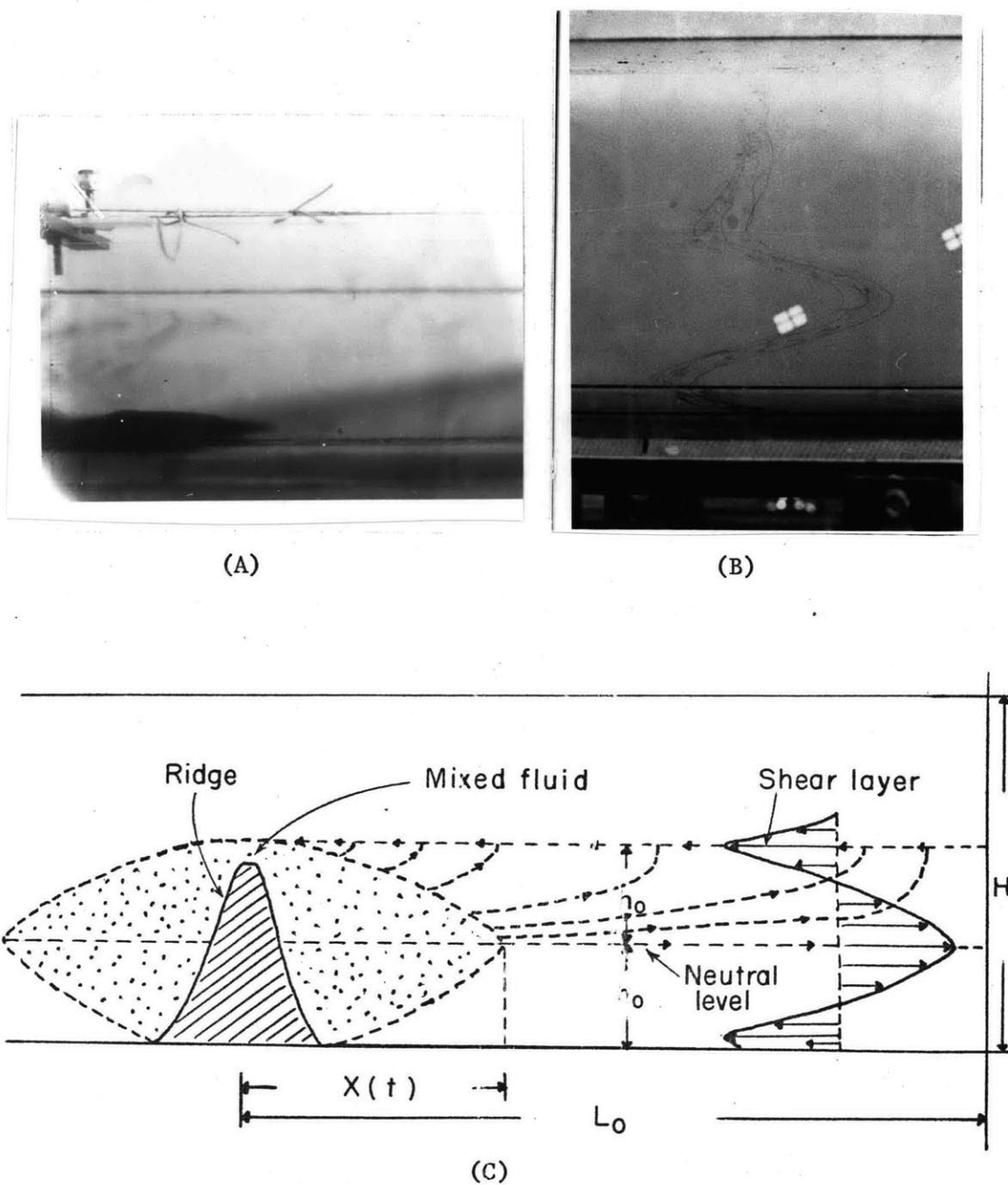ζ_0

X(t)

L_0

H

(C)

Figure 30.   (A) Photograph showing formation of mixed fluid
region (colored here by dark $KMnO_4$ dye).   (B)
Photograph of horizontal velocity profile.   (C)
A sketch of the experimental results showing the
shape of the mixed fluid region, shear layers,
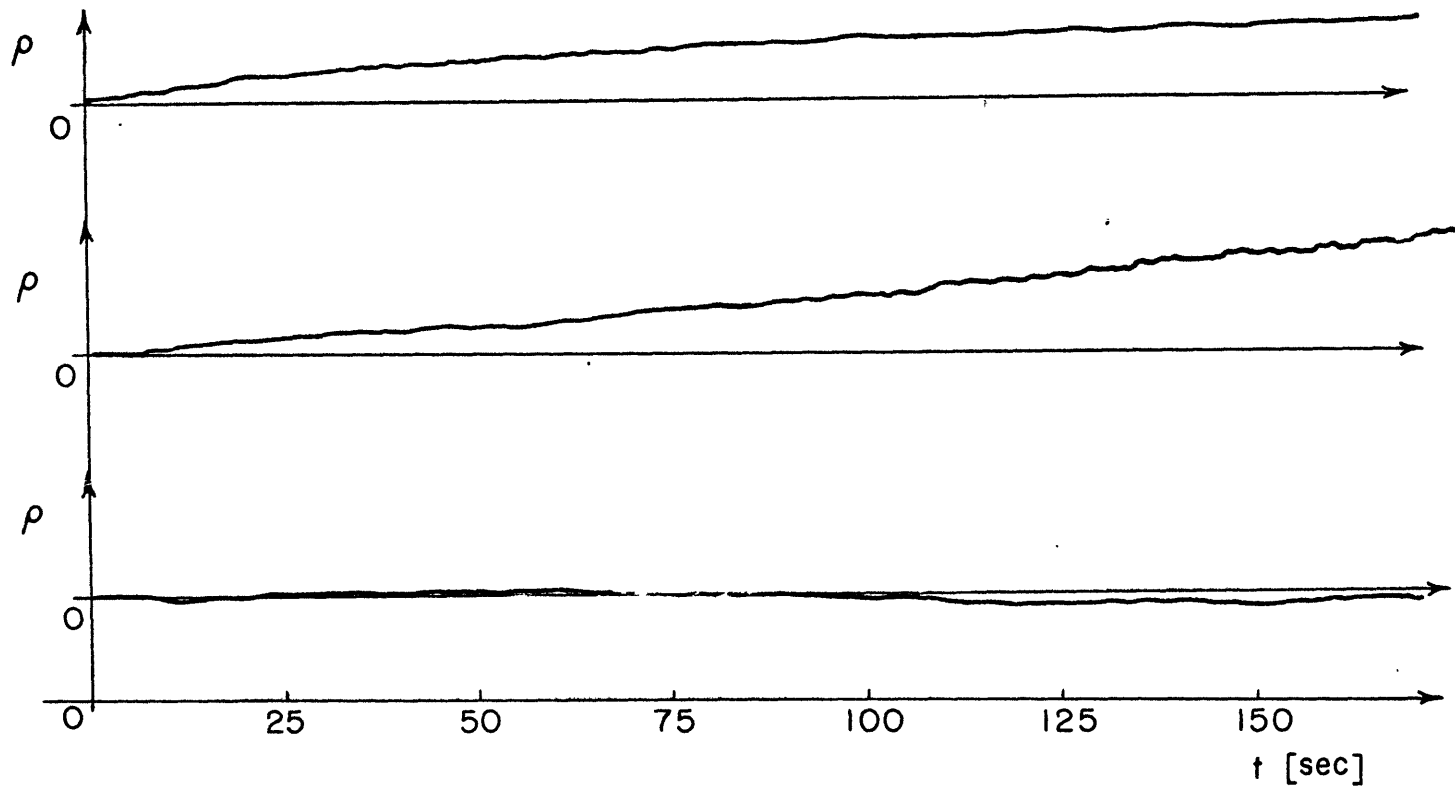and stream lines.

Figure 3/ . Typical density variations from the experimental results on mixing which show the formation of density jump: (A) Below the velocity shear layer (z = h). (B) Inside the shear layer. (C) Above the shear layer.

schematic regimes separately.

A. Interior Region:

The motion of the fluid in this region is quite similar to the slow motion of a solid body in a density stratified fluid (Foster and Saffman, 1970). The governing equations of the interior region are

$$\frac{\partial u}{\partial x} + \frac{\partial w}{\partial z} = 0 \; , \qquad\qquad (5.1)$$

$$\frac{\partial \rho}{\partial t} + w \frac{\partial \rho}{\partial z} + u \frac{\partial \rho}{\partial x} = 0 \; , \qquad\qquad (5.2)$$

$$\frac{\partial \rho}{\partial x} = 0 \; , \qquad\qquad (5.3)$$

$$\frac{\partial p}{\partial z} = -\rho g . \qquad\qquad (5.4)$$

The neglect of the diffusion term in (5.2) is due to the very large Peclet number $P_e = \dfrac{U h_o^2}{K L} \gg 1$, where h_o is the vertical characteristic length, L is the horizontal characteristic length, K is the diffusivity of salt, and U is the typical horizontal velocity. Equations (5.3) and (5.4) are results from the hydrostatic approximation. From (5.3) and (5.4) we have

$$p = p (z, t) \qquad\qquad (5.5)$$

$$\rho = \rho (z, t) \qquad\qquad (5.6)$$

Equations (5.2) and (5.6) imply

$$W = W(z, t).$$ $\qquad (5.7)$

From (5.1) and (5.7), we have

$$u = f(z, t) - x\frac{\partial W}{\partial z}.$$ $\qquad (5.8)$

The boundary condition at the end of the tank is

$$u = 0 \qquad at \qquad x = L.$$ $\qquad (5.9)$

The equation of the interface between the mixed and stratified

fluids is

$$x = g(z, t).$$ $\qquad (5.10)$

Then for a particle which remains on the interface,

$$\frac{D}{Dt}[x - g(z, t)] = 0,$$

or

$$u = \frac{\partial g}{\partial t} + W\frac{\partial g}{\partial z}.$$ $\qquad (5.11)$

Equation (5.8) and (5.9) imply that

$$u = (L - x)\frac{\partial W}{\partial z}.$$ $\qquad (5.12)$

Equations (5.10), (5.11), and (5.12) imply that

$$g_t + W g_z = W_z(L - g)$$ $\qquad (5.13)$

or

$$(L - g)W_z - g_z W - g_t = 0.$$ $\qquad (5.14)$

The solution of (5.14) is

$$w = \frac{\int g_t \, dz + C(t)}{L - g} \, . \tag{5.15}$$

Due to vertical symmetry of the steady flow, the vertical velocity has to vanish at the neutral buoyancy level, i.e.,

$$w = 0 \qquad at \quad z = 0. \tag{5.16}$$

Equation (5.16) then implies

$$w = \frac{1}{L - g} \int_0^z g_t \, dz \, .$$

For reasons which will become clear in the next section, we will choose

$$g = \underline{X}(t) \left[1 - \frac{z^2}{h_0^2} \right] .$$

We then find

$$w = \frac{\underline{X}'(t) \cdot (h_0^2 z - \frac{1}{3} z^3)}{L h_0^2 - \underline{X}(t)(h_0^2 - z^2)} \, , \tag{5.17}$$

and

$$u = (L - x) \frac{\partial w}{\partial z} = \frac{(L - x)}{(L - g)} \cdot (g_t + w g_z)$$

$$= \frac{(L - x)\, \underline{X}'(t)}{L h_0^2 - \underline{X}(t)(h_0^2 - z^2)} \left[(h_0^2 - z^2) - \right.$$

$$\left. \frac{2z\, \underline{X}(t)\, (h_0^2 z - \frac{1}{3} z^3)}{L h_0^2 - \underline{X}(t)\,(h_0^2 - z^2)} \right] \, . \tag{5.18}$$

From (5.2) and (5.18), we have

$$f = f(z, 0),$$ along the characteristic lines.

The characteristic lines and streamfunction respectively are given by

$$\frac{dz}{dt} = \frac{\overline{X}(t)\left(h_0^2 z - \frac{1}{3} z^3\right)}{L h_0^2 - \overline{X}(t)\left(h_0^2 - z^2\right)},$$

$$\psi = (L - x)\frac{\overline{X}'(t)\left(h_0^2 z - \frac{1}{3} z^3\right)}{L h_0^2 - \overline{X}(t)\left(h_0^2 - z^2\right)}. \qquad (5.19)$$

Since both diffusion and viscosity are neglected in the analysis of the unmixed fluid region, discontinuities such as density jumps and velocity shear layers cannot be avoided. The regions $z > h_0$ remain stationary because of the end walls, so that internal boundary layers form to close the recirculation. These fully nonlinear viscous layers help to reduce the vertical velocity to zero, make the density continuous, and carry the backward mass transport. The boundary layers at the end wall reduce the vertical velocity to zero, while the boundary layers at the interfaces between the mixed and unmixed fluids smooth out the density jumps and velocity discontinuities. Further discussion of these boundary layers (with the exception of the interfacial layer) is given by Foster and Saffman (1970).

B. Mixed Region:

The motion of this fluid is complicated. To simplify the situation, we neglect the turbulent motion and weak density gradients inside the mixed region and liken the case to the collapse of a homo-

geneous fluid mass in a density stratified fluid (Schooley and Stewart [1963], Jin Wu [1969], and Mei [1969]). The important difference of the case considered here is that newly mixed fluid is continuously generated by the moving ridge. Assuming the length of the horizontal axis of the mixed fluid X (t) is large and the driving pressure gradient is small, we may again use a quasi-steady approximation, provided that L is so large that the constant Brunt-Vaisala frequency of the unmixed fluid stays constant in time. The governing equations are then

$$ u u_x + w u_z = -p_x + \nu u_{zz} \, , \tag{5.20} $$

$$ u w_x + w w_z = -p_z + \rho g + \nu w_{xx} \, , \tag{5.21} $$

$$ u_x + w_z = 0 \, . \tag{5.22} $$

Guided by the experimental results, the following horizontal column solution is assumed

$$ w = 0 \, , \tag{5.23} $$

$$ u = f(z, t) \, , \tag{5.24} $$

f being a function to be determined later. From (5.20), (5.21), (5.23), and (5.24), the horizontal momentum equation becomes

$$ \alpha \eta \eta_x + \nu u_{zz} = 0 . \tag{5.25} $$

Equation (5.25) means that the driving pressure gradient along the interface between the mixed and stratified fluid is balanced by the viscous force, where η is the height of the interface from the

neutral level and α is the square of the constant Brunt-Vaisala frequency of the stratified fluid.

In order to satisfy (5.25), f(z, t) must assume a certain form. Since η is only a function of x and t, and α is a constant, this implies

$$U = f(z, t) = U_o(t)\left(A(t)z^2 + B(t)z + 1\right), \qquad (5.26)$$

with A(t) and B(t) to be determined. The two boundary conditions for the mixed fluid are

$$\eta = 0 \qquad at \qquad X = \underline{X}(t), \qquad (5.27)$$

$$\eta = h_o \qquad at \qquad X = 0. \qquad (5.28)$$

Although the mathematical forms of the boundary conditions are very simple, their correct physical interpretation is very important. It is well known (Kato and Phillips, 1969) that mixing causes vertical entrainment in a stratified fluid, and the height of vertical entrainment depends crucially on the strength of the mixing process. Thus h_o in (5.28) represents the strength of the mixing process around the ridge, where the boundary condition (5.27) means that the tip of the mixed fluid region has to be at neutral buoyancy level.

It is obvious that there should be a close relation between h_o and the horizontal speed $U_o(t)$ of the tip ($\eta = 0$). From (5.25), (5.26), and (5.27), we have

$$\eta^2 = \frac{-4\nu}{\alpha} \int_x^{\overline{X}(t)} u_o(t) A(t) \, dx$$

$$= \frac{-4\nu}{\alpha} u_o(t) A(t) (\overline{X}(t) - x).$$ \hfill (5.29)

By introducing (5.28) into (5.29), we have

$$u_o(t) = \frac{-\alpha \hbar_o^2}{4\nu} \cdot \frac{1}{A(t)} \cdot \frac{1}{\overline{X}(t)}.$$ \hfill (5.30)

we will now determine the two arbitrary functions A(t) and B(t). Introducing (5.30) into (5.29) yields

$$\eta^2 = \hbar_o^2 \frac{\overline{X}(t) - x}{\overline{X}(t)}$$ \hfill (5.31)

or

$$x = \overline{X}(t) - \frac{\overline{X}(t) \eta^2}{\hbar_o^2}.$$ \hfill (5.32)

This result plus qualitative experimental evidence suggested the form used in the previous section for g(z, t). However, from (5.26), η has to satisfy the following relation

$$x = \eta^2 \int_0^t u_o(t') A(t') \, dt' + \eta \int_0^t u_o(t') B(t') \, dt$$

$$+ \int_0^t u_o(t') \, dt'.$$ \hfill (5.33)

By comparing (5.32) and (5.33), we see that

$$B(t) = 0 \qquad\qquad (5.34)$$

$$\underline{X}(t) = -\hbar_o^2 \int_0^t u_o(t') A(t')\, dt. \qquad\qquad (5.35)$$

Equation (5.34) is an expected result since we have a symmetric flow with respect to $z = 0$. The solution to the integral equation (5.35) is

$$A(t) = -\frac{1}{\hbar_o^2}. \qquad\qquad (5.36)$$

Introducing (5.36) into (5.11) then yields

$$U_o(t) = \frac{\alpha\, \hbar_o^4}{4\nu} \cdot \frac{1}{X(t)}. \qquad\qquad (5.37)$$

This is a very important relationship between the strength of the mixing process and the horizontal collapse speed. The physical interpretations of (5.37) are as follows.

(a) $U_o(t)$ is proportional to the fourth power of h_o; thus U_o depends crucially on the strength of the mixing process around the ridge.

(b) $U_o(t)$ is proportional to α, which is expected since large α means a large driving pressure gradient along the interface.

(c) $U_o(t)$ is decreased by an increase in visco sity ν.

(d) $U_o(t)$ is proportional to $1/\underline{X}(t)$, because as $\underline{X}(t)$ is increased, the driving pressure gradient is decreased.

Other quantities are

$$u(z, t) = u_o(t)\left(\frac{h_o^2 - z^2}{h_o^2}\right), \qquad (5.38)$$

$$\eta(x, t) = h_o\left(1 - \frac{x}{\underline{X}(t)}\right)^{1/2}, \qquad (5.39)$$

$$\underline{X}(t) = \left(\frac{\alpha h_o^4}{2\gamma} t\right)^{1/2}. \qquad (5.40)$$

In order that the above theory may be easily compared with experimental results, (5.40) has to be modified to avoid the sigularity at t = 0. Integrating (5.37) with respect to t, we have

$$X(t) = \left[x_o^2 + \frac{\alpha h_o^4}{2\gamma}(t - t_o)\right]^{1/2} \qquad (5.41)$$

where $x_o = x(t)\big|_{t=t_o}$. We have initially assumed in this theoretical development that $x_o \gg h_o$. The results of a typical mixing experiment are compared in figure 32 for $x_o/h_o = 6.3$ with theoretical curves predicted using (5.41). The rough agreement suggests that the effective viscosity coefficient in the mixing region is of order 1 $cm^2/$ sec (at least 10^2 times the molecular value).

Since the quasi-steady approximation and the assumption of constant α do not accurately apply to these experiments, the theory and experimental results agree only qualitatively. The introduction of rotation would make this problem more interesting (Walin, 1969) and is worthy of further investigation.
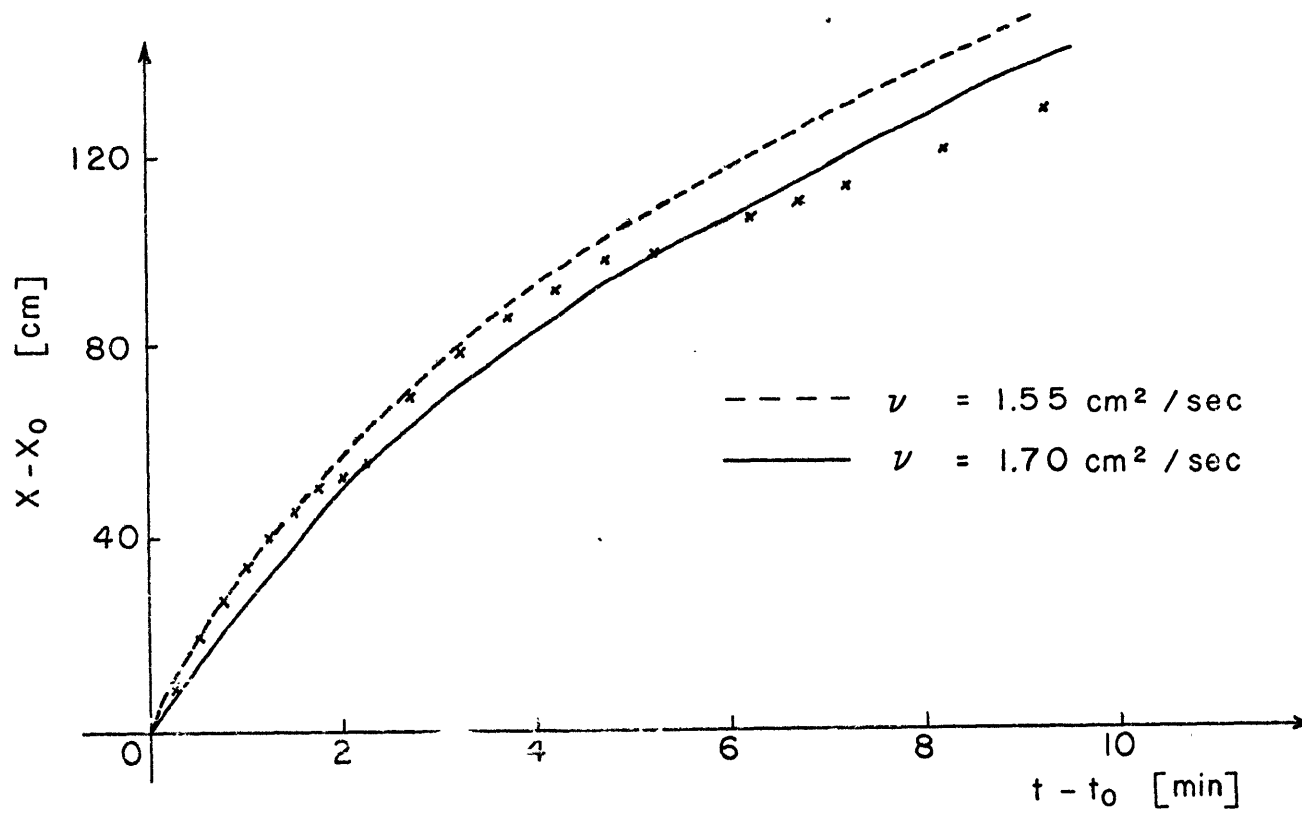
Figure 32. The cross points represent the observed trajectory of the tip of the mixed fluid region in a typical mixing experiment (h_o= 3.8 cm, α= 0.75) where the solid and dash lines represent the theoretical results computed for different viscosity coefficients with x = 24 cm.

6. Conclusion

The experimental results and numerical calculations have already demonstrated that nonlinearity is very important in the generation of long nonlinear internal gravity waves from a local isolated internal disturbance. While wave dispersion in surface and internal waves is similar, a major difference between long surface and internal wave theories is that the basic density stratification of the fluid can even change the sign of the nonlinear effect for internal waves. Thus, an internal solitary wave may exist for both an initial elevation or depression of the stream lines, whereas surface solitary waves exist for only an initial surface elevation. Assuming that the fractional change in the basic density over the vertical characteristic length is small (use Boussinesq approximation), it is found that an internal warm front or depression (corresponding to the first mode) tends to steepen in a typical seasonal thermocline, and long nonlinear internal wave trains will be generated on this depression due to the dispersive effect of the sharp front. A comparison of Halpern's temperature observations in Massachusetts Bay and our numerical results shows that a fully nonlinear model does give accurate estimates for the observed sharp warm front, the phase speed and the wave length of these internal waves. The finite amplitude effect vanishes identically to first order approximation for a linearity stratified fluid of constant Brunt-Vaisala frequency, which is often used. Inclusion of the non-Boussinesq term simply reduces the phase speed of the internal waves.

We should also point out that temperature observations made in

the Straits of Gibraltar by Ziegenbein (1969, 1970), also suggest

the presence of long nonlinear internal waves even though the water

depth is not small in comparison to a typical wave length. This may

be because the thermocline depth rather than the total water depth

becomes the appropriate vertical characteristic length (Benjamin,

1967). A time-dependent KdV equation for this case is under investi-

gation at present.

The experimental results for quasi-steady lee wave trains agree

only qualitatively with ray theory, possibly because the excursion

of the oscillating ridge is not really large enough in comparison to

the wave length of the lee waves. The lee wave regime is bounded by

several limits (mixing, blocking, and the maximum long internal wave

speed). A possible application of this ray theory is to explain some

small amplitude internal wave trains which occur without significant

mean level change in a semi-diurnal tidal flow.

The mixing phenomena due to the moving ridge, which can be

replaced by any other "mixer", is worthy of further investigation.

Our analysis of a very simple model shows that the "mixer" is not only

the source of the mixed fluid but also the sink of the unmixed fluid.

The resulting circulation set up by the "mixer" causes internal

density discontinuities and high velocity shear layers. The final

steady state is that all the fluid below (approximately) the height

of the top of the ridge will become homogeneous, and diffusion will

gradually decrease the subsequent density jump. The summer vertical

temperature profile in Massachusetts Bay seems to give a good proof

of this limiting case.

Acknowledgements

I am very grateful to Prof. Robert Beardsley and Prof. Peter Rhines for their excellent guidence, their moral support, their patience to listen, and their willingness to comment during this study. I would also like to thank Prof. Norman Phillips for his instructive suggestions and for letting me read his unpublished research work on quasi-steady lee waves. I thank Prof. C. C. Mei for his many valuable suggestions and comments and Prof. Erik Mollo-Christensen and Dr. William Simmons for many helpful discussions. I gratefully acknowledge the assistance of Prof. Carl Wunch and Dr. David Cacchione for letting me use their wave tank and probes.

I greatly appreciate the skilled technical assistance given by Mr. Edward Bean of the departmental machine shop during the construction of the experimental apparatus. Shian-yun, my wife made many sacrifices (including her own graduate study) to be a wife of a graduate student. In addition, she typed the first and final draft.

References

Airy, G.B., 1845, Tides and waves. Encyclopaedia Metropolitana, Vol. 5, London

Benjamin, T.B., and Lighthill, M.J., 1954, On cnoidal waves and bores. Proc. Roy. Soc., A224, 448

Benjamin, T.B., 1966, Internal waves of finite amplitude and permanent form. J. Fluid Mech., 25, 241

Benjamin, T.B., 1967, Internal waves of permanent form in fluids of great depth. J. Fluid Mech., 29, 559

Benney, D.J., 1966, Long nonlinear waves in fluid flows. J. Math. Phys., 45, 52

Bremmer, H., 1951, The WKB approximation as the first term of a geometric-optical series. Communications on Pure and Applied Mathematics, Vol. 4

Bretherton, F.P., 1968, Propagation in slowly varying waveguides. Proc. Roy. Soc., A302, 555

Bretherton, F.P., and Garrett, C.J.R., 1968, Wave trains in inhomogeneous moving media. Proc. Roy. Soc., A302, 529

Cacchione, D.A., 1970, Experimental study of internal waves on a slope. Ph.D. Thesis, Massachusetts Institute of Technology and Woods Hole Oceanography Institution

Foster, M.R., and Saffman, P.G., 1970, The drag of a body moving transversely in a confined stratified fluid. J. Fluid Mech., Vol. 43, 407

Gibson, C.H., and Schwarz, W.H., 1963, Detection of conductivity fluctuations in a turbulent flow field. J. Fluid Mech., 16, 357

Halpern, D., 1971, Observations on short period internal waves in Massachusetts Bay. J. of Marine Research, 29, 116

Howard, L.N., 1961, Note on a paper by John W. Miles. J. Fluid
        Mech., 10, 509

Kato, H., and Phillips, O.M., 1969, On the penetration of a turbu-
        lent layer into stratified fluid. J. Fluid Mech., 37, 643

Korteweg, D.J., and DeVries, G., 1895, On the change of form of long
        waves advancing in a rectangular canal and on a new type
        of long stationary waves. Phil. Mag., Series 5, 39, 442

Lemoine, R., 1948, Sur les ondes positives de translation dans les
        canaux et sur ressaut ondulé de faible amplitude.
        La Houille Blanche, No. 2 Grenoble

Lighthill, M.J., 1967, Waves in fluid. Communication on Pure and
        Applied Mathematics, 20, 267

Long, R.R., 1953, Some aspects of the flow of stratified fluid,
        1: A Theoretical investigation. Tellus, 5, 42

Long, R.R., 1954, Some aspects of the flow of stratified fluid,
        2: Experiments with a two-fluid system. Tellus, 6, 97

Long, R.R., 1955, Some aspects of the flow of stratified fluids,
        3: Continuous density gradients. Tellus, 7, 341

Long, R.R., 1965, On the Boussinesq approximation and its role in
        the theory of internal waves. Tellus, 17, 46

Long, R.R., 1970, Blocking effects in flow over obstacles. Tellus,
        22, 471

Madsen, O.S., Mei, C.C., and Savage, R.P., 1971, The evolution of
        time periodic long waves of finite amplitude. J. Fluid
        Mech., 44, 195

Mei, C.C., 1969, Collapse of a homogeneous fluid mass in a strati-
        fied fluid. Proc. 12th Intern. Congr. Appl. Mech.
        (Berlin: Springer), 321

Mei, C.C., and Unluata, U., 1971, Harmonic generation in shallow
        water wave, paper presented by Mei at "Advanced seminars
        on waves on beaches", University of Wisconsin

Miles, J.W., 1961, On the stability of heterogeneous shear flows. J. Fluid Mech., 10, 496

Oster, G., 1965, Density gradients. Sci. Amer., 213, 70

Peregrine, D.H., 1966, Calculations of the development of an undular bore. J. Fluid Mech., 25, 321

Phillips, O.M., George, W.K., and Mied, R.P., 1968, A note on the interaction between internal gravity waves and currents. Deep Sea Research, 15, 267

Rayleigh, Lord, 1876, Phil. Mag. Ser. 5, 257; Papers, 1, 251. Cambridge University Press

Schooley, A.H., and Stewart, R.W., 1963, Experiments with a self-propelled body submerged in a fluid with a vertical density gradient. J. Fluid Mech., 15, 83

Scott, R.J., 1837. Rep. Brit. Ass., p-417

Scott, R.J., 1844. Rep. Brit. Ass., p-311

Stokes, G.G., 1880, Papers, 1, 197-229, 314. Cambridge University Press

Stokes, G.G., 1847, Trans. Camb. Phil. Soc., 8, 441

Turner, J.S., and Kraus, E.B., 1966, A one dimensional model of the seasonal thermocline. I. A laboratory experiment and its interpretation. Tellus, 18, 937

Walin, G., 1969, Some aspects of time-dependent motion of a stratified rotating fluid. J. Fluid Mech., 36, 289

Whitham, G.B., 1965, Nonlinear dispersive waves. Proc. Roy. Soc., A283, 238

Whitham, G.B., 1965, A general approach to linear and nonlinear dispersive waves using a Lagrangian. J. Fluid Mech., 22, 273

Wu, Jin, 1969, Mixed region collapse with internal wave generation in a density stratified medium. J. Fluid Mech., 35, 531

Yih, C.S., 1965, Dynamics of nonhomogeneous fluid. New York
    Macmillan

Zabusky, N.J., and Kruskal, M.D., 1965, Interaction of "soliton"
    in a collisionless plasma and the recurrence of initial
    state. Phyaical Review Letters, 15, 240

Zabusky, N.J., 1967, Synergetic approach to nonlinear wave problems
    (nonlinear partial differential equation, edited by
    Ames, W.F.) Academic Press, New York

Biographical Sketch

The author was born on June 6, 1942 in Szuchung province, China, and raised in Taiwan. He received a B.S. degree in civil engineering from Cheng Kung University in June 1964, and a M.S. degree in geophysics from the Institute of Geophysics, National Central University, in June 1966. He served for one year in the chinese military service before entering M. I. T. in September 1967. He married the former Shian-yun Yao in Cambridge, Massachusetts, in 1969.